1. SELF-SORTING OF DYNAMIC IMINE LIBRARIES UNDER CHEMICAL AND PHYSICAL STIMULI

2. CHARACTERIZATION OF POROUS MATERIALS BASED ON A FLUORINATED TETRAZOLE

A Dissertation Presented to

the Faculty of the Department of Chemistry

University of Houston

In Partial Fulfillment

of the Requirements for the Degree

Doctor of Philosophy

By

Chia-Wei Hsu

May 2016

1. SELF-SORTING OF DYNAMIC IMINE LIBRARIES UNDER CHEMICAL AND PHYSICAL STIMULI

2. CHARACTERIZATION OF POROUS MATERIALS BASED ON A FLUORINATED TETRAZOLE

_____

Chia-Wei Hsu

APPROVED:

_____

Dr. Ognjen Š. Miljanić, Chairman

_____

Dr. Randolph Thummel

_____

Dr. Olafs Daugulis

_____

Dr. Steven Baldelli

_____

Dr. Gregory D. Cuny

_____

Dean, College of Natural Sciences and Mathematics

1. SELF-SORTING OF DYNAMIC IMINE LIBRARIES UNDER CHEMICAL AND PHYSICAL STIMULI

2. CHARACTERIZATION OF POROUS MATERIALS BASED ON A FLUORINATED TETRAZOLE

An Abstract of Dissertation Presented to

the Faculty of the Department of Chemistry

University of Houston

In Partial Fulfillment

of the Requirements for the Degree

Doctor of Philosophy

By

Chia-Wei Hsu

May 2016

ABSTRACT

Chapter 1 introduces the self-sorting processes of dynamic combinaotrial libraries (DCLs) under thermodynamic and kinetic control. Based on the concept of dynamic combinatorial chemistry (DCC), disulfide exchange, imino bond formation, transesterification, and metal-ligand interaction are widely utilized to perform the re-equilibration of molecules. Simplification of multicomponent systems and the manipulation toward the direction of equilibrium are reviewed.

Chapter 2 of this dissertation describes an application of a new external stimulus—adsorption on the silica gel surface—to dynamic imine libraries constructed of as many as four aldehydes and four anilines. During the elution process, imines keep trading their components, resulting in the amplification of the least polar imine which travels down the silica gel-based column the fastest. This process is then iteratively repeated to isolate the next least-polar component in the remaining imine library, eventually simplifying the library from n^2 into n members.

In Chapter 3, we demonstrated iterative simplification of a dynamic imine library constructed from 10 aldehydes and 10 anilines using three orthogonal external stimuli. First, mild oxidation (using molecular iodine as an oxidant) was applied to oxidize the most electron rich imine with the rapid imine exchange. In the second self-sorting step, we obtained a halogenated [2×2] sub-system with bromo- and chloro-substituted imines from the imine library. Third and final step was a slow distillation of the residual imines from the column, leading to the amplification of the least volatile imine in 61% yield. Ultimately, this [10×10] imine library is simplified into two major products and one sub-system after iterative self-sorting.

Chapter 4 will describe the synthesis and characterization of a porous material based on an extensively fluorinated aromatic tristetrazole. This molecule crystallizes in a porous structure which is held together through [N−H···H] hydrogen bonds and electrostatic interactions between C–F units in these molecules. This porous material is compositionally stable up to 270 °C and shows selective adsorption of CO_2 over N_2 (15:1 in mmol g^{-1}) at 195 K and 760 mmHg.

CONTENTS

LIST OF SCHEMES

LIST OF FIGURES AND TABLES

ABBREVIATIONS

4TMSEBP	3,3'-4,4'-*tetrakis*(trimethylsilylethyl)biphenyl
BDBA	1,4-benzenediboronic acids
BET	Brunauer–Emmett–Teller
CFC	chlorofluorocarbon
CI	chemical ionization
COF	covalent organic framework
DCC	dynamic combinatorial chemistry
DCL	dynamic combinatorial library
DMF	*N*,*N*'-dimethylformamide
DMSO-d_6	deuterated dimethylsulfoxide
EI	electron ionization
EtOAc	ethyl acetate
EtOH	ethyl alcohol
ESI	electronspray ionization
FID	flame ionization detector
GC	gas chromatography
H_3BTB	4,4',4"-benzene-1,3,5-tribenzoic acid
HHTP	2,3,6,7,10,11-hexahydroxytriphenylene
HOF	hydrogen-bonded organic framework
HPLC	high performance liquid chromatography
I.D.	inner diameter
IAST	ideal adsorbed solution theory

Me	methyl
MeCN	acetonitrile
MOF	metal organic framework
NaO*t*-Bu	sodium *tert*-butoxide
nCOF	noncovalent organic framework
NMR	nuclear magnetic resonance
Ph	phenyl
PXRD	power X-ray diffraction
RD	reactive distillation
RT	room temperature
TGA	thermogravimetric analysis
THF	tetrahydrofuran
$Ti(OBu)_4$	titanium butoxide
TPBTC	N^1,N^3,N^5-tris(pyridin-4-yl)benzene-1,3,5-tricarboxamide
TTBI	triptycene trisbenzimidazolone

1 Chapter One: Self-sorting via Dynamic Combinatorial Chemistry

1.1 Definition of Self-sorting

In our daily lives, we are often sorting things into certain categories. After laundry, we fold and collect the clothes sorting them into categories such as long/short sleeve t-shirt, pants, and so on. Nature also displays similar phenomena, which simplify lower-order systems to the higher-order ones. For example, the compartmentalization of a biological cell, which results in the formation of different organelles, simplifies a multicomponent system to several major components. Dynamic combinatorial chemistry (DCC) provides insightful studies of interconversion among molecules from mixtures using reversible bond formation.[1] In 2003, Wu and Isaacs defined *the high-fidelity recognition of self from nonself* as "self-sorting."[2] Self-sorting is classified into *thermodynamic self-sorting* and *kinetic self-sorting*. In thermodynamic self-sorting processes, molecules sort and reach the thermodynamic equilibrium; all other self-sorting processes are defined as the kinetic self-sorting. For more-detailed categories, molecules that intend to bind with the same species are classified as *narcissistic self-sorting* (Scheme 1.1, pathway B).[3] Molecules aggregating preferentially with other species are defined as *social self-sorting* (Scheme 1.1, pathways A, C, and D).[4] In 2008, Schalley first introduced the concepts of *integrative* and *non-integrative self-sorting*:[5,6] the former was defined as the formation of a single complex via more than two different subunits which bound in two or more recognition events under positional control (Scheme 1.1, pathway A). The latter was defined as the sorting processes that led to a smaller than the maximum possible set of discrete sub-systems from the components in the

multicomponent system (Scheme 1.1, pathways B−D). In our reviews,[7,8] we provided a distinction between self-sorting and self-assembly. Self-assembly resulted in a single major component from a multicomponent system (with some leftover disordered units); self-sorting usually led to several high-order sub-systems from a low-order multicomponent system. Saha and Schmittel also provided the similar distinction by defining *completive* and *incomplete self-sorting*;[9,10] the former was defined as the use of all components to form one or more assemblies (Scheme 1.1, pathways A−C). The latter resulted in some unused components after sorting (Scheme 1.1, pathway D).

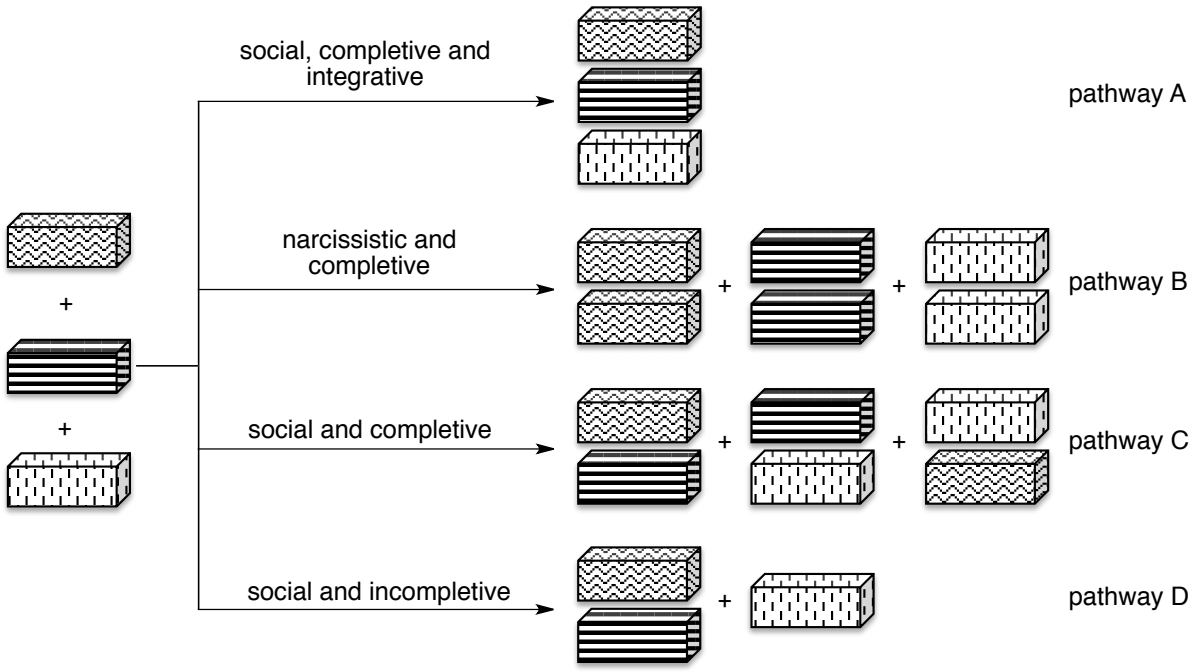

Scheme 1.1 Diagram of different self-sorting processes described in this thesis.

1.2 Thermodynamically Controlled Self-sorting

1.2.1 Thermodynamically Controlled Self-sorting in Purely Organic Systems

Sanders and coworkers were at the vanguard of thermodynamically controlled self-sorting in the 1990s.[11,12] With the equimolar amounts of **1** and **2**, the transesterification

displayed a prominent generation of trimer of **1** (**3**) and dimer of **2** (**4**) as the major products with trace amount of heteromers.

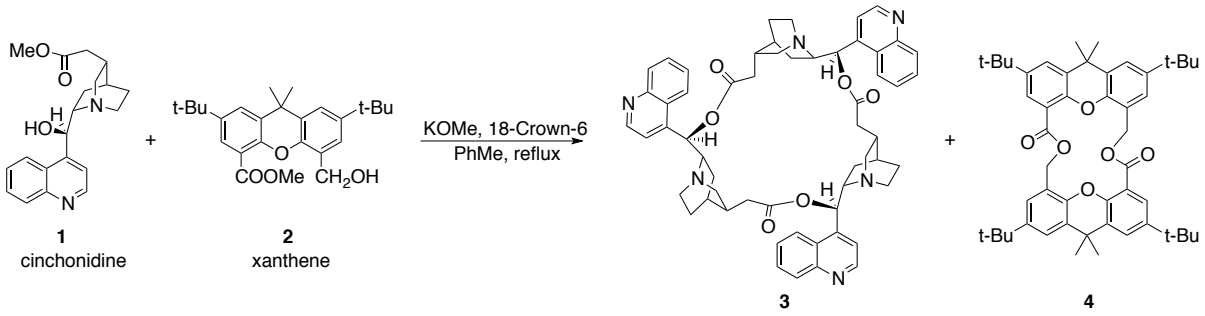

Scheme 1.2 Thermodynamic controlled self-sorting of transesterification.

The control experiment has been carried out by preparing the linear conjugate of **1** and **2**, followed by subjecting this conjugate to the transesterification conditions; this control experiment led to the same trimer **3** and dimer **4** after the system reached the equilibrium.

To unravel further applications of thermodynamic self-sorting, Sanders and Otto introduced reversible disulfide bond formation to manifest the dynamic macrocyclic disulfides in water under thermodynamic control.[1] For instance, in Scheme 1.3, they constructed a disulfide dynamic combinatorial library (DCL) with the equimolar amounts of dithiols (10 mM at pH 7.5 and under ambient temperature) **5**, **6**, **7**, and **8**, followed by the slow oxidation with oxygen and the addition of small amount of base for 24 h.[13] This reversible disulfide exchange led to two major macrocycles: **8**·**6** and **8**·**5**·**5**. They successfully introduced a new dynamic combinatorial library showing self-sorting properties under mild condition (disulfide exchange can take place under neutral or slightly basic conditions).

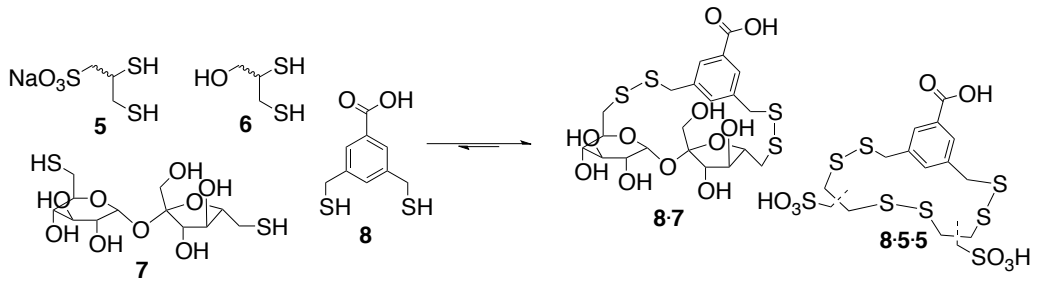

Scheme 1.3 Self-sorting process in a disulfide-based DCL.

Otto et al. applied two different guests to selectively amplify the macrocyclic disulfide—the host—from the starting DCL.[14] In Scheme 1.4, for instance, the starting DCL was fabricated by mixing equimolar amounts of dithiols, **8**, **9**, and **10** in water at pH 8 to 9 in an open vial. Upon electronspray (ESI-MS) ionization analysis, there were 45 macrocyclic disulfides with unique masses. With further separation and analysis of HPLC, there were two major thermodynamic products identified: **9**·**8**·**10** and **8**·**10**. Interestingly, with **11** as the template, this disulfide mixture can sort to **9**·**9**·**10** as the major product; with **12**, **9**·**9**·**9** became the major macrocyclic disulfide.

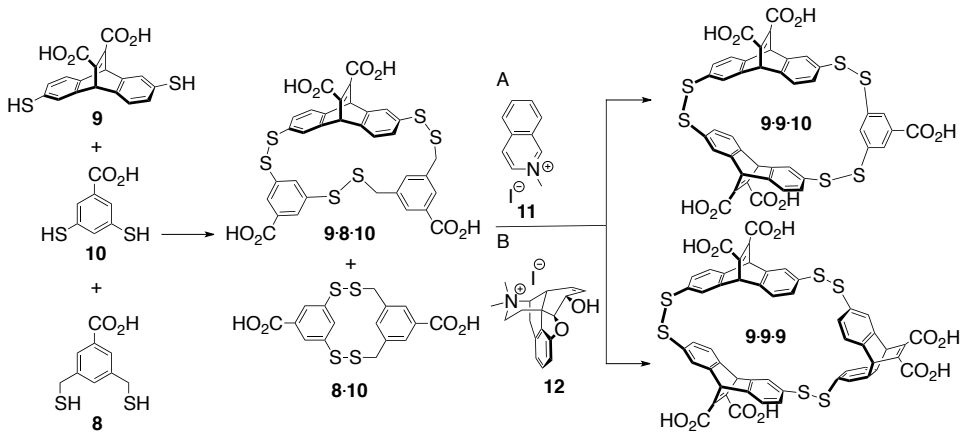

Scheme 1.4 Host-guest conducted disulfide exchange led to two major macrocycles with two different guests.

Pei and coworkers reported an imino bond-based thermodynamically controlled self-sorting by mixing two cyclic dialdehydes (**13** and **14**) with two amines (**15** and **16**)

(Scheme 1.5).[15] In the initial stage, there were some mismatched complexes formed. After the system reached the equilibrium, the dominant complexes were size-matched species **17** and **18**.

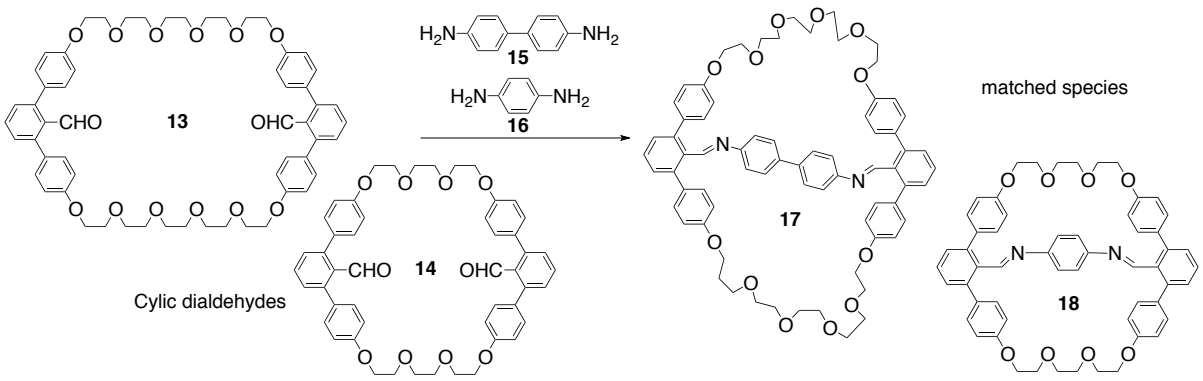

Scheme 1.5 Self-sorting of cyclic dialdehydes and linear aromatic amines formed two size-matched complexes.

Hafezi and Lehn prepared a [2×2] imine DCL by mixing the equimolar amounts of one hydrophobic aldehyde **19** and one hydrophobic amine **22** with one hydrophilic aldehyde **20** and one hydrophilic amine **21** (Scheme 1.6).[16] In the mixed solvent ($MeCN/H_2O$, v/v, 3:2), four possible imines distributed as **23**: 12%, **24**: 35%, **25**: 37%, and **26**: 16%. If NaCl was added to the reaction mixture, it sorted to only two imines due to the phase separation: the one composed of two hydrophobic components in MeCN phase (**24**: 50%) and the other composed of two hydrophilic constituents in the aqueous phase (**25**: 43%).[16] This self-sorting process is reversible: with the phase reunification, the mixture returned to the original distribution.

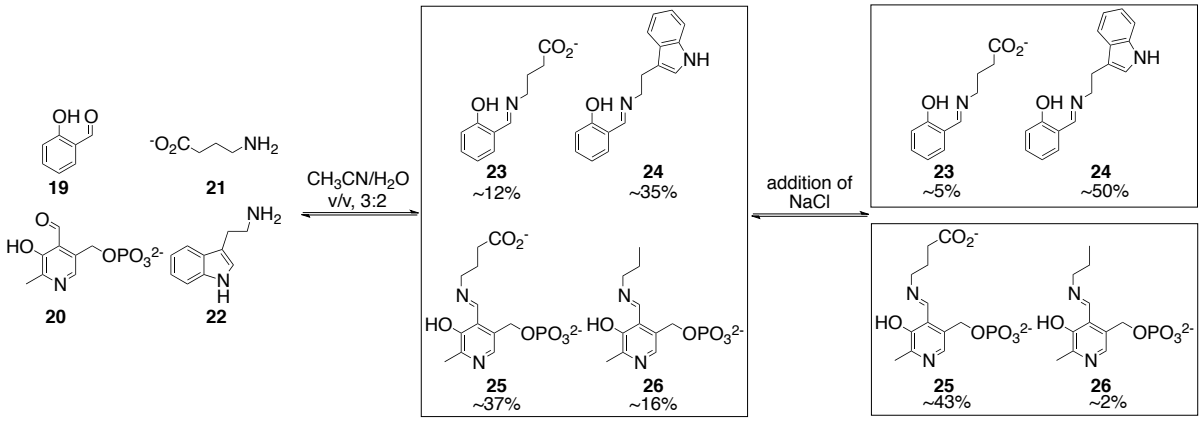

Scheme 1.6 The self-sorting process of a [2×2] imine DCL via the phase separation led to one major imine **23** in aqueous phase and the other major species **25** in organic phase.

Lehn et al. also showed that in the mixed solvent of MeCN/H_2O (v/v, 3:2), the photoisomerization of a pyridyl hydrazone (from *E* to *Z*) released calcium from the *E* isomer and induced the phase separation in the self-sorting system.[17] For the phase reunification and the back-isomerization (*Z* to *E*), sequential addition of hydrochloric acid, then triethylamine, was used. They combined their previous study of imine redistribution with reversible phase separation to this photo-induced phase separation study. They demonstrated that the imine constituents underwent thermodynamically controlled self-sorting process to yield an aqueous phase with hydrophilic imines and an organic phase with hydrophobic imines as the major components under the photo-induced phase separation process. Consequently, the reunification of mixed solvent by treatment with acid, then base, caused the redistribution of imines from the two-phase state to the single-phase state.

Severin et al. reported integrative self-sorting of DCLs among 4-formylphenylboronic acid **27**, 1,3,5-trisaminomethyl-2,4,6-triethylbenzene **28**, and pentaerythritol **29** via imine and boronic ester formation (Scheme 1.7).[18] Regardless of

the competition between aldehydes and boronic acids for the pentaerythritol, the only self-sorted structure **30** was obtained in 94% yield after ball-milling. Two dimensional macrocyclic boronic esters,[19] borasiloxane-,[20] borophosphate-based[21] macrocycles and cages were also reported.

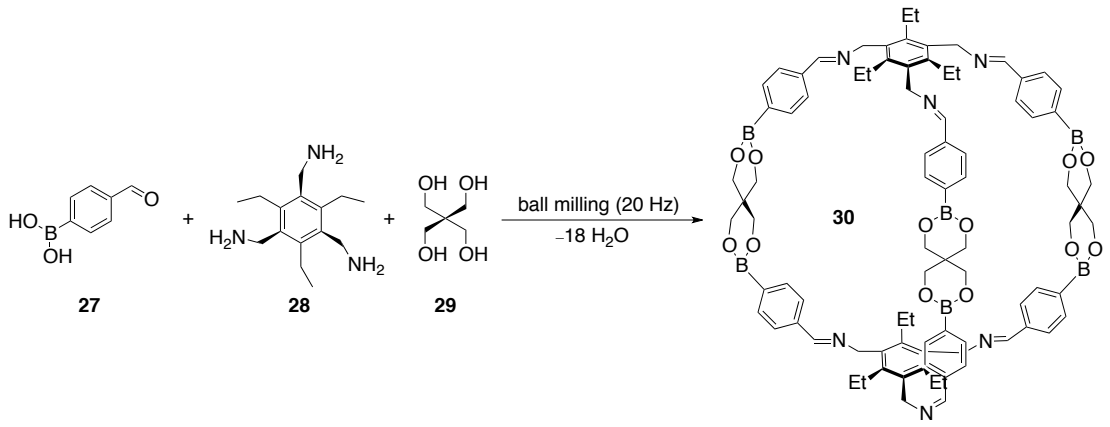

Scheme 1.7 Integrative self-sorting of 4-formylphenylboronic acid **27**, triamine **28**, and pentaerythritol **29**.

Lirag and Miljanić demonstrated that self-sorting in DCLs can be achieved via five reversible reactions,[22] all of which were catalyzed by Brønsted acids: (i) imino bond formation from aldehydes and anilines, (ii) acetalization of aldehydes with alcohols, (iii) boronic ester formation from boronic acids and alcohols, (iv) esterification of carboxylic acids and alcohols, (v) intramolecular dehydration of alcohols forming alkenes. In general, all these reactions should proceed and afford up to 16 possible compounds from 7 starting materials—aldehyde **31**, boronic acid **32**, aniline **33**, diol **34**, primary alcohol **35**, tertiary alcohol **36**, and carboxylic acid **37** (Scheme 1.8). However, the system sorted into only four discrete compounds—imine **38 (**93%), boronic ester **39** (99%), ester **40** (99%), and alkene **41** (98%)—obtained after the reaction reached equilibrium.

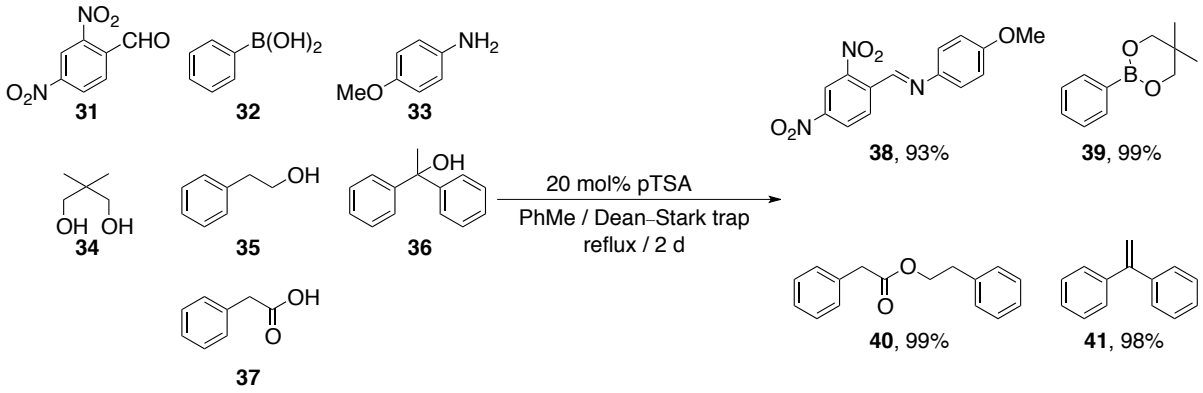

Scheme 1.8 Five potential acid-catalyzed reactions led to only four discrete compounds from one-pot synthesis.

1.2.2 Thermodynamically Controlled Self-sorting in Metal-Ligand Systems

In addition to the purely organic systems mentioned above, Lehn and coworkers reported a series of metal-oligobipyridine ligand constructed double and triple metal helicate complexes.[23,24,25] For example, a mixture of ligands **42**, **43**, and Cu(I) spontaneously assembled into two discrete homomeric double helices—[**42**$_2$Cu$_2$]$^{2+}$ and [**43**$_2$Cu$_2$]$^{2+}$—coordinating with Cu(I) in a tetrahedral geometry (Scheme 1.9).[23]

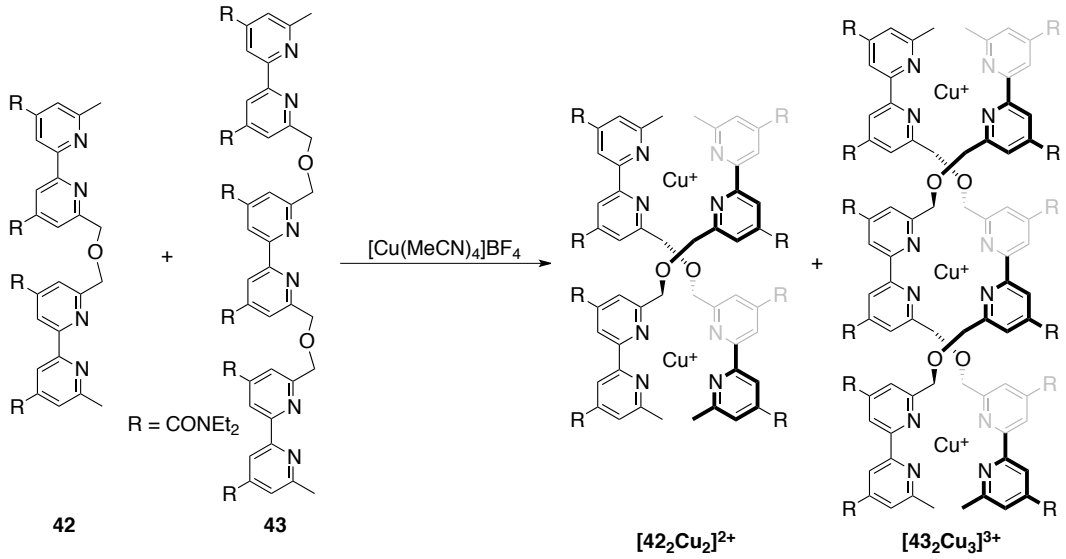

Scheme 1.9 Complexation-driven self-sorting of ligands **42** and **43** in the presence of Cu(I).

This work was extended to an oligobipyridine ligand with five bipyridines, which also engaged in the high-fidelity discrete double helices formation from the mixture of two, three, four, and five bipyridine oligomeric ligands. On the other hand, Lehn et al. also demonstrated that Ni(II) preferably fabricated triple helices with **44** and formed the octahedral geometry at each nickel center.[25] Mixture with 3 equivalents of **44**, 2 equivalents of **45**, 3 equivalents of Ni(II), and 3 equivalents of Cu(I) selectively assembled into one double helix $[\mathbf{45}_2Cu_3]^{3+}$ and one triple helix $[\mathbf{44}_3Ni_3]^{6+}$ (Scheme 1.10).[24] This result revealed that this thermodynamically controlled self-sorting was driven by the steric preference of Ni(II) toward the more exposed bipyridine ligand **44** in the formation of the more crowded octahedral metal complex.

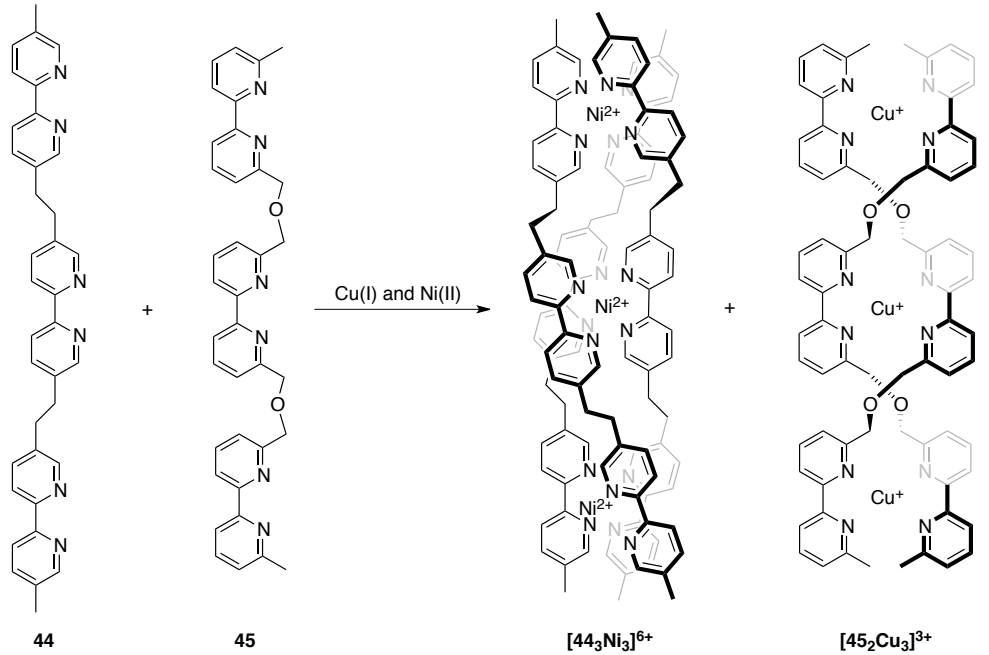

Scheme 1.10 Self-sorting of **44**, **45**, Cu(I), and Ni(II) led to only one triple helicate nickel complex and one double helicate copper complex.

Nitschke and coworkers reported self-sorting protocols based on two reversible reactions: one is imino bond formation providing nitrogen as the coordination site; the

other is metal-ligand interaction. Typically, imines are hydrolyzed quickly in aqueous solvent, but the metal-imine coordination can stabilize the imines. In another words, imines can prevent transition metal such as Cu(I) from oxidation. Nitschke et al. also developed the formation of dynamic Cu(I) helicates, which have a similar structure to Lehn's helicates (Scheme 1.11).[26] The difference is that there is no ligand synthesis: Cu(I) constructively helped the imine formation from mixtures of aldehydes and anilines, by binding to the nitrogen of the imino bond. They also constructed a dynamic imine library (by adding **51**, **52**, and **53**), which was creation by metal complexation of Cu(I) in the aqueous solution to form just two metal-imine complexes (Scheme 1.12).[27]

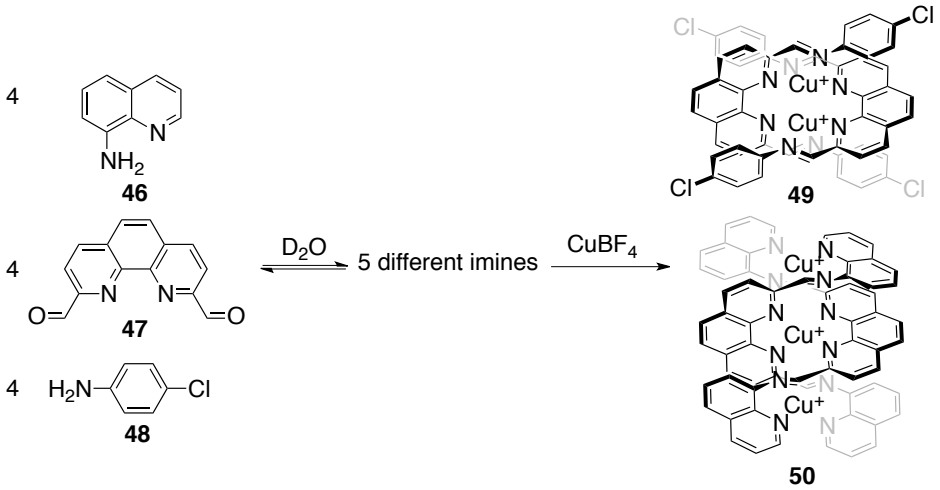

Scheme 1.11 Double helicate self-sorting via Cu(I)−imine interaction.

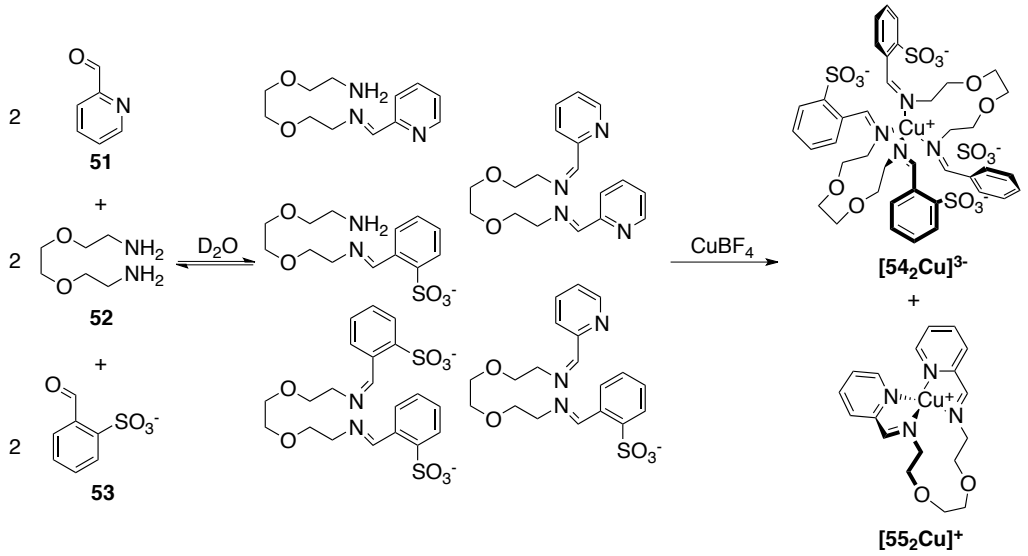

Scheme 1.12 Self-sorting of a mixture of aldehydes (**51** and **53**) and diamine **52** led to two Cu-imine complexes via the stabilization from metal-ligand coordination.

Moreover, Nitschke et al. carried out self-sorting of a more complicated DCL, by adding Fe(II) and Cu(I) to display the "spin-selection" phenomenon (Scheme 1.13).[28] While three equivalents of each aldehyde precursor (**51** and **56**), one equivalent of triamine **57**, and three equivalents of ethanolamine **58** were added into water, a dynamic imine library formed and reached equilibrium with eleven imines in the system. After adding two metal sources—Fe(II) and Cu(I), the self-sorting proceeded spontaneously to only two metal complexes: Fe(**59**)$^{2+}$ and [**60**$_2$Cu]$^+$. The slight steric hindrance between **51** and **56**, a difference of methyl group, led to a favored, diamagnetic, and low-spin state iron complex, Fe(**59**)$^{2+}$, with stronger Fe−N bonds. The non-methylated ligand **60** bound to Cu(I) to form the other complex, [**60**$_2$Cu]$^+$.

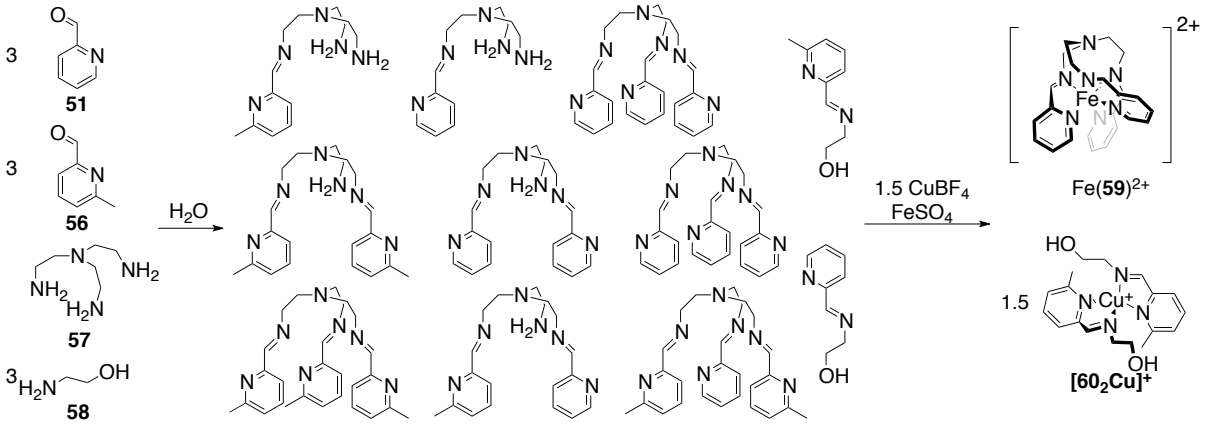

Scheme 1.13 Self-sorting of a mixture with four organic precursors led to two metal-imine complexes: tetrahedral geometric Cu(I) complex **[60**$_2$Cu]$^+$ and octahedral geometric Fe(II) complex Fe(**59**)$^{2+}$.

Nitschke et al. have extended the self-sorting to one-pot syntheses of cage compounds.[29] For example, in Scheme 1.14, a mixture of triamines **61** and **62**, and diamine **16**, which was exposed to excess 2-formylpyridine and Zn(II) at 70 °C, produced only three Zn(II)-imine tetrahedral cages—[**63**$_4$Zn$_4$]$^{8+}$, [**64**$_4$Zn$_4$]$^{8+}$, and [**65**$_4$Zn$_4$]$^{8+}$—based on narcissistic self-sorting (Scheme 1.14). The sequential cage formation was based on the binding geometry: C_2 symmetric diamine **16** could not form the heteroleptic cage with C_3 symmetric triamines **61** or **62**; the distinction between **61** and **62** could lead to the homoleptic structures, face-capped tetrahedral as the result of their Fe(II) analogues.[30] These cage compounds were introduced to bind anions: [**64**$_4$Zn$_4$]$^{8+}$ bound small neutral molecules, such as *t*-BuOH or cyclohexane; [**63**$_4$Zn$_4$]$^{8+}$ and [**65**$_6$Zn$_4$]$^{8+}$ bound anions, such as ClO_4^-, I^-, NO_3^-, and BF_4^-. While the equimolar amounts of these three cages were exposed to 40 equivalents of PF_6^-, 2 equivalents of NO_3^-, and 4 equivalents of cyclohexane, only [**65**$_6$Zn$_4$]$^{8+}$·PF_6^-, [**64**$_4$Zn$_4$]$^{8+}$·cyclohexane, and [**63**$_4$Zn$_4$]$^{8+}$·NO_3^- were observed.

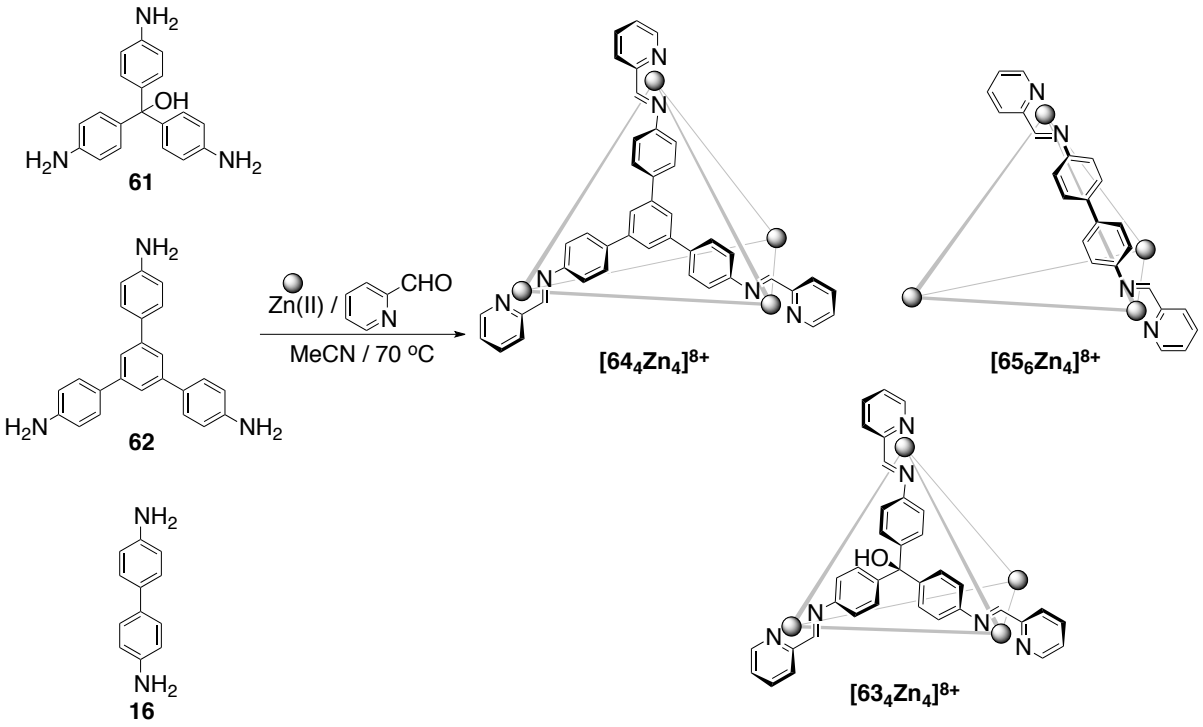

Scheme 1.14 Narcissistic self-sorting of three tridentate imines binding Zn(II) is driven by ligand's symmetry and size. Selective capture of neutral small molecules and anions has been investigated.

Furthermore, they can selectively and sequentially release guests by treatment with 4-methoxyaniline, which can form the more stable imine with 2-formylpyridine and cause the collapse of these three cages in the following order: $[\mathbf{65}_6Zn_4]^{8+}\cdot PF_6^-$, $[\mathbf{64}_4Zn_4]^{8+}\cdot$cyclohexane, and $[\mathbf{63}_4Zn_4]^{8+}\cdot NO_3^-$. These encapsulation/release experiments displayed the potential of chemical syntheses in the one-pot system with programmed subcomponents. This concept was successfully demonstrated as "self-organizing chemical assembly line" with the combination of hetero-Diels-Alder cycloaddition, transformation of endoperoxide into fumaraldehydic acid, followed by 1,4-addition of nitromethane in this one-pot synthetic system.[31]

Stang and coworkers have demonstrated that the self-sorting of pyridine-based ligand donors and platinum (II) acceptors leads to 2D or 3D metallosupramolecules.[32]

The high fidelity is based on the symmetry, polarity, angularity, and size of the ligands, as driving forces between organic donors and Pt(II)-based acceptors. For instance, in Scheme 1.15, they showed directional self-sorting among the ambidenate ligand **64** and organoplatinum acceptors (**67** and **69**) was oriented by the best charge separation to keep only one direction with Pt(II) acceptors (**67** and **69**) and to form metallomacrocycles **68** and **70**.[33]

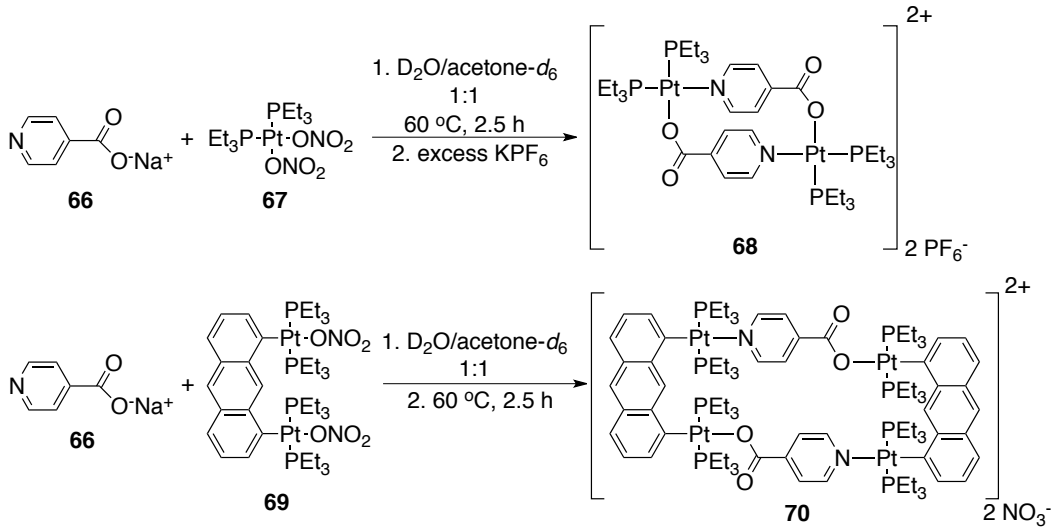

Scheme 1.15 Charge separation-oriented self-sorting process of platinum acceptors and ambidenate ligands.

Their system was extended to coordination-driven self-sorting of 2D polygons upon the exchange of bipyridyl ligand and organoplatinums.[34] The high fidelity of this self-sorting system resulted from the rigid platinum acceptors whose geometries induced the formation of the more thermodynamically stable complexes. In the example of Scheme 1.16, heating **69**, **70**, and **71** in 2:3:5 molar ration for 123 h at 55−60 °C resulted in only two major complexes: rectangle **73** and triangle **74**. NMR spectra showed the iterative self-sorting in this system: after the first 5 hours, there were still some minor signals in the aromatic proton region; ^{1}H NMR spectra slowly simplified to only two

major product signals in the system after heating for 118 more hours. Similar behaviors also showed up in the mixture of **67**, **69**, and **71** (molar ratio: 4:2:6), which was heated to afford square **72** and rectangle **73** as the major products; the mixture of **67**, **70**, and **71** (molar ratio, 4:3:7) also led to square **72** and triangle **73** as the sole major complexes. In Scheme 1.16, the fidelity of self-sorting among three organoplatinum acceptors (**67**, **69**, **70**) and bipyridyl donors **71** was formed slowly from some unknown subunits in the beginning of the sorting process to three major 2D polygons (**72**, **73**, and **74**) after heating for 121−135 h to reach the final thermodynamic equilibrium.

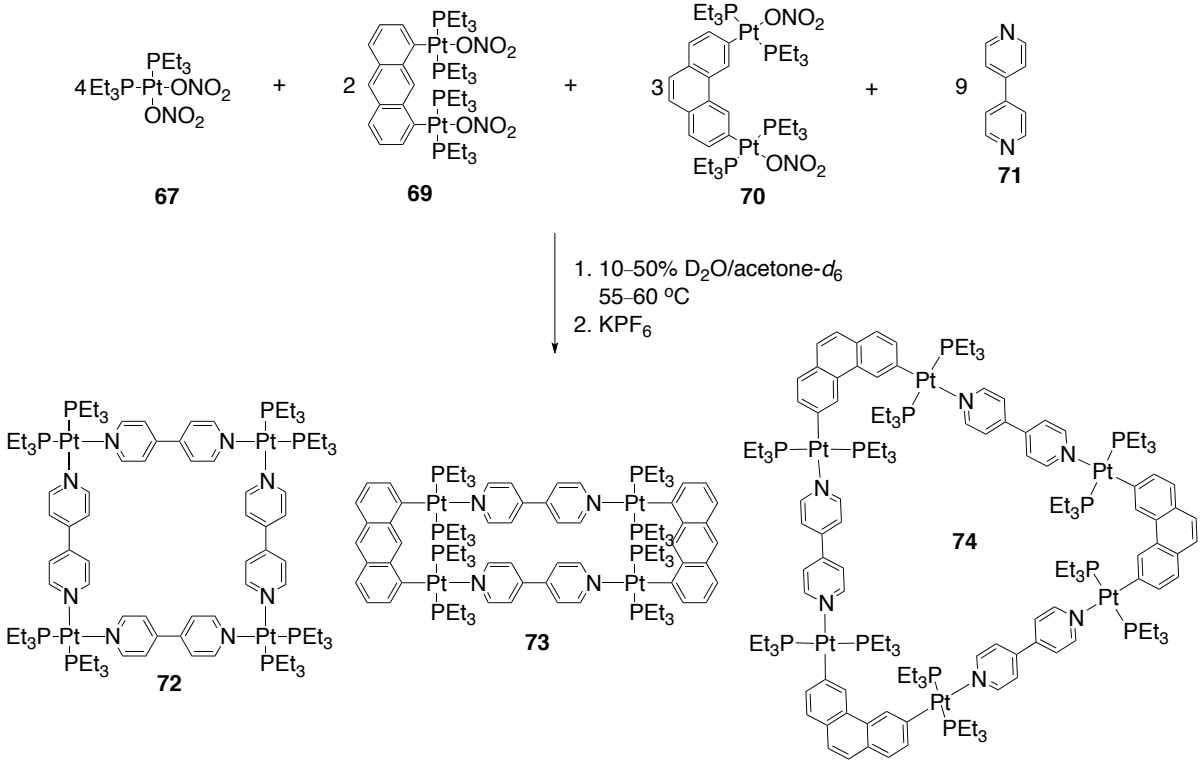

Scheme 1.16 Self-sorting of organoplantinum acceptors **67**, **69,** and **70** with 4,4'-bipyridine **71** selectively fabricated discrete polygons.

All the examples mentioned above belong to homomeric self-sorting with highly symmetric major components. Schmittel and coworkers focused on programmed complexes, which were able to construct low-symmetry complexes with heteromeric

units. They reported an eight-component self-sorting system that resulted in a trisheterometallic scalene triangle.[35] Schmittel et al. manipulated the heteromeric metal-ligand interactions by modifying the structures of ligands electronically and sterically. In the example of Scheme 1.17,[35] for an equimolar mixture of **75**−**80**, Zn(II), and Cu(I), only three metallosupramolecules were obtained: $[Zn(\mathbf{75})(\mathbf{76})]^{2+}$, $[Cu(\mathbf{78})(\mathbf{79})]^{+}$, and **77**·**80**. This resulted from the thermodynamic stability of this starting mixture: **75** and **76** held Zn(II) to form a thermodynamically favored pentacoordinate complex with additional [π···π] stacking; **78**, **79**, and Cu(I) formed a complex $[Cu(\mathbf{78})(\mathbf{79})]^{+}$ from this mixture; **80** prohibited the access from all other ligands except 4-iodopyridine **77**. Based on this result, they extended their research to a three-lateral self-sorting by combining these eight components to form a scalene triangle.[35]

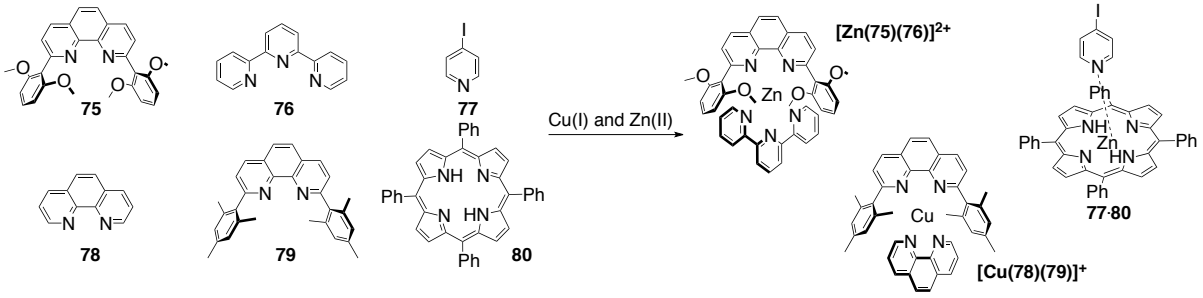

Scheme 1.17 The high fidelity self-sorting of an eight-component mixture led to just three discrete metallomacrocyles.

In Scheme 1.18, Schmittel and coworkers covalently linked **77**/**79**, **76**/**78**, and **75**/**80** and deployed them to Zn(II) and Cu(I). Consequently, the scalene triangle formed, which featured 1.84, 1.60, and 1.44 nm as the lengths of three laterals, from the calculated structure of the complex. In 2013, they utilized the similar strategy to conduct the self-assembly of a low symmetry squalene quadrilateral.[36] Upon mixing all components (**83**, **84**−**87**, Cu(I), and Zn(II)) in 5:1:1:1:1:2:1 ratio, a squalene quadrilateral

was composed of Zn(II) on two corners, Zn-porphyrin on one, and Cu(I) on the final corner. ESI-MS, ^{1}H NMR, ^{1}H−^{1}H COSY NMR, DOSY NMR spectra, and computational analysis proved that this squalene quadrilateral was obtained and the structural assignment was given (Scheme 1.19): Cu−**85**−$Zn_{phorphyrin}$, 1.83 nm; $Zn_{phorphyrin}$−**83**−Zn, 1.50 nm; Zn−**87**−Zn, 1.98 nm; Zn−**86**−Cu, 1.60 nm. This result displayed that a completive and integrative self-sorting with orthogonal metal-ligand interaction under thermodynamic preference. Similar strategies were also introduced in the syntheses of multilateral metallosupramolecules.[37,38]

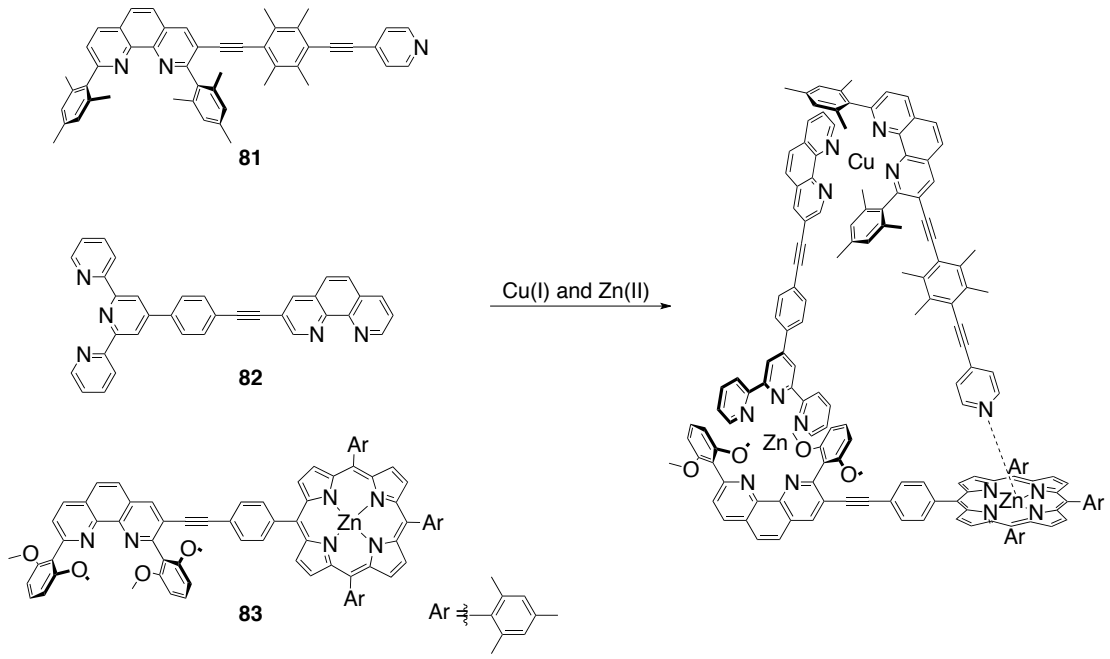

Scheme 1.18 Self-sorting of an equimolar mixture of **81**, **82**, and **83** with Cu(I) and Zn(II) forms a scalene supramolecular triangle.

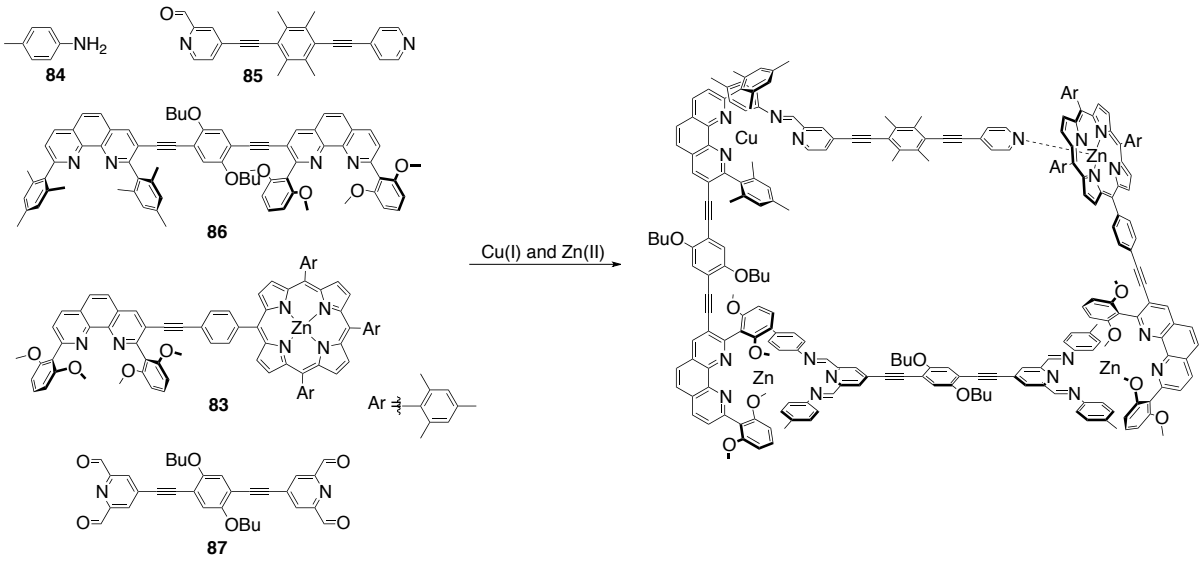

Scheme 1.19 Self-sorting of a seven-component mixture forms a squalene quadrilateral as the sole complex.

1.3 Kinetically Controlled Self-sorting

Kinetically controlled self-sorting processes are less common than thermodynamic self-sorting processes, but they are potentially more relevant to biological systems that operate away from equilibrium. Since 2010, Miljanić's group has demonstrated and developed several kinetically controlled self-sorting DCLs, which work efficiently via chemical or physical external stimuli and successfully simplify n^2 components to only n major components even with decent separation and purity.[39] Kinetic self-sorting systems are commonly based on the Curtin-Hammett principle,[40] which says that the product's distribution is only related to their transition state energy, but not related to the initial distribution of starting materials. Products with lower transition state energy will become more favorable in the reaction. In the following sections chemical stimulus-driven and physical stimulus-driven self-sorting will be introduced.

In a biological cell, several metabolic reactions are happening concurrently without interference. These components can recognize each other selectively and sort into specific products from the complicated ("messy") mixture under either chemical (enzyme catalyzed reaction) or physical (ion channel) control. Mimicking this exquisite concept would allow chemoselectivity in artificial mixtures of precursors, and could not only become a model for biology, but also potentially useful method in the chemical industry, where multiple pure products could be produced in the same reactor.

In 2010, our group introduced the oxidative kinetic self-sorting of imine-based libraries with iodine as the chemical stimulus.[39a] For example, in Scheme 1.20, upon mild oxidation, a nine-imine library composed of three aldehydes and three anilines was simplified as the following order. First, the most electron-rich imine **90** oxidized to benzimidazole **97** and eliminated imines **88**, **89**, **93**, and **96** with the removal of the most electron rich compartments from the library to generate a smaller library—four imines dynamic library—for the further self-sorting. Second, at higher temperature, and with slow injection rate of I_2, imine **92** was oxidized to benzoxazole **98** and the residual imine was the non-reactive **94**. This [3×3] imine library was simplified to three major products while these components underwent imine exchange to replenish the more electron rich species, which could be oxidized the fastest until the corresponding substances were completely depleted.

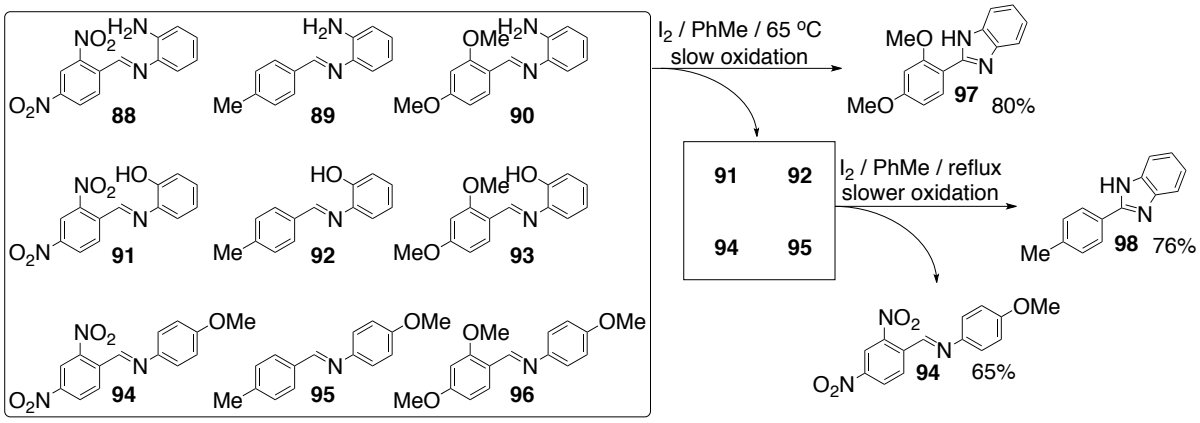

Scheme 1.20 Self-sorting of a dynamic [3×3] imine library via slow addition of iodine from lower temperature to higher temperature.

In this protocol, it is necessary that the oxidation rate is significantly lower than the imine exchange rate to let imines have enough time to re-equilibrate continuously during the slow oxidation. Iodine is a weak enough oxidant for the achievement of this self-sorting. Stronger oxidants such as 2,3-dichloro-5,6-dicyano-1,4-benzoquinone (DDQ) and chloranil oxidized these imines quickly and "froze" the imines composition by instantaneously oxidizing most of the imines in the library. The second factor is the addition rate of iodine. Using a syringe pump to slowly inject iodine solution with low concentration lowers the oxidation rate, but maintains the imine exchange rate. The slow addition preferrentially oxidizes the most electron rich imine. Thus, the direction of equilibrium could favor the replenishment of electron rich/electron rich aldehyde/aniline combination. However, the instantaneous addition of iodine resulted in a significantly lower selectivity because of the more stable and dominant electron poor/electron rich aldehyde/aniline combination in the system.

Kinetically controlled self-sorting can be considered as a dynamic resolution of a mixture. Ramström and coworkers demonstrated that the resolution of a DCL composed

of ten nitroaldol adducts (including enantiomers) which was formed by Henry reaction among five aldehydes and one 2-nitropropane: the kinetically controlled reaction between phenyl acetate and *Burkholderia cepacia* PS-C I lipase produced only two enantiomerically pure nitroacetates with 52% and 33% yields respectively.[41] The same group also demonstrated that lipase-mediated kinetic resolution of a double dynamic system with 24 Strecker adducts (constructed from a reaction of TMSCN with a [3×4] imine library), in which this enzyme selected the most reactive aldehyde and amine components in the acetylation reaction with high enantiomeric purity.[42]

Self-replication is a variant of self-sorting,[43] wherein units of a mixture sort into several systems and one of them is autocatalytic. Philp and coworkers reported some examples of self-replication in an imine-based DCL, in which one imine in the library catalyzed its own formation from the starting aldehydes and anilines.[44] For instance, in Scheme 1.21, Philp et al. started at imine **101** fabricated by aldehyde **100** and amine **99**, whose substituents have hydrogen bond donors and acceptors: aldehyde **100** has a carboxylic acid recognition site and amine **99** has an amidopyridine for the further intramolecular interaction. They demonstrated that not only imine **101** could accelerate its self-production by forming the ternary complex, **99**·**100**·**101**, but the reduced product, amine **102**, could also induce the formation of **101** with the similar ternary complex, **99**·**100**·**102**. However, in the autocatalytic cycle, imine **101** limited the maximum production because **101** remained in the equilibrium with **99** and **101**. In the cross-catalytic cycle, amine **102** didn't equilibrate with **99** and **101** and still produced the ternary complex for the further production of **101**. Thus, it is a better catalyst than **101**.

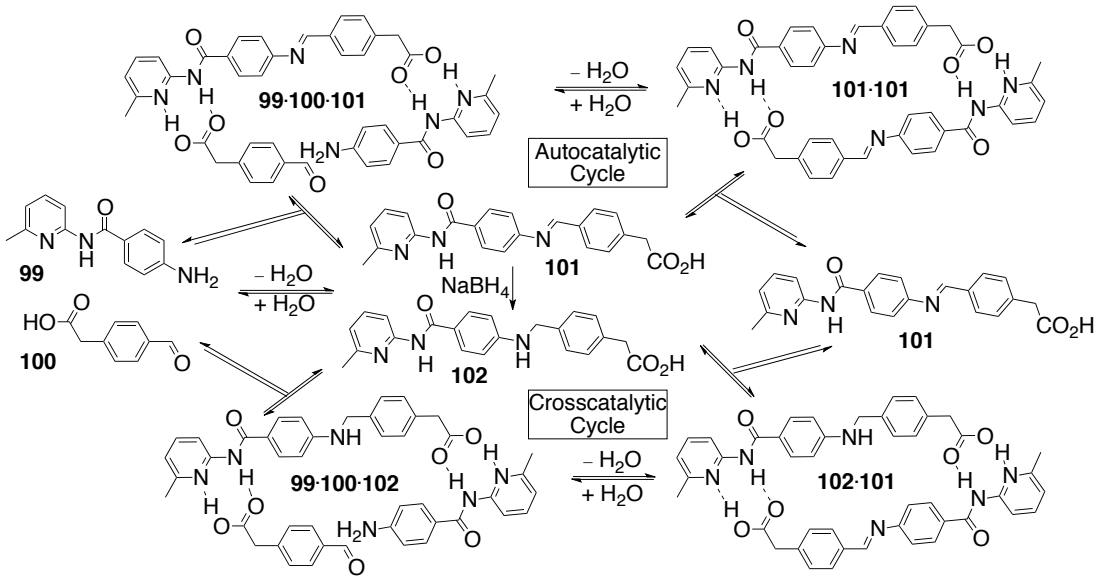

Scheme 1.21 Imine **101** catalyzed the self-replicating process by forming the ternary complex with **99** and **100**. The reduced species **102** also provided the ternary structure to accelerate the production of **101**.

Based on the induction from the ternary complex, Philp et al. introduced the 1,3-dipolar cycloadditon to obtain a product that not only catalyzed its own formation by forming the ternary complex, but also leaked out of the system with no more equilibration.[45,46] For instance, in Scheme 1.22, an equimolar amount of aldehydes **103** and **104**, 4-fluoroaniline **105**, and hydroxylamine **106** resulted in a mixture of two imines (**107** and **110**), and two nitrones (**108** and **109**).[45] Upon the exposure of this mixture to maleimide **111**, the irreversible cycloaddition should occur among nitrones (**108** and **109**) and it should present *cis* and *trans* isomers (*cis* / *trans*-**112** and *cis* / *trans*-**113**). However, only *trans*-**112** could form a ternary complex **108**·**111** *trans*-**112** which selectively conducted the cycloaddition of **108** and **111** to *trans*-**112**. After 16 h, *trans*-**112** contributed over 80% of the products in the system.

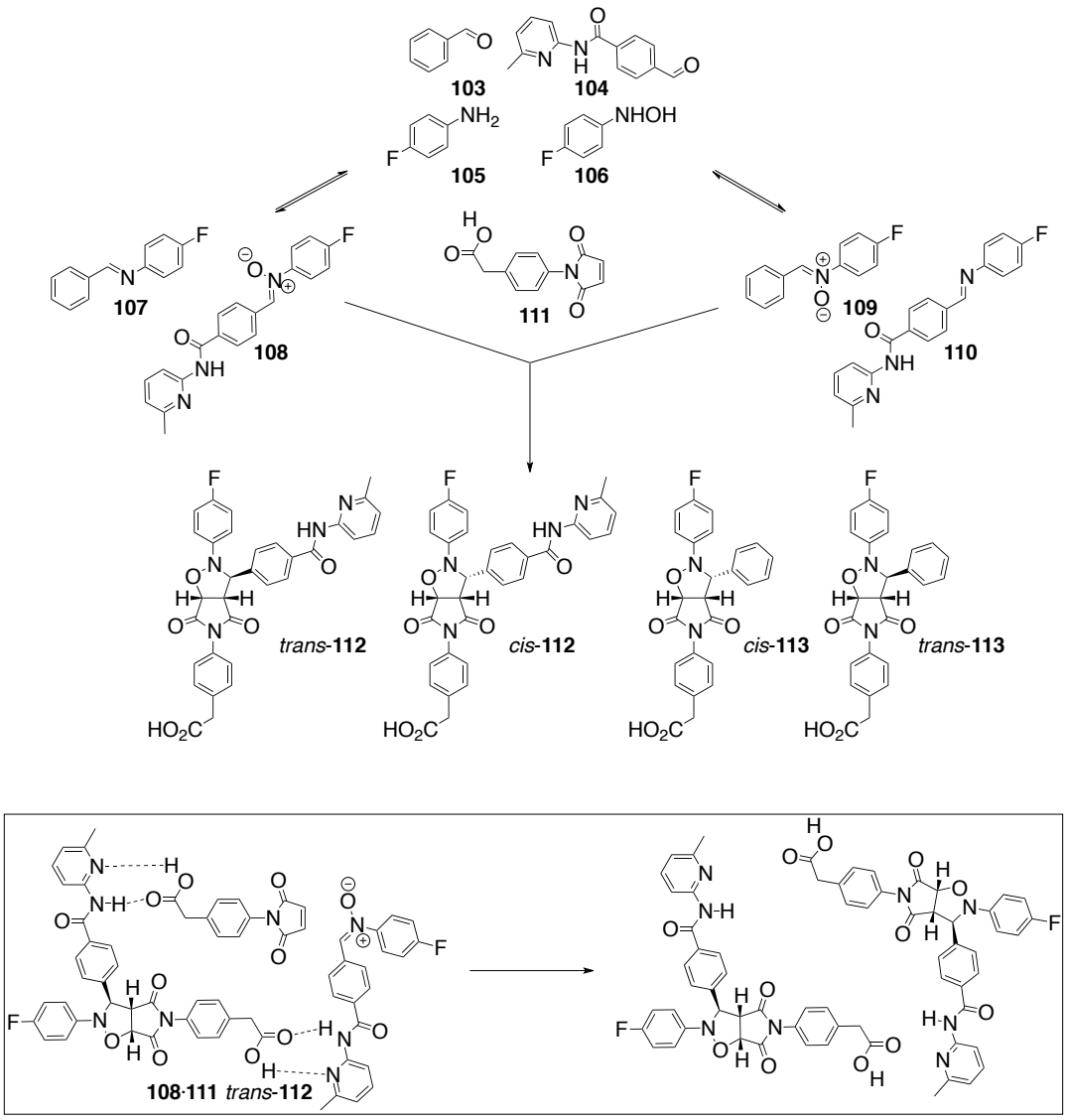

Scheme 1.22 Self-replication of the irreversibly produced cycloaddition product trans-**112** from a DCL. Complex [**108**·**111**·trans-**112**] catalyzed the iterative cycloaddition of precursor **108** with maleimide **111**.

The limitation of kinetically controlled self-sorting via chemical stimuli is that the irreversible reaction rate should be significantly lower than the equilibration rate of components in a DCL, in which this irreversible reaction removed the desired components from the library and enhanced the equilibration until all target components were exhausted. Besides this, physical stimuli are the alternatives to help the components

"leak" out of the library and emerge the self-sorting behavior. In the following section, we will present the systems we have demonstrated with ubiquitous physical stimuli.

Since 2011, we have demonstrated that several physical protocols, such as distillation,[39b,d,e] column chromatography,[39f] and precipitation,[39c] can be used to induce self-sorting behaviors in DCLs. The use of distillation was first introduced to imine-based libraries.[39b] For instance, in Scheme 1.23, in a [3×3] DCL, fabricated by nine imines **114**−**122**, the first reduced pressure distillation (0.10 mmHg) resulted in the most volatile imine **116** (90%), removing in turn imines **114**, **115**, **119**, and **122** from the library. The next distillation with higher temperature (150 °C) isolated imine **118** (94%) and eliminated **117** and **121** to refill **118** and left the least volatile imine **120** (99%) as the distillation residue. This protocol has been extended to a [5×5] imine library.

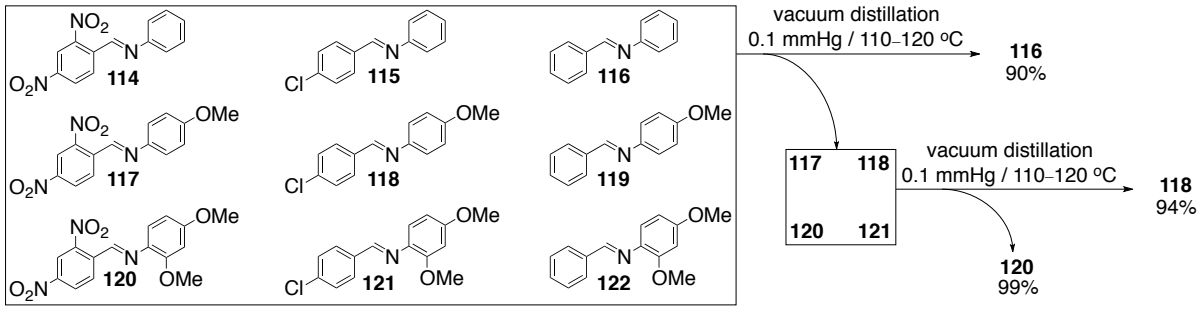

Scheme 1.23 Slow distillation of a [3×3] DCL at high temperature led to three imines with high purities.

As a ubiquitous physical technique, distillation exploits several features of kinetic self-sorting. First, it proceeded at high temperature without solvent, ensuring that imine exchange is much faster than in solution, and the absence of moisture in the solvent prevented the decomposition of imines. Second, distillation also separated these favored imines physically as pure products at different positions of the distillation apparatus. Third, as one of the most common techniques used in the chemical industry, it is likely

the closest method to industrial practice. With the success from distillative imine self-sorting and these factors we mentioned above, we moved our protocol to a more industrially relevant set of chemicals—esters. In the self-sorting of esters, some catalysts are needed, which are NaO*t*-Bu and $Ti(OBu)_4$, to enhance transesterification and afford high fidelity self-sorting.[39d] In Scheme 1.24, nine esters were catalyzed to swap their acyl and alkoxy moieties in the presence of NaO*t*-Bu under vacuum distillation at 50 °C. In the beginning, ester **123** was isolated in 77% yield as the most volatile ester, whose formation eliminated esters **124**, **125**, **126**, and **129** and left a four-ester library for the following step. Under the same condition with longer time, ester **127** was isolated as the distillate (64%) and the residue was ester **131** (80%).

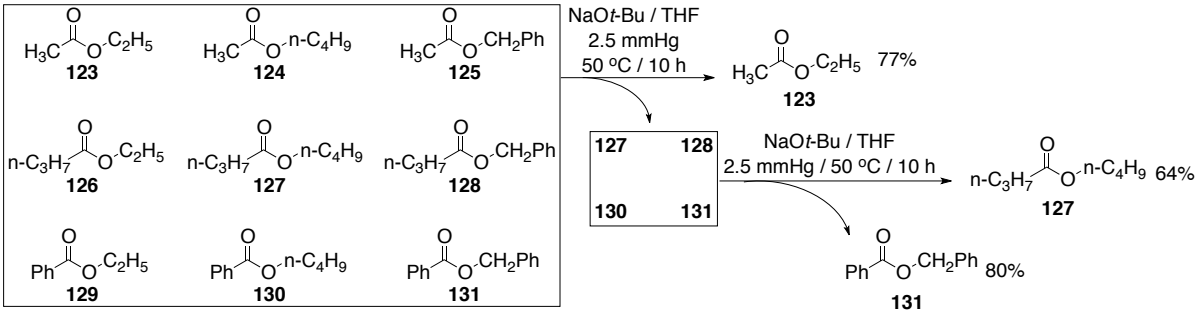

Scheme 1.24 Distillative self-sorting of esters via fast transesterification led to only three esters.

Precipitation is one of the commonly used strategies to purify a compound from a mixture. While the most insoluble compound precipitates, the re-equilibration of the mixture will rapidly "refill" this compound. If this process is repeated iteratively, several components could be isolated from the mixture in the sequential precipitation. Other than distillation and adsorption, which needs to be performed at higher temperature to enhance fast imine exchange rates, precipitation usually proceeded at lower temperature, thus subjecting it to slower equilibration.

We have investigated the precipitative self-sorting of dynamic imine libraries.[39c] Major imines could be collected and separated after the precipitation at each stage based on significant solubility differences. For example, in Scheme 1.25, after equimolar amounts of aldehydes **103**, **134**, and **31**, anilines **132**, **33**, and **133** were dissolved in EtOH, this mixture was subjected to slow addition of water (which reduced the solubility of the imines). Only three imines were obtained: **120**, **135**, and **116** in descending order of solubilities (**116**: 13.3 mmol/L, **135**: 0.2 mmol/L, **120**: <0.1 mmol/L). This selectivity was driven by the lowest solubility of **120**, followed by more soluble **135**, then the most soluble imine **116**. The precipitation of **120** and **135** left the only aldehyde **103** and aniline **132** in the solution, which constructed the most soluble imine **116** as the third major component.

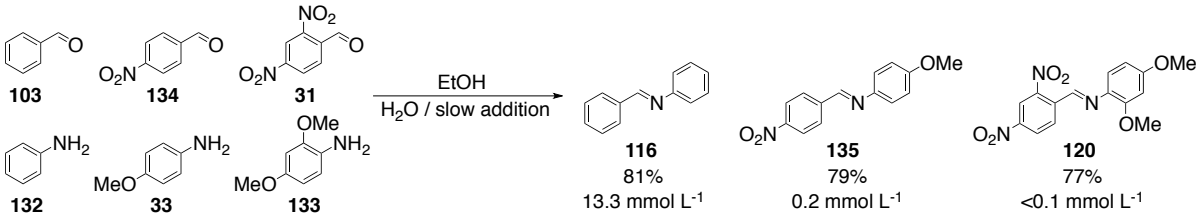

Scheme 1.25 Self-sorting of a [3×3] imine library driven by slowly adding H_2O into EtOH to decrease the solubility of imines led to only three discrete imines by removing the least soluble imine **120**, then **135**. The most soluble imine **116** stayed in the library.

1.4 Conclusion and Outlook

Self-sorting processes are based on the thermodynamically or kinetically preferred behaviors of mixtures and the direction of equilibrium can be manipulated with different strategies. Since the 1990s, comprehensive studies of these processes have created several new perspectives to approach this concept via the thermodynamically favored metal-ligand interaction, host-guest chemistry, reversible covalent bond formation (imino

bond, disulfide exchange, transesterification) and benefit the chemical education by introducing various reversible reactions and Le Châtelier's principle. Either physical or chemical stimulus can trigger self-sorting events and result in high fidelity simplification of a multicomponent system.

In the regime of thermodynamically controlled self-sorting, researchers have moved on from the symmetric system to the asymmetric one. Schmittel et al. pushed the margin of their work toward a highly asymmetric metallomacrocycle constructed from several binding units. Their integrative self-sorting is more similar to natural systems and inspires sophisticated applications. For much more complex DCLs, some starting materials may have the similar enthalpy of their thermodynamic products. This may result in lower fidelity of the sorted products. It will be exciting to see new systems, which can take the entropic challenges with much higher complexity.

Kinetically controlled self-sorting processes have revealed several irreversible stimuli which successfully help the desired component "leak" out of the reaction mixture through reaction pathway with a lower transition energy barrier. The maximum complexity of DCLs is currently up to a [5×5] imine library (25 imines available in the same mixture). In the second chapter, I am going to present one new physical stimulus—adsorption of imines on silica gel—that was used to obtain high fidelity self-sorting and carry out the separation via column chromatography. In the third chapter, I will show that three orthogonal stimuli—oxidation, adsorption, and distillation, can be applied to a [10×10] imine DCL for iterative self-sorting.

1.5 References

[1] (a) Reek, J. N. H.; Otto, S. *Dynamic Combinatorial Chemistry*; Wiley, 2010; (b) Cougnon, F. B. L.; Sanders, J. K. M. *Acc. Chem. Res.* **2012**, *45*, 2211−2221; (c) Otto, S. *Acc. Chem. Res.* **2012**, *45*, 2200−2210; (d) Li, J.; Nowak, P.; Otto, S. *J. Am. Chem. Soc.* **2013**, *135*, 9222−9239; (e) Corbett, P. T.; Leclaire, J.; Vial, L.; West, K. R.; Wietor, J.-L.; Sanders, J. K. M.; Otto, S. *Chem. Rev.* **2006**, *106*, 3652−3711.

[2] Wu, A.; Isaacs, L. *J. Am. Chem. Soc.* **2003**, *125*, 4831−4835.

[3] Kondo, T.; Oyama, K.-I.; Yoshida, K. *Angew. Chem. Int. Ed. Engl.* **2001**, *40*, 894−897.

[4] Shivanyuk, A.; Rebek, J. Jr. *J. Am. Chem. Soc.* **2002**, *124*, 12074−12075.

[5] Jiang, W.; Winkler, H. D. F.; Schalley, C. A. *J. Am. Chem. Soc.* **2008**, *130*, 13852–13853.

[6] Jiang, W.; Schalley, C. A. *Proc. Natl. Acad. Sci. USA* **2009**, *106*, 10425−10429.

[7] Osowska, K.; Miljanić, O. Š. *Synlett* **2011**, *2011*, 1643−1648.

[8] Qing Ji; Lirag, R. C.; Miljanić, O. Š. *Chem. Soc. Rev.* **2014**, *43*, 1873−1884.

[9] Mahata, K.; Schmittel, M. *J. Am. Chem. Soc.* **2009**, *131*, 16544−16554.

[10] Lal Saha, M.; Schmittel, M. *Org. Biomol. Chem.* **2012**, *10*, 4651−4684.

[11] Rowan, S. J.; Hamilton, D. G.; Brady, P. A.; Sanders, J. K. M. *J. Am. Chem. Soc.* **1997**, *119*, 2578−2579.

[12] Rowan, S. J.; Brady, P. A.; Sanders, J. K. M. *Angew. Chem. Int. Ed.* **1996**, *35*, 2143−2145.

[13] Otto, S.; Furlan, R. L. E.; Sanders, J. K. M. *J. Am. Chem. Soc.* **2000**, *122*, 12063−12064.

[14] Otto, S.; Furlan, R. L. E.; Sanders, J. K. M. *Science* **2002**, *297*, 590−593.

[15] Han, J.-M.; Pan, J.-L.; Lei, T.; Liu, C.; Pei, J. *Chem. Eur. J.* **2010**, *16*, 13850−13861.

[16] Hafezi, N.; Lehn, J.-M. *J. Am. Chem. Soc.* **2012**, *134*, 12861−12868.

[17] Vantomme, G.; Hafezi, N.; Lehn, J.-M. *Chem. Sci.* **2014**, *5*, 1475−1483.

[18] Içli, B.; Christinat, N.; Tönnemann, J.; Schüttler, C.; Scopelliti, R.; Severin, K. *J. Am. Chem. Soc.* **2009**, *131*, 3154−3155.

[19] Christinat, N.; Scopelliti, R.; Severin, K. *Angew. Chem. Int. Ed.* **2008**, *47*, 1848−1852.

[20] Pascu, M.; Ruggi, A.; Scopelliti, R.; Severin, K. *Chem. Commun.* **2013**, *49*, 45−47.

[21] Tönnemann, J.; Scopelliti, R.; Severin, K. *Eur. J. Inorg. Chem.* **2013**, 5071−5074.

[22] Lirag, R. C.; Miljanić, O. Š. *Chem. Commun.* **2014**, *50*, 9401−9404.

[23] Krämer, R.; Lehn, J.-M.; Marquis-Rigault, A. *Proc. Natl. Acad. Sci. USA* **1993**, *90*, 5394−5398.

[24] Lehn, J.-M.; Rigault, A.; Jay, S.; Harrowfield, J.; Chevrier, B.; Moras, D. *Proc. Natl. Acad. Sci. USA* **1987**, *84*, 2565−2569.

[25] Krämer, R.; Lehn, J.-M.; De Cian, A.; Fischer, J. *Angew. Chem. Int. Ed. Engl.* **1993**, *32*, 703−706.

[26] Hutin, M.; Frantz, R.; Nitschke, J. R. *Chem. Eur. J.* **2006**, *12*, 4077−4082.

[27] Schultz, D.; Nitschke, J. R. *Proc. Natl. Acad. Sci.* **2005**, *102*, 11191−11195.

[28] Schultz, D.; Nitschke, J. R. *Angew. Chem. Int. Ed.* **2006**, *45*, 2453−2456.

[29] Jiménez, A.; Bilbeisi, R. A.; Ronson, T. K.; Zarra, S.; Woodhead, C.; Nitschke, J. R. *Angew. Chem. Int. Ed.* **2014**, *53*, 4556−4560.

[30] Bilbeisi, R. A.; Clegg, J. K.; Elgrishi, N.; Hatten, X. d.; Devillard, M.; Breiner, B.; Mal, P.; Nitschke, J. R. *J. Am. Chem. Soc.* **2012**, *134*, 5110−5119.

[31] Salles, A. G.; Zarra, S.; Turner, R. M.; Nitschke, J. R. *J. Am. Chem. Soc.* **2013**, *135*, 19143−19146.

[32] Northrop, B. H.; Zheng, Y.-R.; Chi, K.-W.; Stang, P. J. *Acc. Chem. Res.* **2009**, *42*, 1554−1563.

[33] Chi, K.-W.; Addicott, C.; Arif, A. M.; Stang, P. J. *J. Am. Chem. Soc.* **2004**, *126*, 16569−16574.

[34] Addicott, C.; Das, N.; Stang, P. J. *Inorg. Chem.* **2004**, *43*, 5335−5338.

[35] Mahata, K.; Saha, M. L.; Schmittel, M. *J. Am. Chem. Soc.* **2010**, *132*, 15933−15935.

[36] Saha, M. L.; Schmittel, M. *J. Am. Chem. Soc.* **2013**, *135*, 17743−17746.

[37] Mahata, K.; Schmittel, M. *J. Am. Chem. Soc.* **2009**, *131*, 16544−16554.

[38] Saha, M. L.; Mittal, N.; Bats, J. W.; Schmittel, M. *Chem. Commun.* **2014**, *50*, 12189−12192.

[39] (a) Osowska, K.; Miljanić, O. Š. *J. Am. Chem. Soc.* **2011**, *133*, 724−727; (b) Osowska, K.; Miljanić, O. Š. *Angew. Chem. Int. Ed.* **2011**, *50*, 8345−8349; (c) Lirag, R. C.; Osowska, K.; Miljanić, O. Š. *Org. Biomol. Chem.* **2012**, *10*, 4847−4850; (d) Ji, Q.; Miljanić, O. Š. *J. Org. Chem.* **2013**, *78*, 12710−12716; (e)

Ji, Q.; El-Hamdi, N. S.; Miljanić, O. Š. *J. Chem. Educ.* **2014**, *91*, 830−833; (f) Hsu, C.-W.; Miljanić, O. Š. *Angew. Chem. Int. Ed.* **2015**, *54*, 2219−2222.

[40] Gold, V. *Pure Appl. Chem.* **1979**, *51*, 1725−1801.

[41] Vongvilai, P.; Angelin, M.; Larsson, R.; Ramström, O. *Angew. Chem. Int. Ed.* **2007**, *46*, 948−950.

[42] Vongvilai, P.; Ramström, O. *J. Am. Chem. Soc.* **2009**, *131*, 14419−14425.

[43] Patzke, V.; von Kiedrowski, G. *ARKIVOC* **2007**, 293−310.

[44] del Amo, V.; Slawin, A. M. Z.; Philp, D. *Org. Lett.* **2008**, *10*, 4589−4592.

[45] Sadownik, J. W.; Philp, D. *Angew. Chem. Int. Ed.* **2008**, *47*, 9965−9970.

[46] Allen, V. C.; Robertson, C. C.; Turega, S. M.; Philp, D. *Org. Lett.* **2010**, *12*, 1920−1923.

2 Chapter Two: Adsorption-driven Self-sorting of Dynamic Imine Libraries[1]

2.1 Introduction

The differential adsorption of compounds from a liquid or gaseous mixture on solid materials is of critical importance in the fields of heterogeneous catalysis, surface sensing, separations, and even in theories of the origin of life.[2] Adsorption of components of dynamic combinatorial libraries (DCLs)[3] should additionally result in substantial redistribution of the material among the equilibrating species so that the best-adsorbed species are amplified at the expense of their less-well-adsorbed counterparts. Further benefits can come from the use of open systems which do not establish a thermodynamic equilibrium and can amplify even small differences in equilibrium partition coefficients to yield synthetically useful product distributions. In this Chapter, I present such a case: simplification of dynamic libraries containing as many as 16 components into just four final products during the course of column chromatography on silica gel.

Dynamic combinatorial chemistry (DCC) studies equilibrating compound mixtures which can respond to external stimuli by increasing the proportion of (i.e. amplifying) those library components that best adopt to the disturbing stimulus, at the expense of those that do not. This error-correcting mechanism allows production of thermodynamically stabilized species in yields that are often quantitative, as the material can be continuously recycled across shallow potential-energy surfaces until the thermodynamic minimum is reached. This key benefit of DCC is also its key drawback as working in a closed system at equilibrium does not allow the production of kinetically favored products.

By switching instead to an open system with a continuous flow of material, kinetic and thermodynamic factors can work together, so that kinetically controlled products can be produced in high yields enabled by continuous recycling of precursors before they enter an irreversible removal process.[4] We and others have explored this behavior to achieve self-sorting,[3, 5] dynamic kinetic resolution,[6] and self-replication.[7] Our work demonstrated that iterative application of an irreversible kinetic stimulus in an open system results in a cascade of disproportionation processes, simplifying a library containing n^2 members into just n products. The stimulus for these self-sorting processes can be a chemical reaction[8] or a physical transformation, such as distillation,[9] precipitation,[10] or transfer of materials between two liquid phases.[11] Herein, we show that DCL members can be amplified based on the difference in their partition coefficients between the mobile and the stationary phase during the course of column chromatography.[12]

2.2 Results and Discussion

We hypothesized that slow elution of a dynamic combinatorial library constructed from some of the imines **134**–**116** (Figure 2.1) would amplify the least polar component that elutes first. As this occurred, its more polar counterparts that share either the same aldehyde or amine starting components as this least polar imine, would disproportionate to replenish the least polar imine and to amplify the most polar imine at the expense of species of intermediate polarity (illustrated on a mixture of imines **139**–**143** in Scheme 2.1).[13]

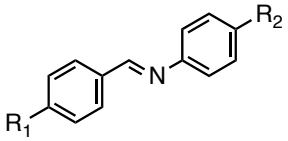

	R_2				
R_1	Br	Me	OMe	COOH	H
Br	**134**	**138**	**142**	**145**	–
Me	**135**	**139**	**95**	**146**	–
MeO	**136**	**140**	**143**	**147**	–
HOOC	**137**	**141**	**144**	**148**	**150**
H	–	–	–	**149**	**116**

Figure 2.1 Structures of imines employed in this study.

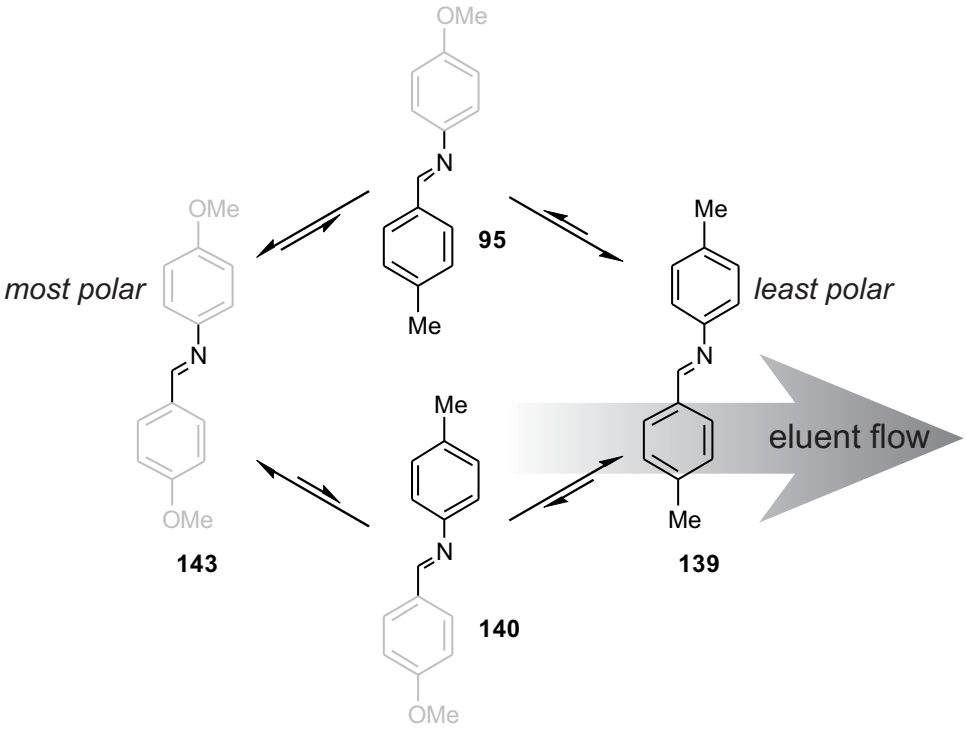

Scheme 2.1 Simplification of a [2×2] imine library during the course of column chromatography. The least polar imine **139** combines the two black components and travels fastest through the column. As it is being depleted, the two crossover components (**95** and **140**) react to produce more of **139**, while simultaneously amplifying the most polar fraction **143**, which combines the two gray "sticky" components.

Each of the examined imine libraries was formed by mixing equimolar amounts of the requisite aldehydes and anilines in toluene as the solvent, followed by heating the mixture at reflux for 12 hours. During the heating, H_2O was removed using a Dean-Stark trap. Once dehydration was complete, the toluene was evaporated and the crude imine

library mixture was pre-adsorbed onto oven-dried silica with an approximate mass 2.5 times higher than that of the crude reaction mixture. This solid mixture was placed on top of a chromatography column (inner diameter 150 mm) which was preloaded with a layer of oven-dried silica gel (10–20 cm high). Finally, the part of the column containing the silica gel was wrapped in a heating tape, which was used to keep the column at approximately 50 °C. In the first experiment, a mixture of imines **139**, **95**, **140**, and **143** was prepared and analyzed by ^{1}H NMR spectroscopy. The relative ratios of the four imines were calculated to be 1.00:0.65:0.66:0.99 (Figure 2.2a, gray vertical bars), respectively. Column chromatography of this mixture was initially performed with a 100:1 v/v mixture and then with a 20:1 v/v mixture of hexane and EtOAc. Two major fractions were isolated. In the first fraction, the dominant product was **139** (85±1%), as determined by integration of the resonance signals in the ^{1}H NMR spectrum of this fraction by comparison with an internal standard 1,3,5-trimethoxybenzene. Similar analysis of the second fraction revealed **143** as the major component (89±1%) and a small amount of **140** (8±0.2%). In essence, fast elution of the least polar imine **139** disturbed the equilibrium distribution, forcing **95** and **140** to react and replenish the removed **139**—until their constituents were completely consumed in the process. The most polar imine **143**—which did not share either of the components of **139**—was also amplified in the mixture at the expense of its counterparts of intermediate polarity (Figure 2.2a, white bars).

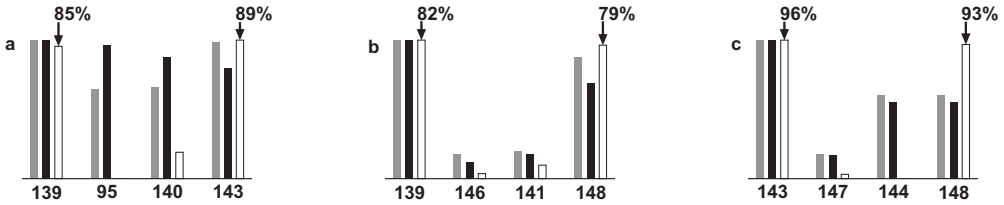

Figure 2.2 Relative normalized distributions of imine components in three [2×2] imine libraries before (gray bars) and after (black bars) addition of silica gel. The white bars show the total yields of individual imines from the isolated fractions, which were determined using the integrals of resonance signals in the ^{1}H NMR spectra with an internal standard.

As this experiment required the addition of a significant amount of silica gel to the imine mixture, we next confirmed that this addition does not significantly change the equilibrium. The initial mixture was combined with approximately 2.5 times greater mass of silica gel and then heated at reflux in toluene overnight. After the removal of silica gel by filtration, integration of the resonance signals in the ^{1}H NMR spectrum of the resultant solution revealed a **139**:**95**:**140**:**143** ratio of 1:0.96:0.88:0.80, suggesting that silica gel does not dramatically change the ratio of the library members (Figure 2.2a, black bars). As only the solution composition was monitored, the measured changes in library composition can be interpreted as a consequence of differences in adsorption on silica gel among the various imines in the mixture.

Two additional [2×2] experiments were performed. In the first (Figure 2.2b), imines **139**, **146**, **141**, and **148** were similarly analyzed with and without silica gel, before being subjected to column chromatography. This mixture was biased from the outset: the equilibrated library shows a high preference for the formation of the least polar imine **139** (relative abundance 1.00) and the most polar **148** (0.88), relative to their counterparts of intermediate polarity (**146**: 0.18, **141**: 0.20). This ratio changed minimally upon addition of silica gel. Ultimately, chromatography—eluting first with a mixture of hexane/EtOAc

(20:1 v/v) and then with pure THF—led to the isolation of **139** (82±1%) as the dominant component of the first fraction, followed by **148** (79±3%) as the major component in the second fraction. Small amounts of **146** (3±0.1%) and **141** (8±0.3%) were also detected.

In the final [2×2] system (Figure 2.2c), the initial distribution was between the first two experiments—biased towards the least polar imine **143** and the most polar imine **148**, but not as dramatically as in the previous experiment. Column chromatography significantly amplified this bias, producing **143** in 96±1% yield and **148** in 93±3% yield.

In a more complex [3×3] system, three aldehyde and three amine starting materials were reacted together to yield a mixture of nine imines, the distribution of which is also represented by gray vertical bars (Figure 2.3). The proportion of the most abundant imine in the mixture, imine **143**, is approximately six times greater than that of the least abundant member of the library, imine **146**. Upon addition of silica, this distribution equalizes somewhat, with the **143**/**146** ratio decreasing to approximately 3.5. Column chromatography of the system initially employed pure hexane as the eluent. The polarity of the eluent was then increased to hexane/EtOAc 100:1 v/v and then to a 10:1 ratio, and was finally changed to pure THF. Imine **139** was isolated in the first fraction in 80±1% yield, essentially consuming (almost) all of benzaldehyde and aniline constituents in the process. The second small fraction contained 12±0.2% of **140**, while the third fraction carried **143** (81±1%). In the final fraction, imine **148** dominated (89±3%), and small amounts of **141** (4±0.1%) were also detected.

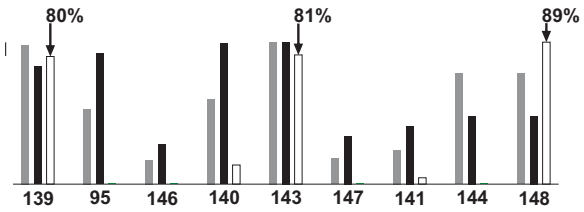

Figure 2.3 Relative normalized distributions of imine components in the [3×3] imine library before (gray bars) and after (black bars) addition of silica gel. The white bars show the total yields of individual imines from the isolated fractions, which were determined using the integrals of resonance signals in the ^{1}H NMR spectra with an internal standard.

The final [4×4] experiment started with a mixture of 16 imines in which the most abundant imine **139** was present in approximately threefold excess relative to the least abundant imine **146** (Figure 2.4, gray bars). Upon addition of silica gel the relative abundances changed, leaving **140** as the imine with the highest proportion and **137** as the least concentrated member of the library ([**140**]/[**137**]=2.44). Column chromatography—eluting first with hexane/toluene (10:1 v/v, then 8:1), then with hexane/EtOAc (40:1, then 10:1, then 2:1), and finally with pure THF—enabled us to isolate six distinct fractions: a) the first fraction composed mostly of **134** (64±1%); b) the second fraction with small amounts of **138** (1±0.1%) and **135** (3±0.1%); c) the third fraction, which was a mixture of **139** (78±1%), **138** (17±0.1%), **135** (13±0.1%), and an additional amount of **134** (3±0.02%); d) the fourth fraction composed of **136** (5±0.1%) and **140** (8±0.1%); e) the fifth fraction made up mostly of **143** (80±1%) and some **136** (5±0.1%); and f) a final fraction as a mixture of **148** (76±3%), **141** (2±0.1%), **137** (2±0.1%), and **145** (1±0.1%). Conceptually, rapid elution of **134** forced imines **138**–**145** to react with **135**, **136**, and **137** to replenish **134**. After elution of **134** is completed, the original 16-imine library lost these seven members and was reduced in size to form a [3×3] library which now had **139**

as the least polar member. In the next step, its elution consumed **95**, **146**, **140**, and **141**, decreasing the size of the leftover library to just 4 members, and so on.

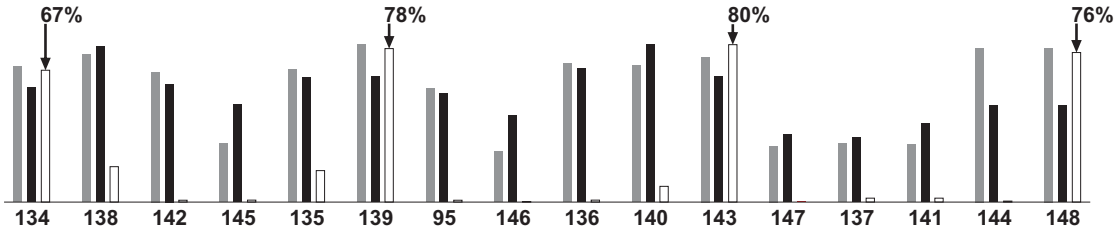

Figure 2.4 Relative normalized distributions of imine components in the [4×4] imine library before (gray bars) and after (black bars) addition of silica gel. The white bars show the total yields of individual imines from the isolated fractions, which were determined using the integrals of resonance signals in the ^{1}H NMR spectra with an internal standard.

This procedure is limited in resolution. Each of the isolated imines is eluted in several fractions and that is a necessary feature of this procedure. For example, in the experiment shown in Figure 2.3, imine **139** is eluted as three separate fractions, although they may not be collected as such. The amount of **139** that is present in the initial mixture is eluted quickly. The remainder of **139** has to be produced on the column by disproportionation of partners that a) contain its constituents and b) elute at approximately the same rate. Thus, **95** and **140**—which are of comparable polarity—produce the second batch of **139**, while **146** and **141** elute later and are responsible for the production of the third batch of **139**. With larger libraries, it is likely that there will be overlap of multiple fractions, and thus the amplification loses fidelity as the library increases in complexity.

Based on the same logic, an even more curious transmutation experiment was performed (Scheme 2.2). Equimolar amounts of pure **150** and **149** (which both contain one highly polar and one highly nonpolar component) were loaded onto a silica gel

column, and eluted first with hexane/EtOAc (40:1 v/v) and subsequently with pure THF. The first isolated fraction contained **148** (92%) and the second **116** (94%). This is a particularly unusual column chromatography experiment, given that two compounds eluted from the column are different than the two loaded compounds.

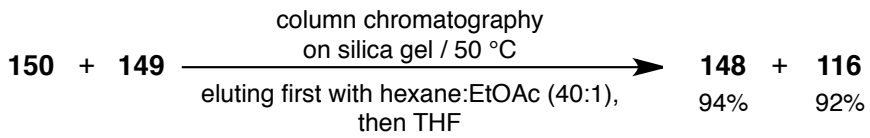

Scheme 2.2 Transmutation of imines during column chromatography.

2.3 Conclusion

In conclusion, we have shown that complex libraries of equilibrating compounds can simplify in composition during the course of column chromatography on silica gel. This process could easily be combined with chemical reactions—by, for example, performing a chromatographic separation on a column impregnated with a catalyst—resulting in multidimensional simplification of complex libraries. In the future, we will attempt to automate and monitor this procedure using an HPLC instrument. Such an extension would allow the use of this dynamic procedure as a physical chemistry tool to, for example, determine polarity indicators[14] in a direct competition experiment. This method will also be expanded to other adsorbents and dynamic compound classes.[15]

2.4 Experimental Section

2.4.1 General Methods and Materials

Reagents and solvents were purchased from commercial suppliers and used without further purification, with the exception of PhMe and hexane, which were dried over molecular sieves. Round bottom flasks (50 mL) and Dean-Stark traps were used as

the standard part of the reaction apparatus for the syntheses of imine libraries. Column chromatography was performed in a 305 mm-long chromatography column with an 127 mm inner diameter with light air flow. Silica gel (60 Å, 40−63 μm, Sorbent Technology) was oven-dried and used as the adsorbent for dry-loaded sample preparation and column chromatography. External heating of the chromatography column was achieved using a heating tape (52 W, 1.3 cm width, ~0.6 m length, produced by Thermo Scientific) at 30 V. Before wrapping the heating tape around the column (in all experiments), an additional layer of silica gel was added (~2 cm height) to the top of the column. After the addition of the eluent into the column, the heat was not applied until the first drops of solvent came out from the bottom end of the column. All NMR spectra were collected on a JEOL ECA-500 spectrometer with working frequencies of 500 MHz for ^{1}H NMR and 125 MHz for ^{13}C NMR nuclei. Chemical shifts are reported in ppm units relative to the residual signal of the solvent ($CDCl_3$: 7.26 ppm, DMSO-d_6: 2.49 ppm). ^{13}C NMR spectra were recorded with simultaneous decoupling of ^{1}H nuclei. The NMR internal standard for yield determination was 1,3,5-trimethoxybenzene (Alfa Aesar, 99%). The melting points were measured on a Barnstead International Mel-TEMP(R) apparatus, and are uncorrected. The mass spectra were obtained via LCQ Deca XP Plus from Thermo Finnigan (ESI-MS) or TRACE MS Plus from Thermo Finnigan (EI-MS). Fourier transform infrared spectra were measured by Nicolet MAGNA-IR 860 Fourier transform spectrometer using KBr pellet technique. All of the studied imines have been previously reported in the literature, with the exception of **137**, **141**, and **144**—for which no NMR data had been reported. Synthetic procedures and NMR data for these imines are given in the following section.

2.4.2 Syntheses of Possible Imine Candidates

4-[[(4-Bromophenyl)imino]methyl]benzoic acid (**137**)

A mixture of 4-formylbenzoic acid (140 mg, 0.933 mmol) and 4-bromoaniline (160 mg, 0.933 mmol) was added into a 50 mL round bottom flask, along with PhMe (20 mL). The solution was heated at reflux for 12 h with a Dean-Stark trap. After that time, PhMe was evaporated in vacuo, and the resulting solid was washed with hexane, to give the title compound as a dark green solid in 62% yield (177 mg).

137: ^{1}H NMR (DMSO-d_6, 500 MHz): 8.72 (s, 1H), 8.09−7.99 (m, 4H), 7.62−7.60 (d, $^{3}J_{H-H}$=8.6 Hz, 2H), 7.28−7.27 (d, $^{3}J_{H-H}$=8.6 Hz, 2H) ppm. ^{13}C NMR (DMSO-d_6, 125 MHz): 166.9, 160.7, 150.2, 139.4, 133.2, 132.1, 129.8, 128.8, 123.4, 119.1 ppm. Melting point: 273−274 °C (lit. 273 °C).[16] ESI-MS (ESI negative mode): Calcd for $136_4H_9BrNO_2^-$ [$(M-1)^{-1}$]: 301.98. Found: 302.01. IR (KBr, neat): 3050−2540 (br, O−H stretching), 1680 (s, C=O, stretching), 1620 (s, C=N, stretching), 1480, 1430 (s, aromatic C−C, stretching), 1290 (s, O−H bending), 1000−800 (m−s, aromatic C−H bending) cm^{-1}.

4-[[(4-Methylphenyl)imino]methyl]benzoic acid (**141**)

A mixture of 4-formylbenzoic acid (140 mg, 0.933 mmol) and 4-methylaniline (100 mg, 0.933 mmol) was added into a 50 mL round bottom flask, along with PhMe (20 mL). The solution was heated at reflux for 12 h with a Dean-Stark trap. After that time, PhMe was evaporated in vacuo, and the resulting solid was washed with hexane, to give the title compound as a light yellow solid in 91% yield (203 mg).

141: ^{1}H NMR ($CDCl_3$, 500 MHz): 8.55 (s, 1H), 8.21−8.19 (d, $^{3}J_{H-H}$=8.6 Hz, 2H), 8.02−8.00 (d, $^{3}J_{H-H}$=8.0 Hz, 2H), 7.24−7.18 (m, 4H), 2.39 (s, 3H) ppm. ^{1}H NMR

(DMSO-d_6, 500 MHz): 8.72 (s, 1H), 8.06−8.01 (m, 4H), 7.23 (s, 4H), 2.32 (s, 3H) ppm. ^{13}C NMR (DMSO-d_6, 125 MHz): 166.9, 158.8, 148.3, 139.8, 136.0, 132.8, 129.8, 129.7, 128.6, 121.2, 20.6 ppm. Melting point: 262−265 °C (lit. 265 °C).[16] EI-MS: Calcd for $136_5H_{13}NO_2^+$: 239.09. Found: 239.24. IR (KBr, neat): 2980−2540 (br, O−H stretching), 1680 (s, C=O, stretching), 1620 (s, C=N, stretching), 1500, 1420 (s, aromatic C−C, stretching), 1290 (s, O−H bending), 900−700 (m−s, aromatic C−H bending) cm^{-1}.

4-[[(4-Methoxyphenyl)imino]methyl]benzoic acid (**144**)

A mixture of 4-formylbenzoic acid (140 mg, 0.933 mmol) and 4-methoxyaniline (115 mg, 0.933 mmol) was added into a 50 mL round bottom flask, along with PhMe (20 mL). The solution was heated at reflux for 12 h with a Dean-Stark trap. After that time, PhMe was evaporated in vacuo, and the resulting solid was washed with hexane, to give the title compound as a light yellow solid in 93% yield (222 mg).

144: ^{1}H NMR (DMSO-d_6, 500 MHz): 8.74 (s, 1H, E isomer), 8.71 (s, 1H, Z isomer), 8.05−8.00 (m, 4H), 7.37−7.34 (m, 2H), 7.01−6.98 (m, 2H), 3.78 (s, 3H) ppm. ^{13}C NMR (DMSO-d_6, 125 MHz): 167.0, 158.4, 157.3, 143.6, 140.0, 132.6, 129.7, 128.4, 122.3, 114.5, 55.3 ppm. Melting point: 213−215 °C (lit. 216 °C).[16] ESI-MS (ESI negative): Calcd for $136_5H_{13}NO_3^{-1}$ (M^{-1}): 255.09. Found: 255.11. IR (KBr, neat): 3080−2530 (br, O−H stretching), 1690 (s, C=O, stretching), 1620 (s, C=N, stretching), 1500, 1430 (s, aromatic C−C, stretching), 1250 (s, O−H bending), 1190−835 (m−s, aromatic C−H bending) cm^{-1}.

2.4.3 Adsorption-Driven Self-Sorting of [2×2] Imine Libraries

Experiment #1

4-Methyl-*N*-[(4-methylphenyl)methylene]benzenamine (**139**) and 4-Methoxy-*N*-[(4-methoxyphenyl)methylene]benzenamine (**143**)

Equimolar amounts of 4-methylbenzaldehyde (110 μL, 0.933 mmol), 4-methoxybenzaldehyde (114 μL, 0.933 mmol), 4-methylaniline (100 mg, 0.933 mmol) and 4-methoxyaniline (115 mg, 0.933 mmol) were added into a 50 mL round bottom flask, along with PhMe (20 mL). The mixture was heated at reflux for 12 h, and a Dean-Stark trap was used to remove H_2O. Then, PhMe was removed in vacuo to afford a mixture of four imines as a light brown solid. This mixture was preadsorbed onto silica gel (approx. 1 g) and then added on top of a chromatography column, which was pre-loaded with an approx. 10 cm-high layer of oven-dried silica gel. The column was then wrapped with a heating tape and heated to approx. 50 °C. The elution was performed first with hexane (300 mL), followed by a 100:1 hexane/EtOAc (v/v, 200 mL), and 10:1 hexane/EtOAc (v/v, 110 mL) mixtures, and finally with pure EtOAc (100 mL). Three fractions were isolated. In the first, imine **139** was the dominant product (85% yield, based on an internal standard calculation with 171 mg of the crude product and 22.3 mg of the internal standard, see Figure 2.5). The second fraction contained imine **140** as the major component (8% yield, based on an internal standard calculation with 27 mg of the crude compound and 9.7 mg of the internal standard, see Figure 2.6). The final fraction contained imine **143** (89% yield, based on an internal standard calculation with 224 mg of the crude compound and 21 mg of the internal standard, see Figure 2.7).

139: ^{1}H NMR ($CDCl_3$, 500 MHz): 8.44 (s, 1H), 7.81−7.80 (d, $^{3}J_{H-H}$=8.0 Hz, 2H), 7.30−7.28 (d, $^{3}J_{H-H}$=7.5 Hz, 2H), 7.22−7.15 (m, 4H), 2.43 (s, 3H), 2.39 (s, 3H) ppm. Spectral data agree with the previous literature report.[17]

140: ^{1}H NMR ($CDCl_3$, 500 MHz): 8.40 (s, 1H), 7.86−7.84 (m, 2H), 7.20−7.12 (m, 4H), 7.02−6.97 (m, 2H) ppm. Spectral data agree with the previous literature report.[18]

143: ^{1}H NMR ($CDCl_3$, 500 MHz): 8.41 (s, 1H), 7.86−7.83 (m, 2H), 7.24−7.21 (m, 2H), 6.99−6.91 (*m*, 4H), 3.86 (*s*, 3H), 3.82 (*s*, 3H) ppm. Spectral data agree with the previous literature report.[19]

Calculation of the Yields based on the Integration of ^{1}H NMR Spectra

Internal standard 1,3,5-trimethoxybenzene (22.3 mg, 0.133 mmol) was added into 171 mg of crude **139**. From the integration of the ^{1}H NMR spectrum (Figure 2.5), the number of moles of **139** was calculated to be 0.133 mmol × 5.93 = 0.789 mmol. Thus, the yield of **139** is 0.789 mmol ÷ 0.933 mmol = 85%. Analogous calculations have been performed for all other imines of interest.

Yield of **140**: 9.7 mg ÷ 168.19 g mol^{-1} = 0.058 mmol →→ 0.058 mmol × 1.25 = 0.073 mmol →→0.073 mmol ÷ 0.933 mmol = 8% (Figure 2.6).

Yield of **143**: 21.3 mg ÷ 168.19 g mol^{-1} = 0.127 mmol →→ 0.127 mmol × 6.53 = 0.829 →→ 0.829 mmol ÷ 0.933 mmol = 89% (Figure 2.7).

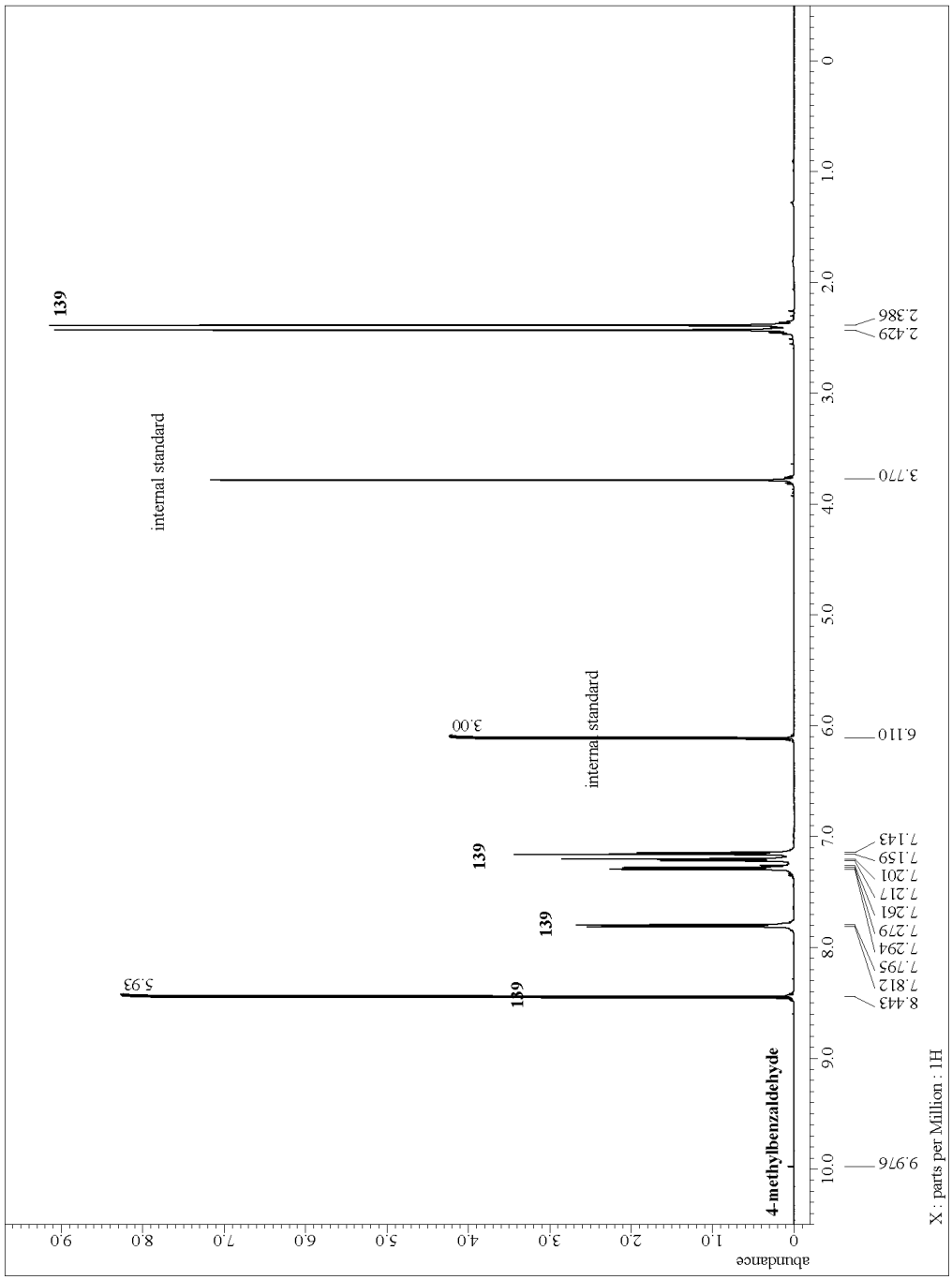

Figure 2.5 ^{1}H NMR spectrum of the first eluted fraction in Experiment #1. Imine **139** is the dominant component.

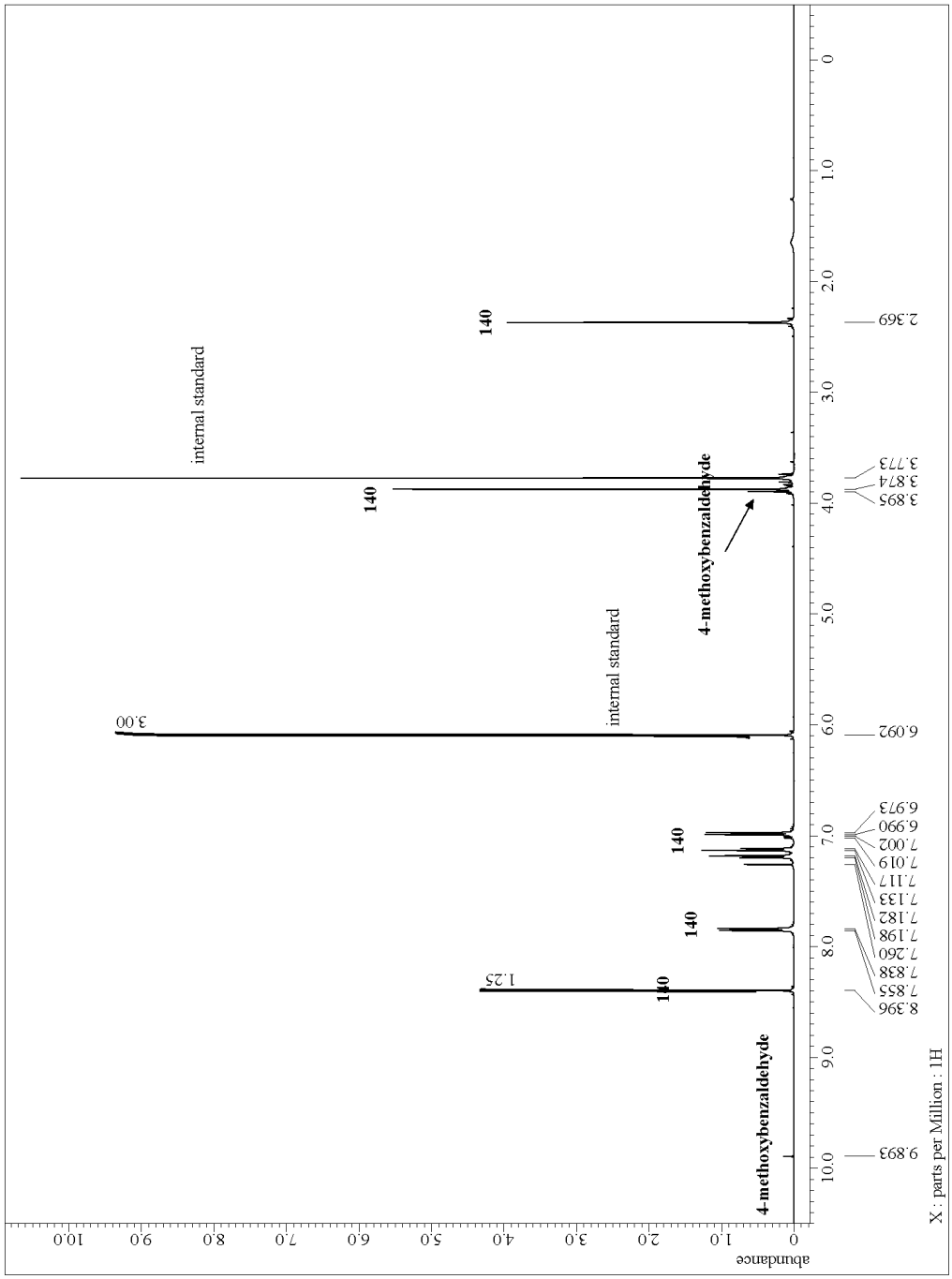

Figure 2.6 ^{1}H NMR spectrum of the second eluted fraction in Experiment #1. Imine **140** is the dominant component.

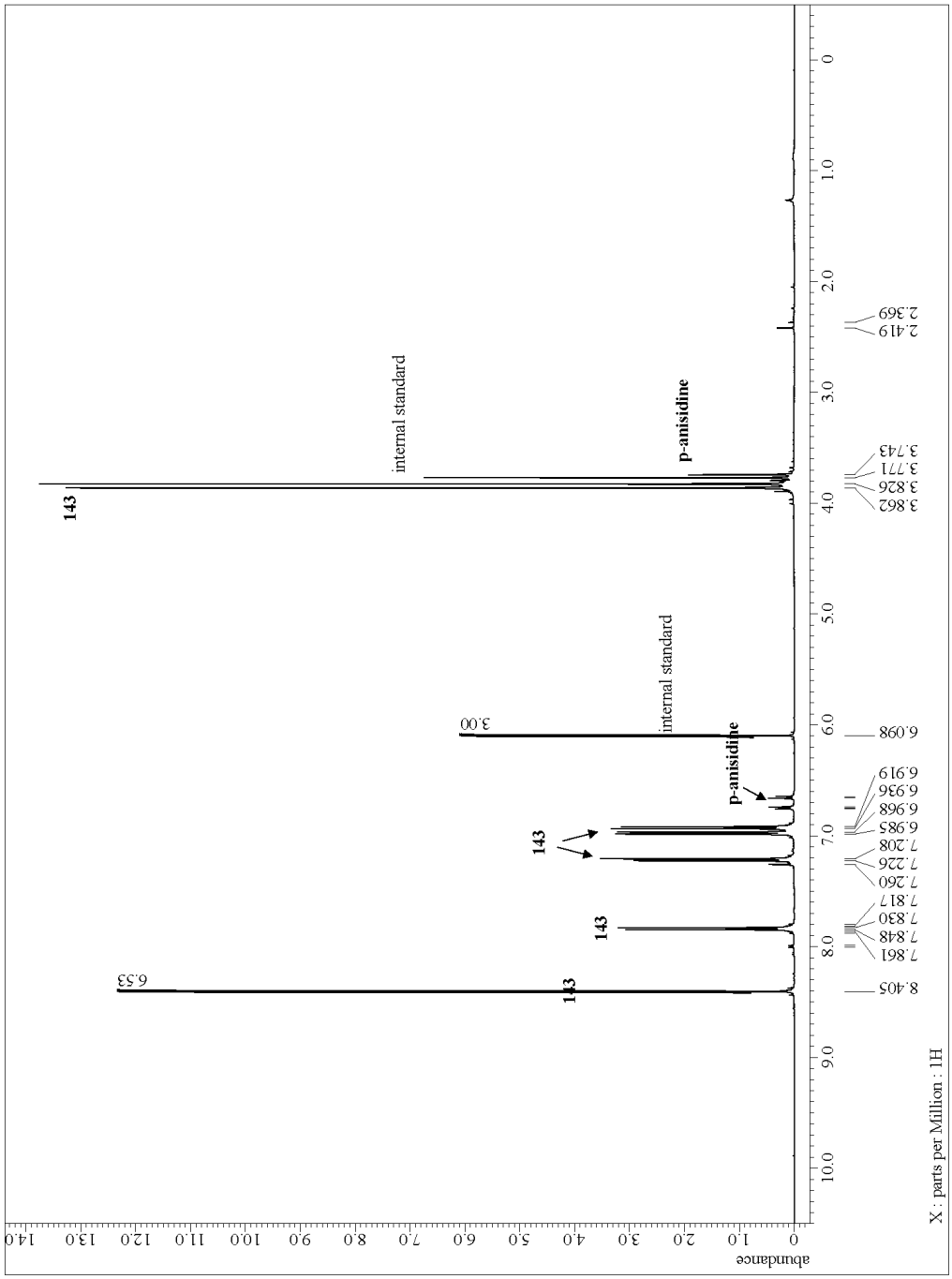

Figure 2.7 ^{1}H NMR spectrum of the third eluted fraction in Experiment #1. Imine **143** is the dominant component.

Experiment #2

4-Methyl-*N*-[(4-methylphenyl)methylene]benzenamine (**139**) and 4-[[(4-carboxyphenyl)imino]methyl]benzoic acid (**148**)

Equimolar amounts of 4-methylbenzaldehyde (110 μL, 0.933 mmol), 4-formylbenzoic acid (140 mg, 0.933 mmol), 4-methylaniline (100 mg, 0.933 mmol) and 4-aminobenzoic acid (128 mg, 0.933 mmol) were added into a 50 mL round bottom flask, along with PhMe (20 mL). The mixture was heated at reflux for 12 h, and a Dean-Stark trap was used to remove H_2O. Then, PhMe was removed in vacuo to afford a mixture of four imines as a yellow solid. This mixture was preadsorbed onto silica gel (approx. 1 g) and then added on top of a chromatography column, which was pre-loaded with an approx. 10 cm-high layer of oven-dried silica gel. The column was then wrapped with a heating tape and heated to approx. 50 °C. The elution was performed first with 20:1 hexane/EtOAc (v/v, 210 mL) mixture and then with pure THF (600 mL). Two fractions were isolated. In the first, imine **139** was the dominant product (79% yield, based on an internal standard calculation with 169 mg of the crude product and 21.4 mg of the internal standard, see Figure 2.8). The second fraction contained imine **148** as the major component (79% yield, based on an internal standard calculation with 23.8 mg crude compound mixed with 5.6 mg internal standard, see Figure 2.9), along with smaller amounts of **139** (3%), **146** (3%), and **141** (8%).

139: ^{1}H NMR ($CDCl_3$, 500 MHz): 8.44 (s, 1H), 7.81−7.80 (d, $^3J_{H–H}$=8.0 Hz, 2H), 7.30−7.28 (d, $^3J_{H–H}$=7.5 Hz, 2H), 7.22−7.15 (m, 4H), 2.43 (s, 3H), 2.39 (s, 3H) ppm. Spectral data agree with the previous literature report.[17]

146: ^{1}H NMR (DMSO-d_6, 500 MHz): 8.58 (s, 1H), 7.97−7.95 (m, 2H), 7.85−7.83

(d, $^{3}J_{H-H}$=8.0 Hz, 2H), 7.35−7.34 (d, $^{3}J_{H-H}$=8.1 Hz, 2H), 7.30−7.28 (m, 2H), 2.38 (s, 3H) ppm. Spectral data agree with the previous literature report.[20]

141: ^{1}H NMR (DMSO-d_6, 500 MHz): 8.71 (s, 1H), 8.08−8.04 (m, 4H), 7.22 (s, 4H), 2.32 (s, 3H) ppm. Spectral data agree with the previous literature report.[16]

148: ^{1}H NMR (DMSO-d_6, 500 MHz): 8.72 (s, 1H), 8.08−8.04 (m, 4H), 8.00−7.97 (m, 2H), 7.36−7.34 (m, 2H) ppm. Spectral data agree with the previous literature report.[21]

Calculation of the Yields Based on the Integration of ^{1}H NMR Spectra

The yield of **139** in the first fraction: the number of moles of internal standard is 21.4 mg ÷ 168.19 g mol^{-1} = 0.127 mmol →→ the number of moles of **139** is 0.127 mmol × 5.77 = 0.733 mmol →→ the yield of **139** is 0.733 mmol ÷ 0.933 mmol = 79% (Figure 2.8). In the second fraction: the number of moles of internal standard is 5.6 mg ÷ 168.19 g mol^{-1} = 0.033 mmol →→ the number of moles of **139** is 0.033 mmol × 0.049 × 467 mg ÷ 23.8 mg = 0.032 mmol→→ the yield of **139** is 0.032 mmol ÷ 0.933 mmol = 3% (Figure 2.9). The total yield of **139** is 79% + 3% = 82%.

The yield of **146**: the number of moles of internal standard is 5.6 mg ÷ 168.19 g mol^{-1} = 0.033 mmol →→ the number of moles of **146** is 0.033 mmol × 0.038 × 467 mg ÷ 23.8 mg = 0.025 mmol →→ the yield of **146** is 0.025 mmol ÷ 0.933 mmol = 3% (Figure 2.9).

The yield of **141**: the number of moles of internal standard is 5.6 mg ÷ 168.19 g mol^{-1} = 0.033 mmol →→ the number of moles of **141** is 0.033 mmol × 0.12 × 467 mg ÷ 23.8 mg = 0.078 mmol →→ the yield of **141** is 0.078 mmol ÷ 0.933 mmol = 8% (Figure 2.9).

The yield of **148**: the number of moles of internal standard is 5.6 mg ÷ 168.19 g mol^{-1} = 0.033 mmol →→ the number of moles of **148** is 0.033 mmol × 1.14 × 467 mg ÷ 23.8 mg = 0.738 mmol →→ the yield of **148** is 0.738 mmol ÷ 0.933 mmol = 79% (Figure 2.9).

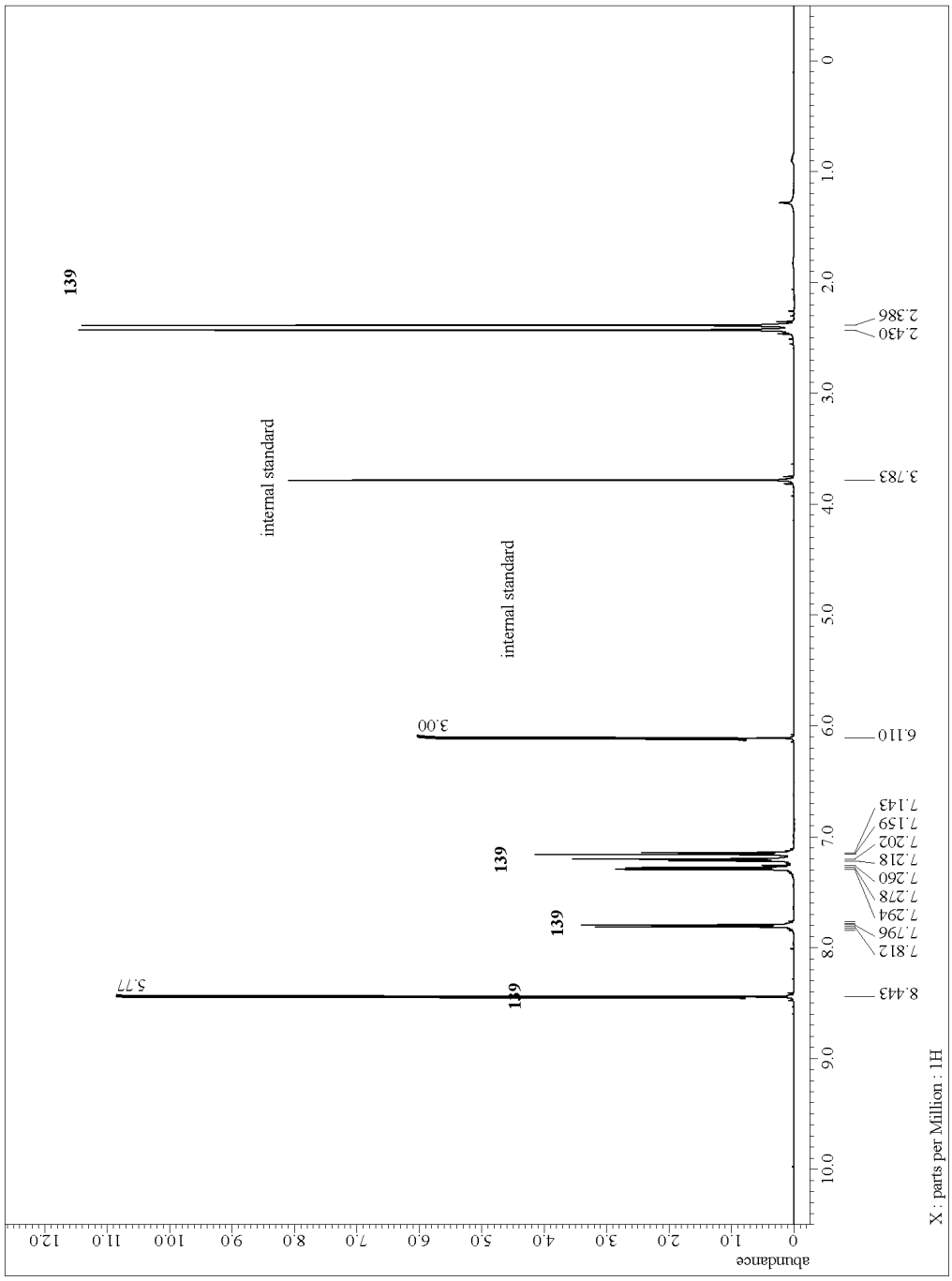

Figure 2.8 ^{1}H NMR spectrum of the first eluted fraction in Experiment #2. Imine **139** is the dominant component.

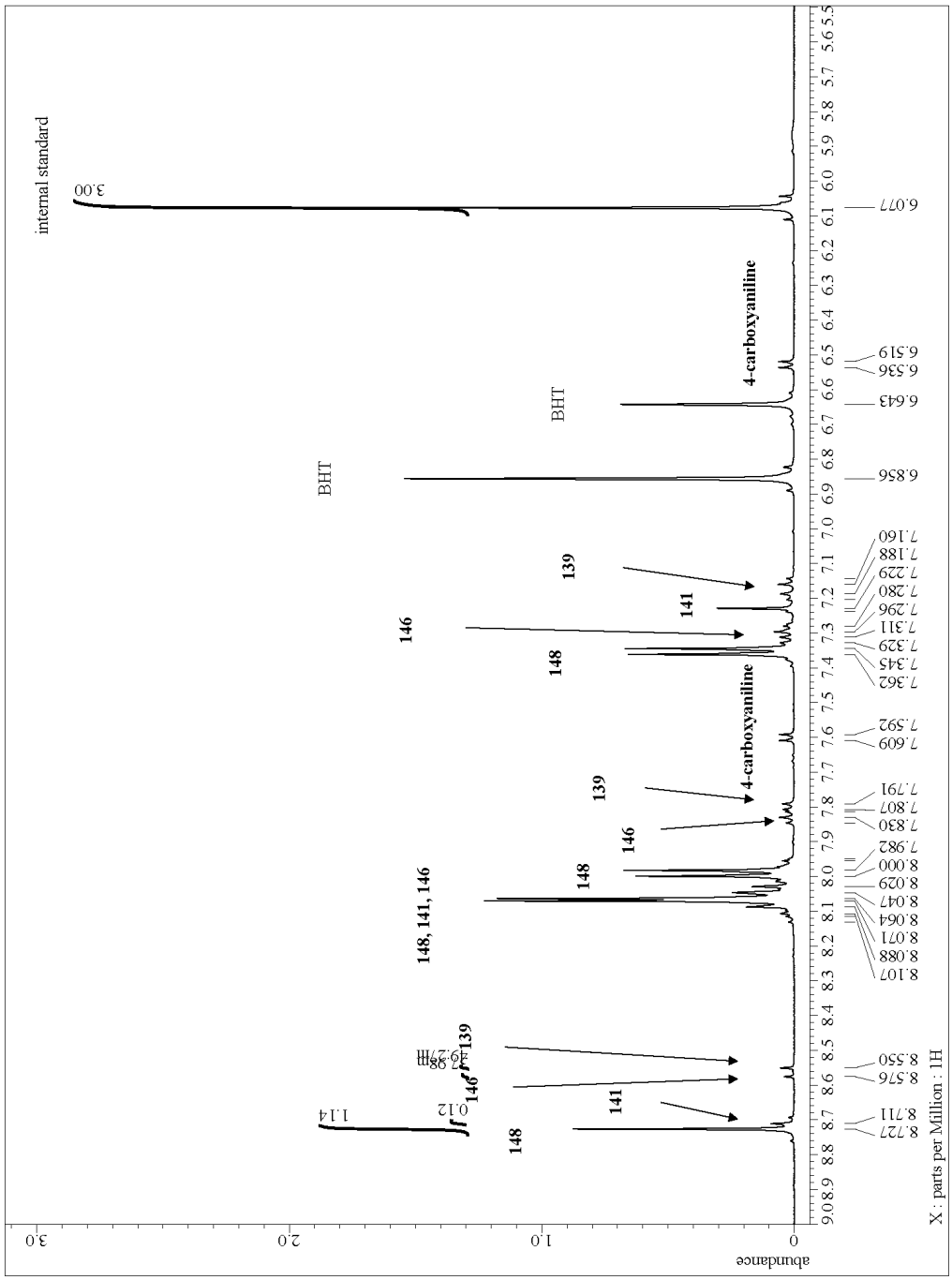

Figure 2.9 ^{1}H NMR spectrum of the second eluted fraction in Experiment #2. Imine **148** is the dominant component, but small amounts of imines **139**, **146**, and **141** also noticeable.

Experiment #3

4-Methoxy-*N*-[(4-methoxyphenyl)methylene]benzenamine (**143**) and 4-[[(4-carboxyphenyl)imino]methyl]benzoic acid (**148**)

Equimolar amounts of 4-methoxybenzaldehyde (114 μL, 0.933 mmol), 4-formylbenzoic acid (140 mg, 0.933 mmol), 4-methoxyaniline (115 mg, 0.933 mmol) and 4-aminobenzoic acid (128 mg, 0.933 mmol) were added into a 50 mL round bottom flask, along with PhMe (20 mL). The mixture was heated at reflux for 12 h, and a Dean-Stark trap was used to remove H_2O. Then, PhMe was removed in vacuo to afford a mixture of four imines as a yellow solid. This mixture was preadsorbed onto silica gel (approx. 1 g) and then added on top of a chromatography column, which was preloaded with an approx. 10 cm-high layer of oven-dried silica gel. The column was then wrapped with a heating tape and heated to approx. 50 °C. The elution was performed first with 10:1 hexane/EtOAc (v/v, 220 mL) mixture and then with pure THF (700 mL). Two fractions were isolated. In the first, imine **143** was the dominant product (88% yield, based on an internal standard calculation with 208 mg of the crude product and 22.9 mg of the internal standard, see Figure 2.10). The second fraction contained imine **148** as the major component (93% yield, based on an internal standard calculation with 20 mg of the crude compound and 7.2 mg of the internal standard, see Figure 2.11), along with smaller amounts of **143** (8%) and **147** (3%).

143: ^{1}H NMR ($CDCl_3$, 500 MHz: 8.41 (*s*, 1H), 7.86−7.83 (m, 2H), 7.24−7.21 (m, 2H), 6.99−6.91 (m, 4H), 3.86 (s, 3H), 3.82 (s, 3H) ppm. ^{1}H NMR (DMSO-d_6, 500 MHz: 8.53 (s, 1H), 7.85−7.84 (d, $^3J_{H-H}$=8.6 Hz, 2H), 7.24−7.23 (d, $^3J_{H-H}$=9.2 Hz, 2H), 7.05−7.04 (d, $^3J_{H-H}$=9.2 Hz, 2H), 6.96−6.94 (d, $^3J_{H-H}$=9.2 Hz, 2H), 3.82 (s, 3H), 3.76 (s,

3H) ppm. Spectral data agree with the previous literature report.[19]

147: ^{1}H NMR (DMSO-d_6, 500 MHz): 8.54 (s, 1H), 7.97−7.94 (m, 2H), 7.91−7.87 (m, 2H), 7.29−7.26 (m, 2H), 7.10−7.07 (m, 2H), 3.83 (s, 3H) ppm. Spectral data agree with the previous literature report.[20]

148: ^{1}H NMR (DMSO-d_6, 500 MHz): 8.72 (s, 1H), 8.08−8.04 (m, 4H), 8.00−7.97 (m, 2H), 7.36−7.34 (m, 2H) ppm. Spectral data agree with the previous literature reports.[21]

Calculation of the Yields based on the Integration of ^{1}H NMR Spectra

The yield of **143** in the first fraction: the number of moles of internal standard is 22.9 mg ÷ 168.19 g mol^{-1} = 0.136 mmol, the number of moles of **143** is 0.136 mmol × 6.01 = 0.817 mmol, the yield of **143** is 0.817 mmol ÷ 0.933 mmol = 88% (Figure 2.10); In the second fraction: the number of moles of internal standard is 7.2 mg ÷ 168.19 g mol^{-1} = 0.043 mmol, the number of moles of **143** is 0.043 mmol × 0.068 × 497 mg ÷ 20 mg = 0.073 mmol, the yield of **143** is 0.073 mmol ÷ 0.933 mmol = 8% (Figure 2.11). The total yield of **143** is 88% + 8% = 96%.

The yield of **147**: the number of moles of internal standard is 7.2 mg ÷ 168.19 g mol^{-1} = 0.043 mmol, the number of moles of **147** is 0.043 mmol × 0.028 × 497 mg × 20 mg = 0.030 mmol, the yield of **147** is 0.030 mmol × 0.933 mmol = 3% (Figure 2.11).

The yield of **148**: the number of moles of internal standard is 7.2 mg ÷ 168.19 g mol^{-1} = 0.043 mmol, the number of moles of **148** is 0.043 mmol × 0.81 × 497 mg ÷ 20 mg = 0.866 mmol, the yield of **148** is 0.866 mmol ÷ 0.933 mmol = 93% (Figure 2.11).

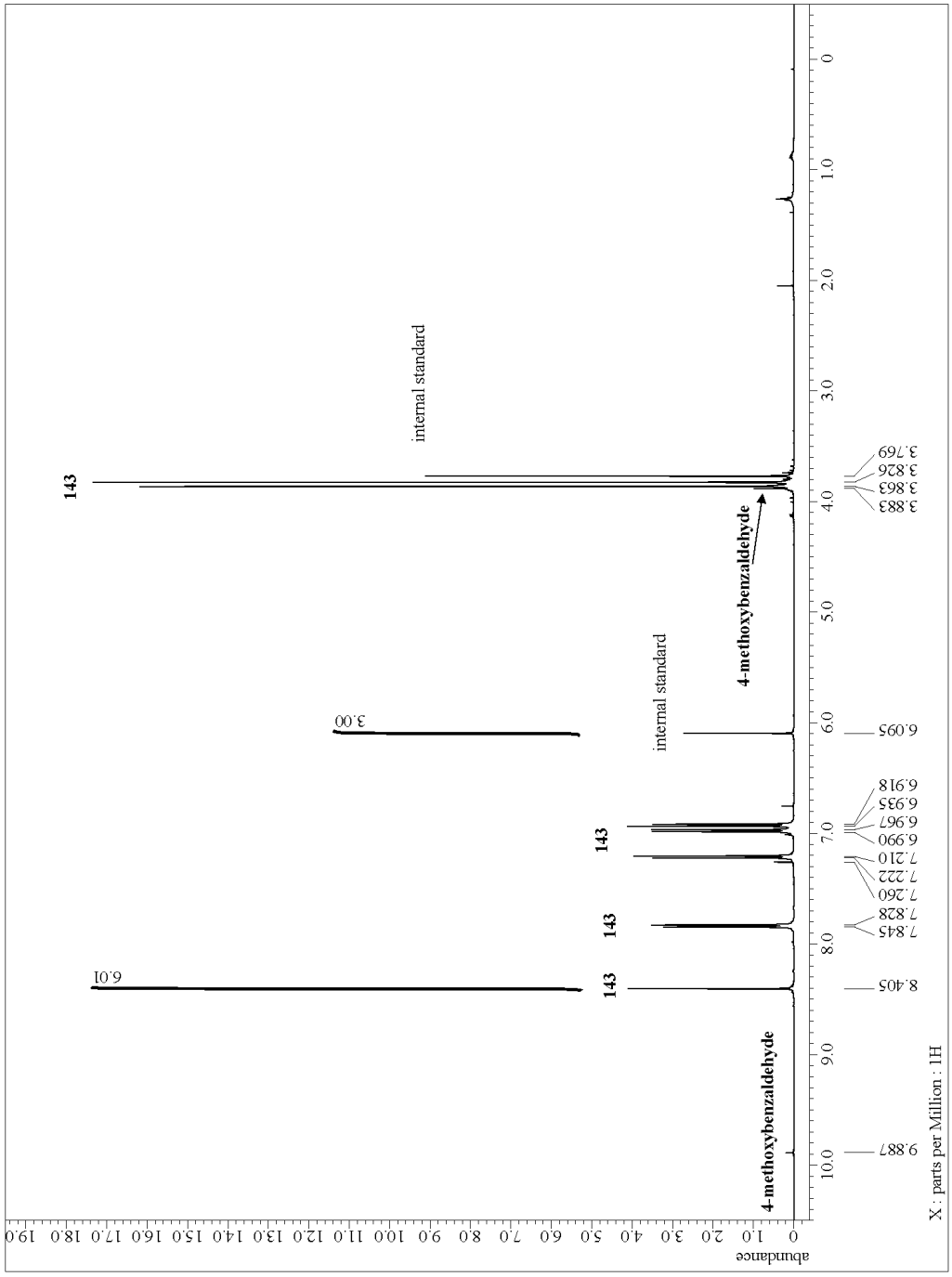

Figure 2.10 ^{1}H NMR spectrum of the first isolated fraction from Experiment #3. Imine **143** is the dominant component.

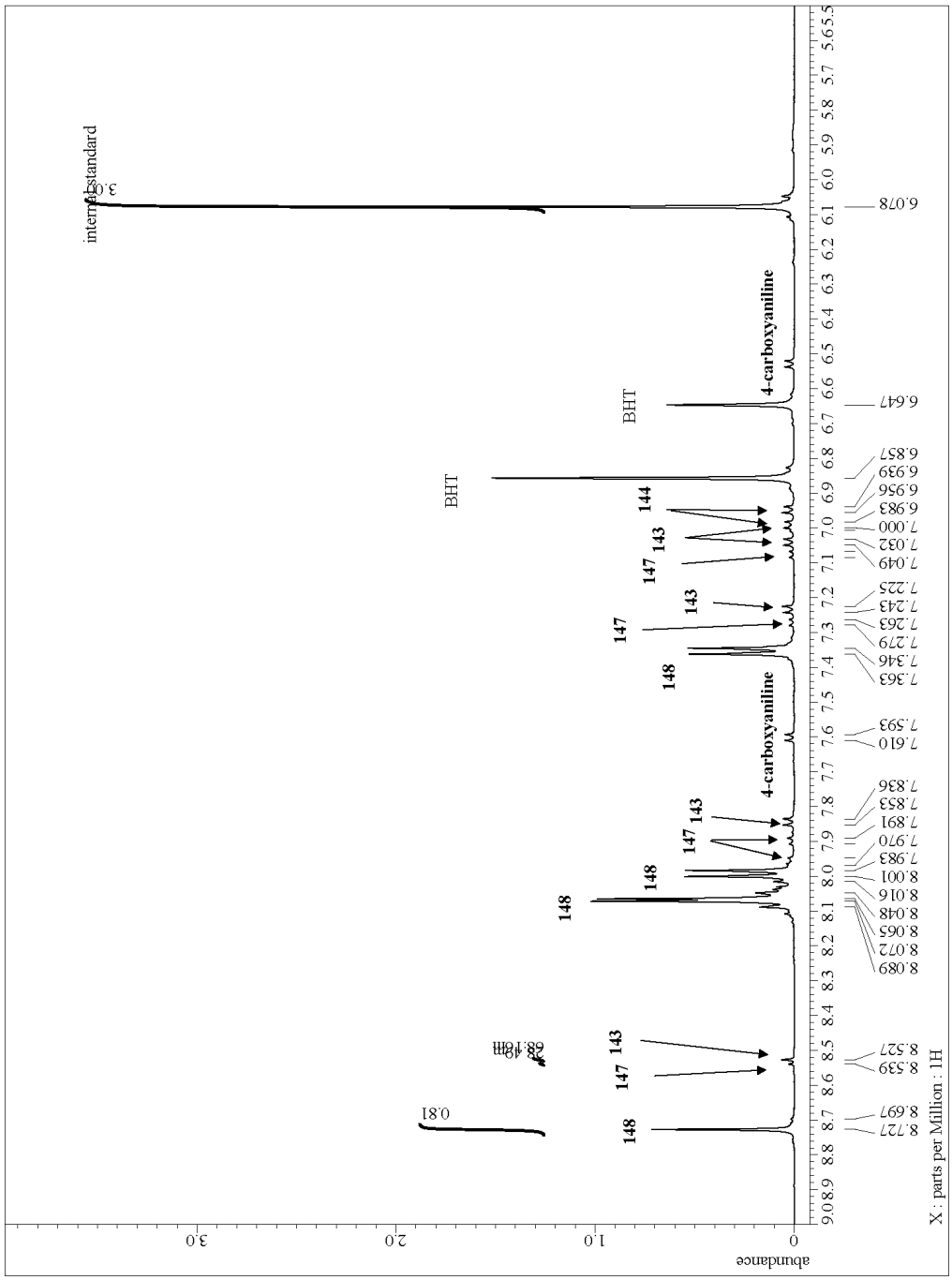

Figure 2.11 ^{1}H NMR spectrum of the second isolated fraction from Experiment #3. Imine **148** is the dominant component, but small amounts of imines **143** and **147** are also present.

2.4.4 Adsorption-Driven Self-Sorting of a [3×3] Imine Library

Experiment #4

4-Methyl-*N*-[(4-methylphenyl)methylene]benzenamine (**139**), 4-Methoxy-*N*-[(4-methoxyphenyl)methylene]benzenamine (**143**) and 4-[[(4-carboxyphenyl)imino]methyl]benzoic acid (**148**)

Equimolar amounts of 4-methylbenzaldehyde (110 μL, 0.933 mmol), 4-methoxybenzaldehyde (114 μL, 0.933 mmol), 4-formylbenzoic acid (140 mg, 0.933 mmol), 4-methylaniline (100 mg, 0.933 mmol), 4-methoxyaniline (115 mg, 0.933 mmol) and 4-aminobenzoic acid (128 mg, 0.933 mmol) were added into a 50 mL round bottom flask, along with PhMe (20 mL). The mixture was heated at reflux for 12 h, and a Dean-Stark trap was used to remove H_2O. Then, PhMe was removed in vacuo to afford a mixture of nine imines as a yellow solid. This mixture was preadsorbed onto silica gel (approx. 1.5 g) and then added on top of a chromatography column, which was pre-loaded with an approx. 10 cm-high layer of oven-dried silica gel. The column was then wrapped with a heating tape and heated to approx. 50 °C. The elution was performed first with pure hexane (300 mL), then with a 100:1 hexane/EtOAc (v/v, 200 mL) and 10:1 hexane/EtOAc (v/v, 220 mL) mixtures and finally with pure THF (600 mL). Four fractions were isolated. In the first, imine **139** was the dominant product (80% yield, based on an internal standard calculation with 160 mg of the crude product and 20.9 mg of the internal standard, see Figure 2.12). The second fraction contained imine **140** as the major component (12% yield, based on an internal standard calculation with 26 mg of the crude compound and 10.2 mg of the internal standard, see Figure 2.13) with small amounts of **139** (0.4%). The third fraction contained mostly imine **143** (81% yield, based

on an internal standard calculation with 191 mg of the crude material and 21.6 mg of the internal standard, see Figure 2.14). Finally, the fourth fraction contained imines **141** and **148** in 4% and 89% yields, respectively (based on an internal standard calculation with 20 mg of the crude material, mixed with 7.5 mg of the internal standard, see Figure 2.15).

139: ^{1}H NMR ($CDCl_3$, 500 MHz): 8.44 (s, 1H), 7.81−7.80 (d, $^{3}J_{H-H}$=8.0 Hz, 2H), 7.30−7.28 (d, $^{3}J_{H-H}$=7.5 Hz, 2H), 7.22−7.15 (m, 4H), 2.43 (s, 3H), 2.39 (s, 3H) ppm. Spectral data agree with the previous literature report.[17]

140: ^{1}H NMR ($CDCl_3$, 500 MHz): 8.40 (s, 1H), 7.86−7.84 (m, 2H), 7.20−7.12 (m, 4H), 7.02−6.97 (m, 2H) ppm. Spectral data agree with the previous literature report.[18]

143: ^{1}H NMR ($CDCl_3$, 500 MHz): 8.41 (s, 1H), 7.86−7.83 (m, 2H), 7.24−7.21 (m, 2H), 6.99−6.91 (m, 4H), 3.86 (s, 3H), 3.82 (s, 3H) ppm. Spectral data agree with the previous literature report.[19]

141: ^{1}H NMR (DMSO-d_6, 500 MHz): 8.71 (s, 1H), 8.08−8.04 (m, 4H), 7.22 (s, 4H), 2.32 (s, 3H) ppm. Spectral data agree with the previous literature report.[16]

148: ^{1}H NMR (DMSO-d_6, 500 MHz): 8.72 (s, 1H), 8.08−8.04 (m, 4H), 8.00−7.97 (m, 2H), 7.36−7.34 (m, 2H) ppm. Spectral data agree with the previous literature report.[21]

Calculation of the Yields based on the Integration of ^{1}H NMR Spectra

The yield of **139** in the first fraction: the number of moles of internal standard is 20.9 mg ÷ 168.19 g mol^{-1} = 0.124 mmol, the number of moles of **139** is 0.124 mmol × 6.03 = 0.748 mmol, the yield of **139** is 0.748 mmol ÷ 0.933 mmol = 80% (Figure 2.12). In the second fraction: the number of moles of internal standard is 10.2 mg ÷ 168.19 g mol^{-1} = 0.061 mmol, the number of moles of **139** is 0.061 mmol × 0.064 = 0.004 mmol,

the yield of **139** is 0.004 mmol ÷ 0.933 mmol = 0.4% (Figure 2.13). The total yield of **139** is 80% + 0.4% = 80%

The yield of **140**: the number of moles of internal standard is 10.2 mg ÷ 168.19 g mol^{-1} = 0.061 mmol, the number of moles of **140** is 0.061 mmol × 1.81 = 0.110 mmol, the yield of **140** is 0.110 mmol ÷ 0.933 mmol = 12% (Figure 2.13).

The yield of **143**: the number of moles of internal standard is 21.6 mg ÷ 168.19 g mol^{-1} = 0.128 mmol, the number of moles of **143** is 0.128 mmol × 5.91 = 0.756 mmol, the yield of **143** is 0.756 mmol ÷ 0.933 mmol = 81% (Figure 2.14).

The yield of **141**: the number of moles of internal standard is 7.5 mg ÷ 168.19 g mol^{-1} = 0.045 mmol, the number of moles of **141** is 0.045 mmol × 0.037 × 474 mg ÷ 20 mg = 0.036 mmol, the yield of **141** is 0.036 mmol ÷ 0.933 mmol = 4% (Figure 2.15).

The yield of **148**: the number of moles of internal standard is 7.5 mg ÷ 168.19 g mol^{-1} = 0.045 mmol, the number of moles of **148** is 0.045 mmol × 0.83 × 474 mg ÷ 20 mg = 0.832 mmol, the yield of **148** is 0.832 mmol ÷ 0.933 mmol = 89% (Figure 2.15).

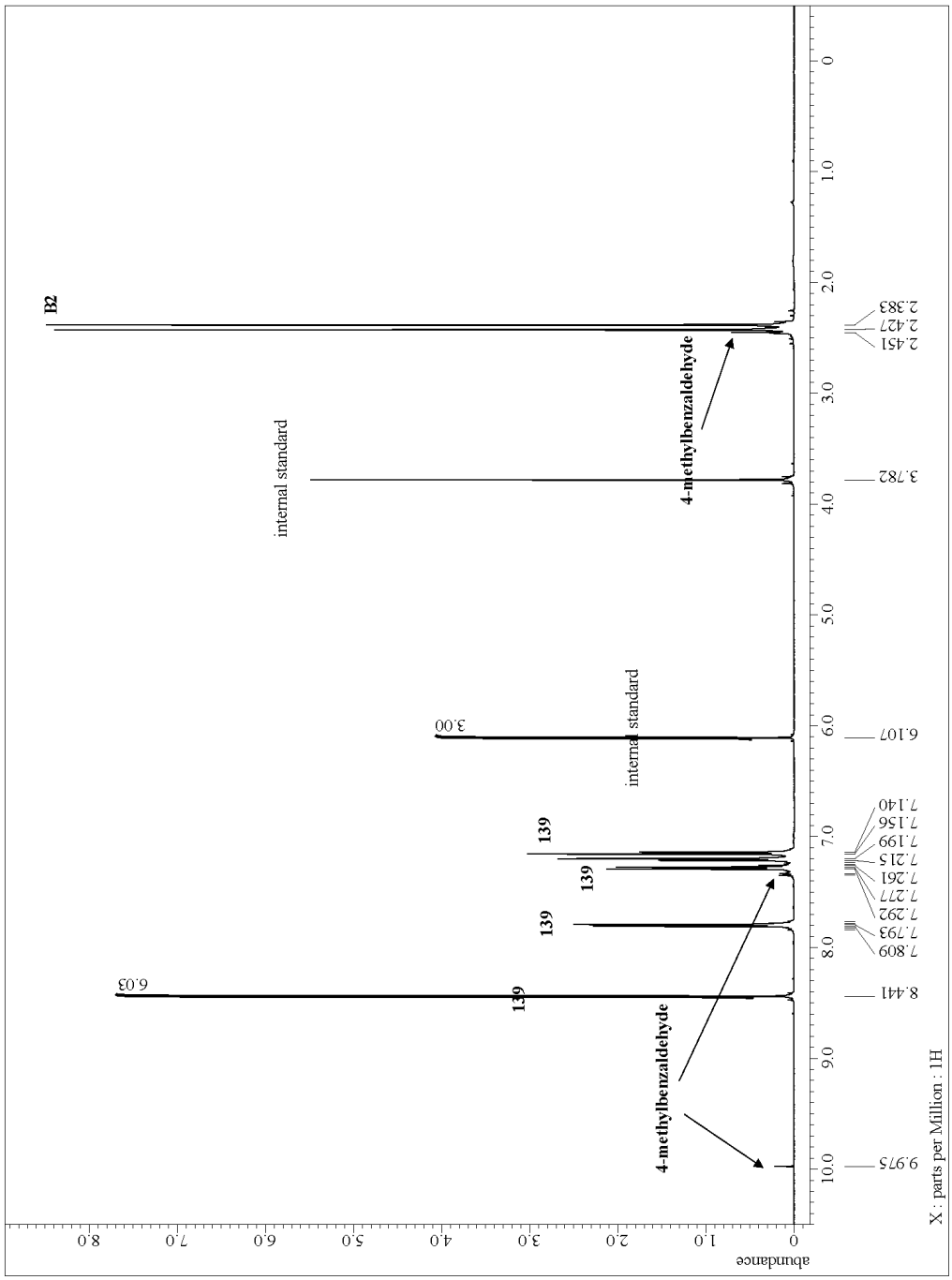

Figure 2.12 ^{1}H NMR spectrum of the first isolated fraction from Experiment #4. Imine **139** is the dominant component.

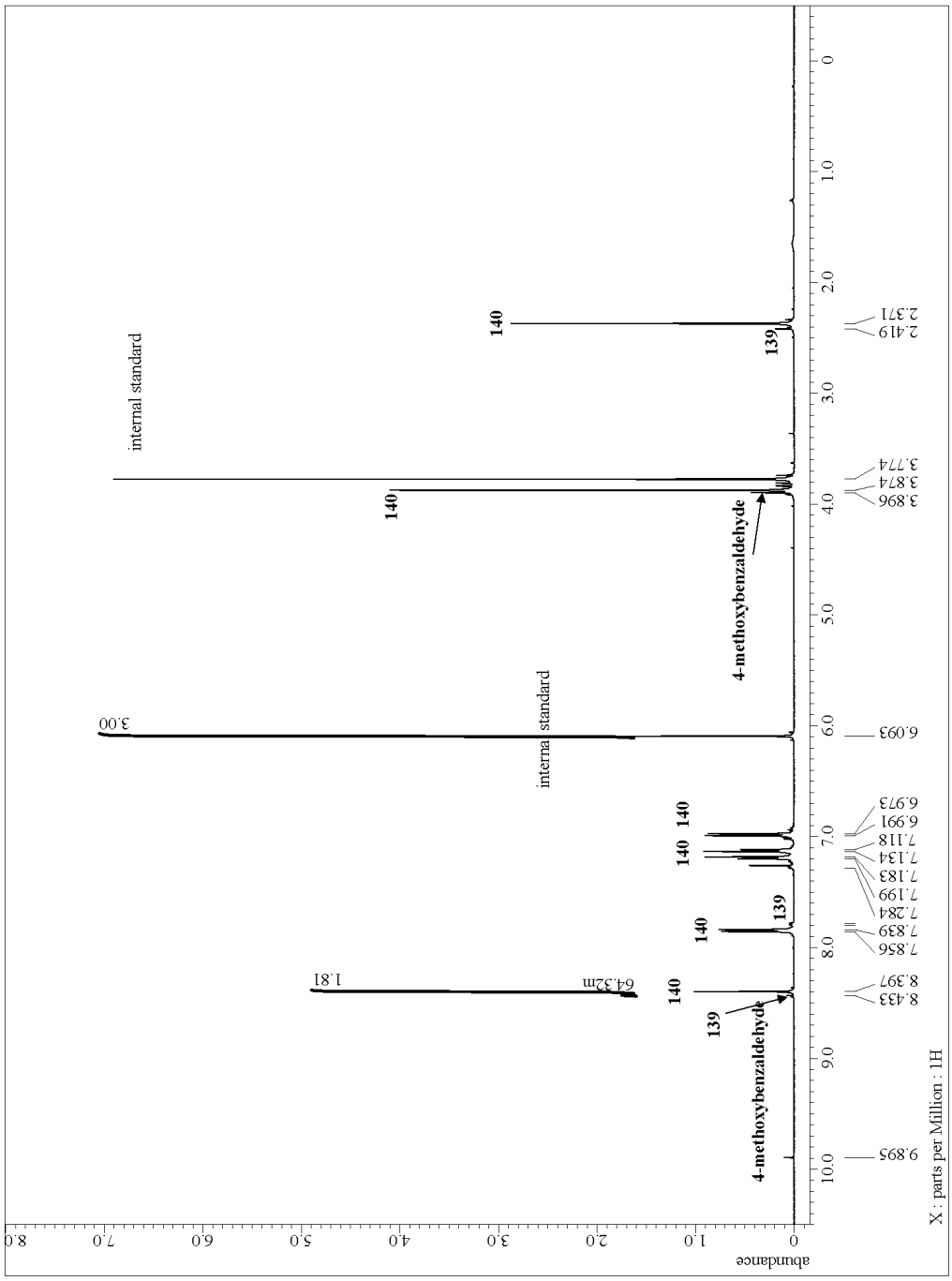

Figure 2.13 ^{1}H NMR spectrum of the second isolated fraction from Experiment #4. Imine **140** is the dominant component, and very small amounts of **139** are present.

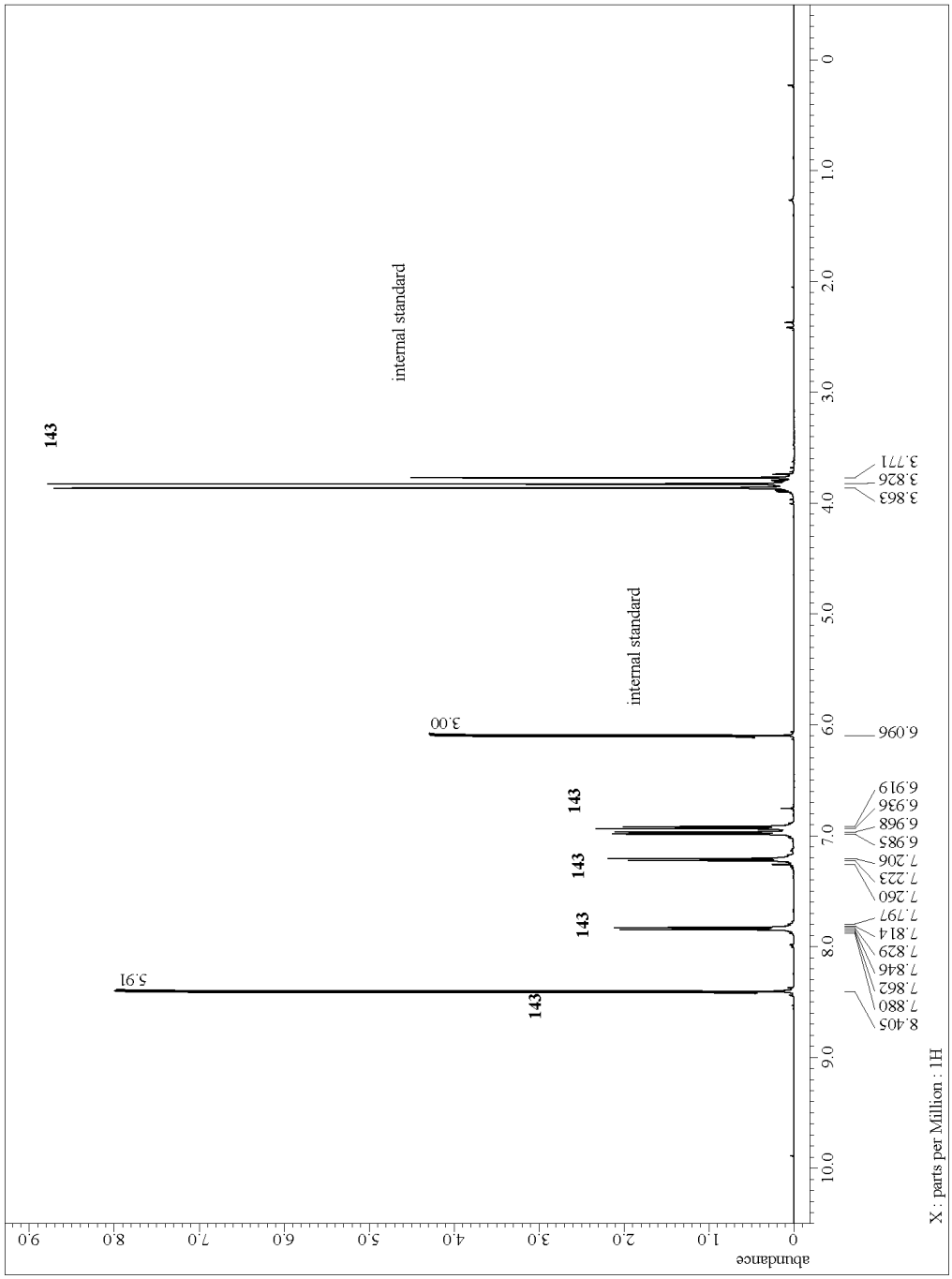

Figure 2.14 ^{1}H NMR spectrum of the third isolated fraction from Experiment #4. Imine **143** is the dominant component.

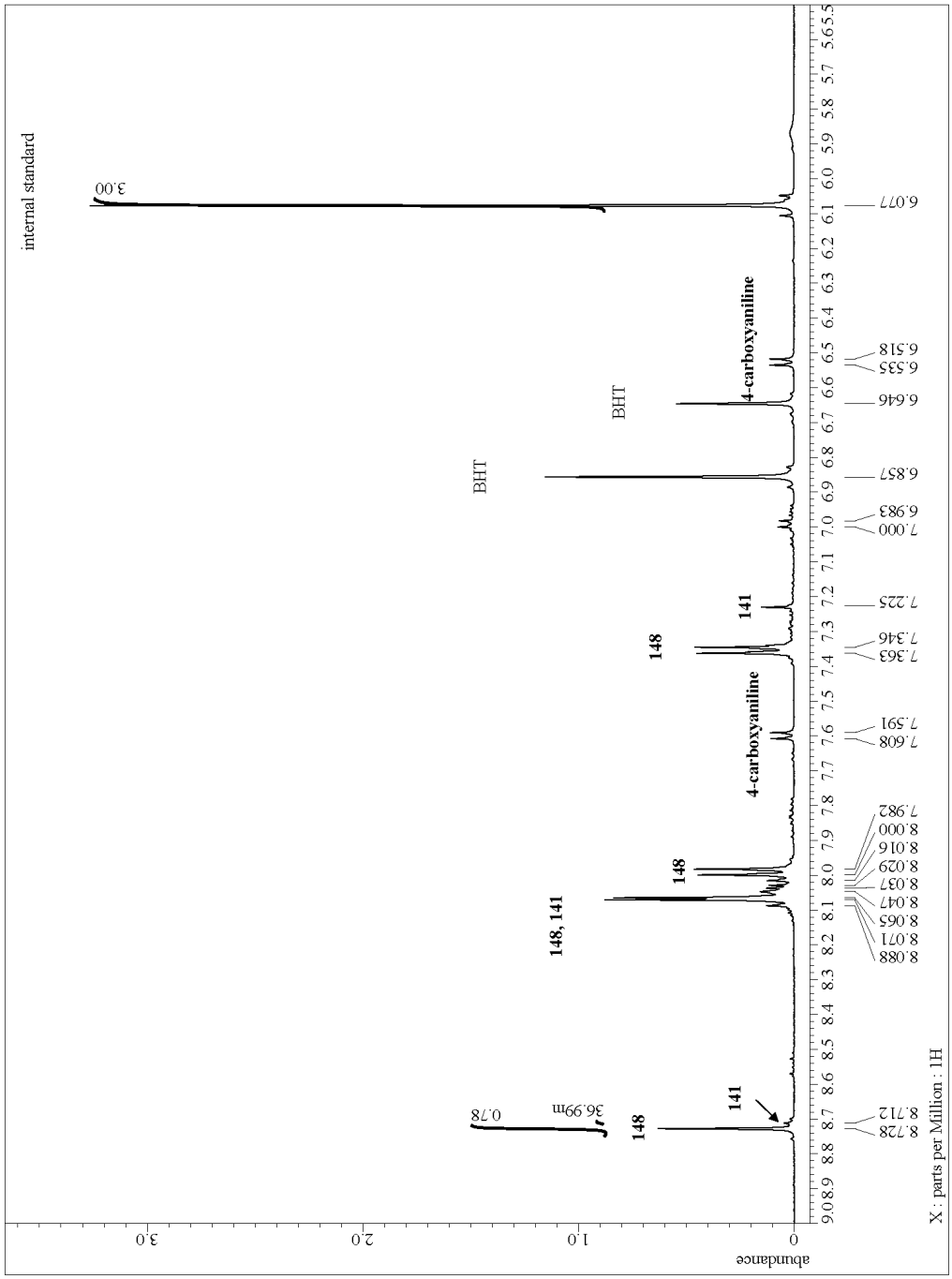

Figure 2.15 ^{1}H NMR spectrum of the fourth isolated fraction from Experiment #4. Imines **141** and **148** are the two major components, with imine **148** being dominant.

2.4.5 Adsorption-Driven Self-Sorting of a [4×4] Imine Library

Experiment #5

4-Bromo-*N*-[(4-bromophenyl)methylene]benzenamine (**134**), 4-Methyl-*N*-[(4-methylphenyl)methylene]benzenamine (**139**), 4-Methoxy-*N*-[(4-methoxyphenyl)methylene]benzenamine (**143**) and 4-[[(4-carboxyphenyl)imino]methyl]benzoic acid (**148**)

Equimolar amounts of 4-bromobenzaldehyde (173 mg, 0.933 mmol), 4-methylbenzaldehyde (110 μL, 0.933 mmol), 4-methoxybenzaldehyde (114 μL, 0.933 mmol), 4-formylbenzoic acid (140 mg, 0.933 mmol), 4-bromoaniline (160 mg, 0.933 mmol), 4-methylaniline (100 mg, 0.933 mmol), 4-methoxyaniline (115 mg, 0.933 mmol) and 4-aminobenzoic acid (128 mg, 0.933 mmol) were added into a 50 mL round bottom flask, along with PhMe (20 mL). The mixture was heated at reflux for 12 h, and a Dean-Stark trap was used to remove H_2O. Then, PhMe was removed in vacuo to afford a mixture of nine imines as a yellow solid. This mixture was preadsorbed onto silica gel (approx. 2.5 g) and then added on top of a chromatography column, which was pre-loaded with an approx. 20 cm-high layer of oven-dried silica gel. The column was then wrapped with a heating tape and heated to approx. 50 °C. The elution was performed first with 10:1 hexane/PhMe (v/v, 220 mL) and 8:1 hexane/PhMe (v/v, 360 mL) mixtures, then with 40:1 hexane/EtOAc (v/v, 205 mL), 10:1 hexane/EtOAc (v/v, 220 mL), and 2:1 hexane/EtOAc (v/v, 150 mL) mixtures, and finally with pure THF (400 mL). Six fractions were isolated. In the first, imine **134** was the dominant product (64% yield, based on an internal standard calculation with 228 mg of the crude product and 25.6 mg of the internal standard, see Figure 2.16). The second fraction contained imines **138** and

135 as the major components (1% and 3% yields, respectively, based on an internal standard calculation with 29 mg of the crude material and 11.6 mg of the internal standard, see Figure 2.17). The third fraction contained mostly imine **139** (78% yield, based on an internal standard calculation with 274 mg of the crude material and 26.4 mg of the internal standard, see Figure 2.18), along with some **134** (3%), **138** (17%), and **135** (13%). The fourth fraction contained small amounts of imines **136** and **140** (5% and 8% yields, respectively, based on an internal standard calculation with 46 mg of the crude material mixed with 15.7 mg of internal standard, Figure 2.19). The fifth fraction contained a small amount of imine **136**, along with much more of imine **143** (1% and 8% yields, respectively, based on an internal standard calculation with 199 mg of the crude material mixed with 22.8 mg of internal standard, Figure 2.20). The final fraction was dominated by imine **148** (76% yield, based on an internal standard calculation with 21.3 mg of the crude sample mixed with 4.4 mg of the internal standard, see Figure 2.21). Trivial amounts of **145** (1%), **137** (2%), and **141** (2%) could also be identified in this last fraction.

134: ^{1}H NMR ($CDCl_3$, 500 MHz): 8.37 (s, 1H), 7.77−7.75 (d, $^{3}J_{H-H}$=8.1 Hz, 2H), 7.62−7.60 (d, $^{3}J_{H-H}$=8.6 Hz, 2H), 7.51−7.50 (d, $^{3}J_{H-H}$=8.6 Hz, 2H), 7.09−7.08 (*d*, $^{3}J_{H-H}$=8.6 Hz, 2H) ppm. Spectral data agree with the previous literature report.[22]

138: ^{1}H NMR ($CDCl_3$, 500 MHz): 8.42 (s, 1H), 7.78−7.76 (d, $^{3}J_{H-H}$=8.6 Hz, 2H), 7.61−7.60 (d, $^{3}J_{H-H}$=8.6 Hz, 2H), 7.21−7.14 (m, 4H), 2.38 (s, 3H) ppm. Spectral data agree with the previous literature report.[23]

145: ^{1}H NMR (DMSO-d_6, 500 MHz): 8.64 (s, 1H), 7.98−7.97 (d, $^{3}J_{H-H}$=8.1 Hz, 2H), 7.90−7.74 (m, 4H), 7.33−7.32 (d, $^{3}J_{H-H}$=8.6 Hz, 2H) ppm. Spectral data agree with

the previous literature report.[20]

135: ^{1}H NMR ($CDCl_3$, 500 MHz): 8.38 (s, 1H), 7.77−7.60 (m, 4H), 7.52−7.50 (m, 2H), 7.10−7.08 (m, 2H), 2.37 (s, 3H), 2.39 (s, 3H) ppm. Spectral data agree with the previous literature report.[24]

139: ^{1}H NMR ($CDCl_3$, 500 MHz): 8.44 (s, 1H), 7.81−7.80 (d, $^{3}J_{H-H}$=8.0 Hz, 2H), 7.30−7.28 (d, $^{3}J_{H-H}$=7.5 Hz, 2H), 7.22−7.15 (m, 4H), 2.43 (s, 3H), 2.39 (s, 3H) ppm. Spectral data agree with the previous literature report.[17]

136: ^{1}H NMR ($CDCl_3$, 500 MHz): 8.34 (s, 1H), 7.85−7.83 (d, $^{3}J_{H-H}$=8.6 Hz, 2H), 7.50−7.48 (d, $^{3}J_{H-H}$=8.6 Hz, 2H), 7.08−7.06 (d, $^{3}J_{H-H}$=8.6 Hz, 2H), 7.00−6.98 (d, $^{3}J_{H-H}$=8.6 Hz, 2H), 3.88 (s, 3H) ppm. Spectral data agree with the previous literature report.[25]

140: ^{1}H NMR ($CDCl_3$, 500 MHz): 8.40 (s, 1H), 7.86−7.84 (m, 2H), 7.20−7.12 (m, 4H), 7.02−6.97 (m, 2H) ppm. Spectral data agree with the previous literature report.[18]

143: ^{1}H NMR ($CDCl_3$, 500 MHz): 8.41 (s, 1H), 7.86−7.83 (m, 2H), 7.24−7.21 (m, 2H), 6.99−6.91 (m, 4H), 3.86 (s, 3H), 3.82 (s, 3H) ppm. Spectral data agree with the previous literature report.[19]

137: ^{1}H NMR (DMSO-d_6, 500 MHz): 8.72 (s, 1H), 8.09−7.99 (m, 4H), 7.62−7.60 (d, $^{3}J_{H-H}$=8.6 Hz, 2H), 7.28−7.27 (d, $^{3}J_{H-H}$=8.6 Hz, 2H) ppm. Spectral data agree with the previous literature report.[16]

141: ^{1}H NMR (DMSO-d_6, 500 MHz): 8.71 (s, 1H), 8.08−8.04 (m, 4H), 7.22 (s, 4H), 2.32 (s, 3H) ppm. Spectral data agree with the previous literature report.[16]

148: ^{1}H NMR (DMSO-d_6, 500 MHz): 8.72 (s, 1H), 8.08−8.04 (m, 4H), 8.00−7.97 (m, 2H), 7.36−7.34 (m, 2H) ppm. Spectral data agree with the previous literature report.[21]

Calculation of the Yields based on the Integration of ^{1}H NMR Spectra

The yield of **134** in the first fraction: the number of moles of internal standard is 25.6 mg ÷ 168.19 g mol^{-1} = 0.152 mmol, the number of moles of **134** is 0.152 mmol × 3.92 = 0.596 mmol, the yield of **134** is 0.596 mmol ÷ 0.933 mmol = 64% (Figure 2.16). In the third fraction: the number of moles of internal standard is 26.4 mg ÷ 168.19 g mol^{-1} = 0.157 mmol, the number of moles of **134** is 0.157 mmol × 0.17 = 0.027 mmol, the yield of **134** is 0.027 mmol ÷ 0.933 mmol = 3% (Figure 2.18). Total yield of **134** is 64% + 3% = 67%.

The yield of **138**: the number of moles of internal standard is 11.6 mg ÷ 168.19 g mol^{-1} = 0.069 mmol, the number of moles of **138** is 0.069 mmol × 0.091 = 0.006 mmol, the yield of **138** is 0.006 mmol ÷ 0.933 mmol = 1% (Figure 2.17). In the third fraction: the number of moles of internal standard is 26.4 mg ÷ 168.19 g mol^{-1} = 0.157 mmol, the number of moles of **138** is 0.157 mmol × 0.98 = 0.154 mmol, the yield of **138** is 0.154 mmol ÷ 0.933 mmol = 17% (Figure 2.18). Total yield of **138** is 1% + 17% = 18%.

The yield of **135** in the second fraction: the number of moles of internal standard is 11.6 mg ÷ 168.19 g mol^{-1} = 0.069 mmol, the number of moles of **135** is 0.069 mmol × 0.43 = 0.030 mmol, the yield of **135** is 0.030 mmol ÷ 0.933 mmol = 3% (Figure 2.17). In the third fraction: the number of moles of internal standard is 26.4 mg ÷ 168.19 g mol^{-1} = 0.157 mmol, the number of moles of **135** is 0.157 mmol × 0.77 = 0.121 mmol, the yield of **135** is 0.121 mmol ÷ 0.933 mmol = 13% (Figure 2.18). Total yield of **135** is 3% + 13% = 16%.

The yield of **139**: the number of moles of internal standard is 26.4 mg ÷ 168.19 g mol^{-1} = 0.157 mmol, the number of moles of **139** is 0.157 mmol × 4.62 = 0.725 mmol,

the yield of **139** is 0.725 mmol ÷ 0.933 mmol = 78% (Figure 2.18).

The yield of **136** in the fourth fraction: the number of moles of internal standard is 15.7 mg ÷ 168.19 g mol^{-1} = 0.093 mmol, the number of moles of **136** is 0.093 mmol × 0.47 = 0.044 mmol, the yield of **136** is 0.044 mmol ÷ 0.933 mmol = 5% (Figure 2.19). In the fifth fraction: the number of moles of internal standard is 22.8 mg ÷ 168.19 g mol^{-1} = 0.136 mmol, the number of moles of **136** is 0.136 mmol × 0.050 = 0.007 mmol, the yield of **136** is 0.007 mmol ÷ 0.933 mmol = 1% (Figure 2.20). The total yield of **136** is 5% + 1% = 6%.

The yield of **140**: the number of moles of internal standard is 15.7 mg ÷ 168.19 g mol^{-1} = 0.093 mmol, the number of moles of **140** is 0.093 mmol × 0.85 = 0.079 mmol, the yield of **140** is 0.079 mmol ÷ 0.933 mmol = 8% (Figure 2.19).

The yield of **143**: the number of moles of internal standard is 22.8 mg ÷ 168.19 g mol^{-1} = 0.136 mmol, the number of moles of **143** is 0.136 mmol × 5.52 = 0.751 mmol, the yield of **143** is 0.751 mmol ÷ 0.933 mmol = 80% (Figure 2.20).

The yield of **137**: the number of moles of internal standard is 4.4 mg ÷ 168.19 g mol^{-1} = 0.026 mmol, the number of moles of **137** is 0.026 mmol × (0.078 ÷ 2) × 412 mg ÷ 21.3 mg = 0.020 mmol, the yield of **137** is 0.020 mmol ÷ 0.933 mmol = 2% (Figure 2.21).

The yield of **141**: the number of moles of internal standard is 4.4 mg ÷ 168.19 g mol^{-1} = 0.026 mmol, the number of moles of **141** is 0.026 mmol × (0.12 ÷ 4) × 412 mg ÷ 21.3 mg = 0.015 mmol, the yield of **141** is 0.015 mmol ÷ 0.933 mmol = 2% (Figure 2.21).

The yield of **148**: the number of moles of internal standard is 4.4 mg ÷ 168.19 g

mol^{-1} = 0.026 mmol, the number of moles of **148** is 0.026 mmol × 1.48 ×412 mg ÷ 21.3 mg − 0.015 (mmol of **141**) − 0.020 (mmol of **137**) = 0.709 mmol, the yield of **148** is 0.709 mmol ÷ 0.933 mmol = 76% (Figure 2.21).

The yield of **145**: the number of moles of internal standard is 4.4 mg ÷ 168.19 g mol^{-1} = 0.026 mmol, the number of moles of **145** is 0.026 mmol × 0.026 × 412 mg ÷ 21.3 mg = 0.013 mmol, the yield of **145** is 0.013 mmol ÷ 0.933 mmol = 1% (Figure 2.21).

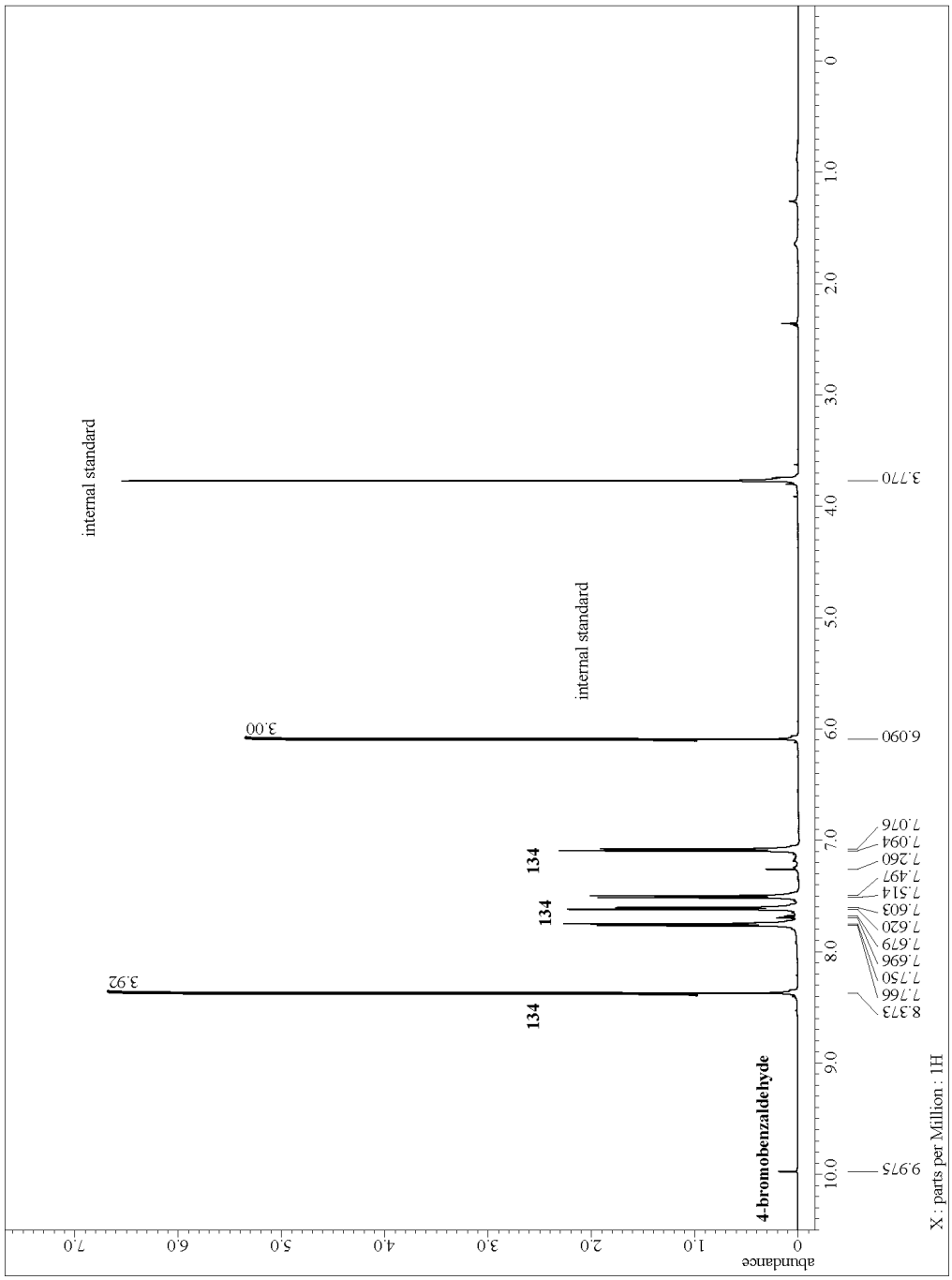

Figure 2.16 ^{1}H NMR spectrum of the first isolated fraction from Experiment #5. Imine **134** is the major product.

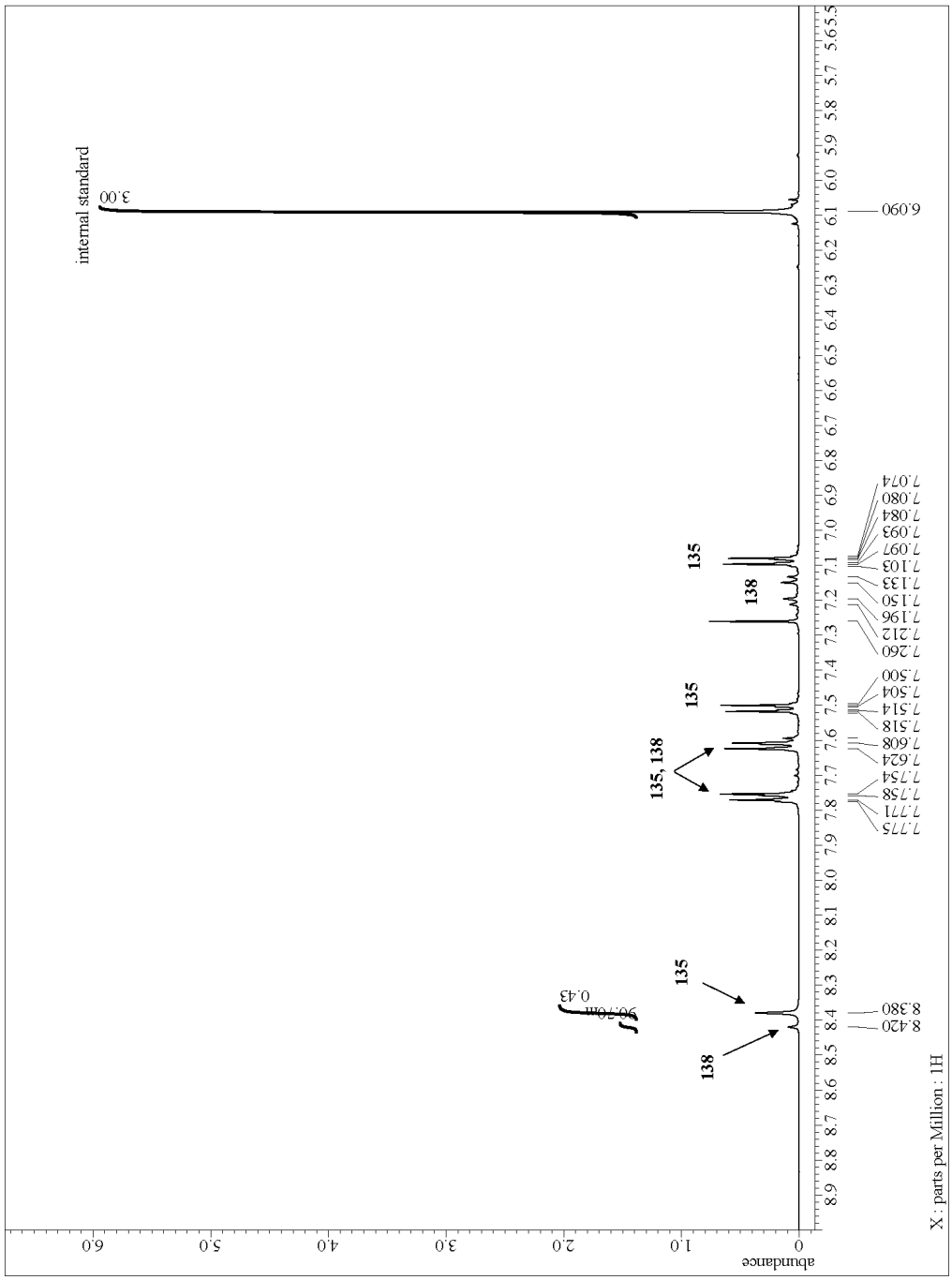

Figure 2.17 ^{1}H NMR spectrum of the second isolated fraction from Experiment #5. Imines **138** and **135** are the two major components.

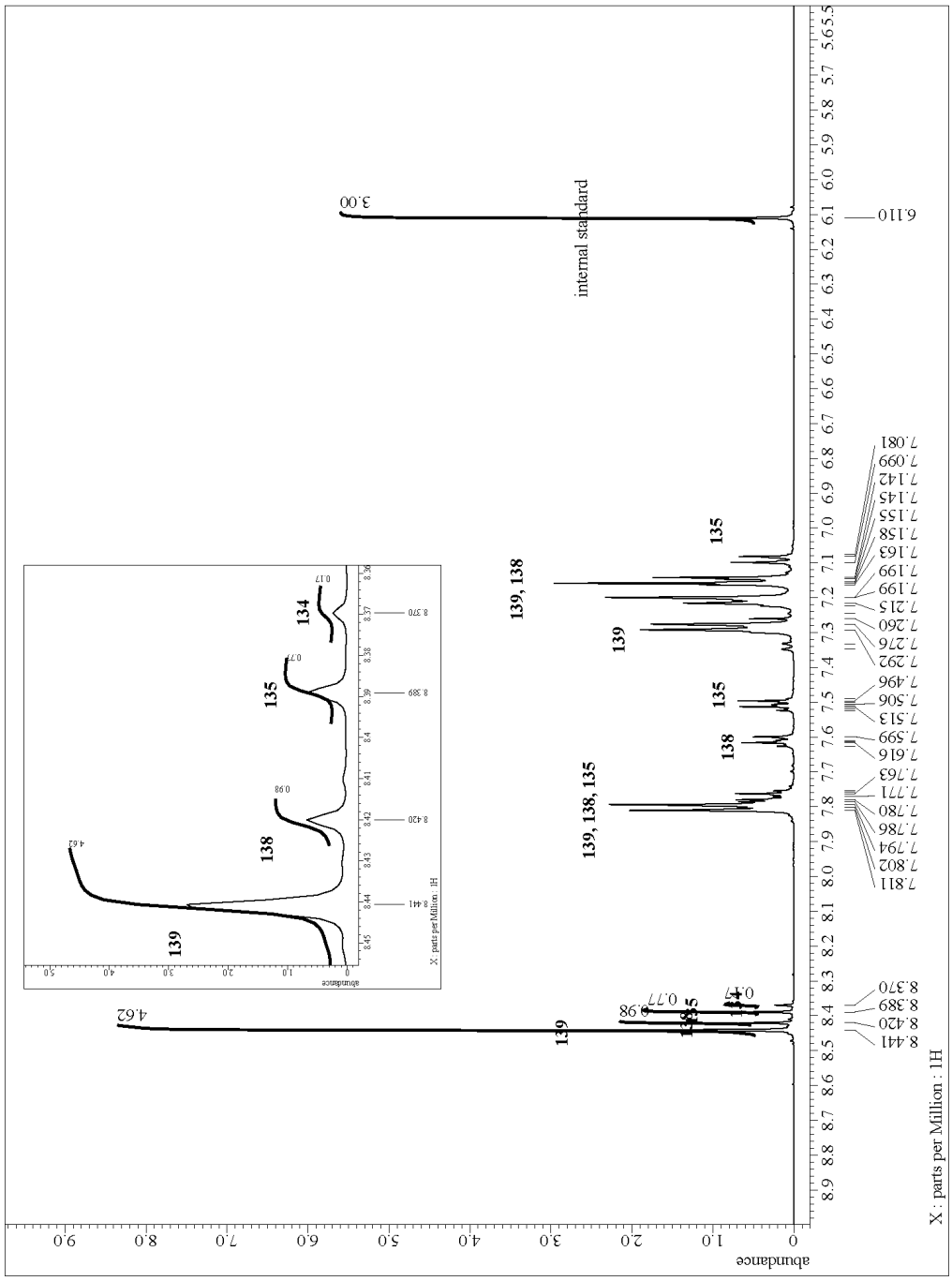

Figure 2.18 ^{1}H NMR spectrum of the third isolated fraction from Experiment #5. Imines **134**, **138**, **135**, and **95** are the major components.

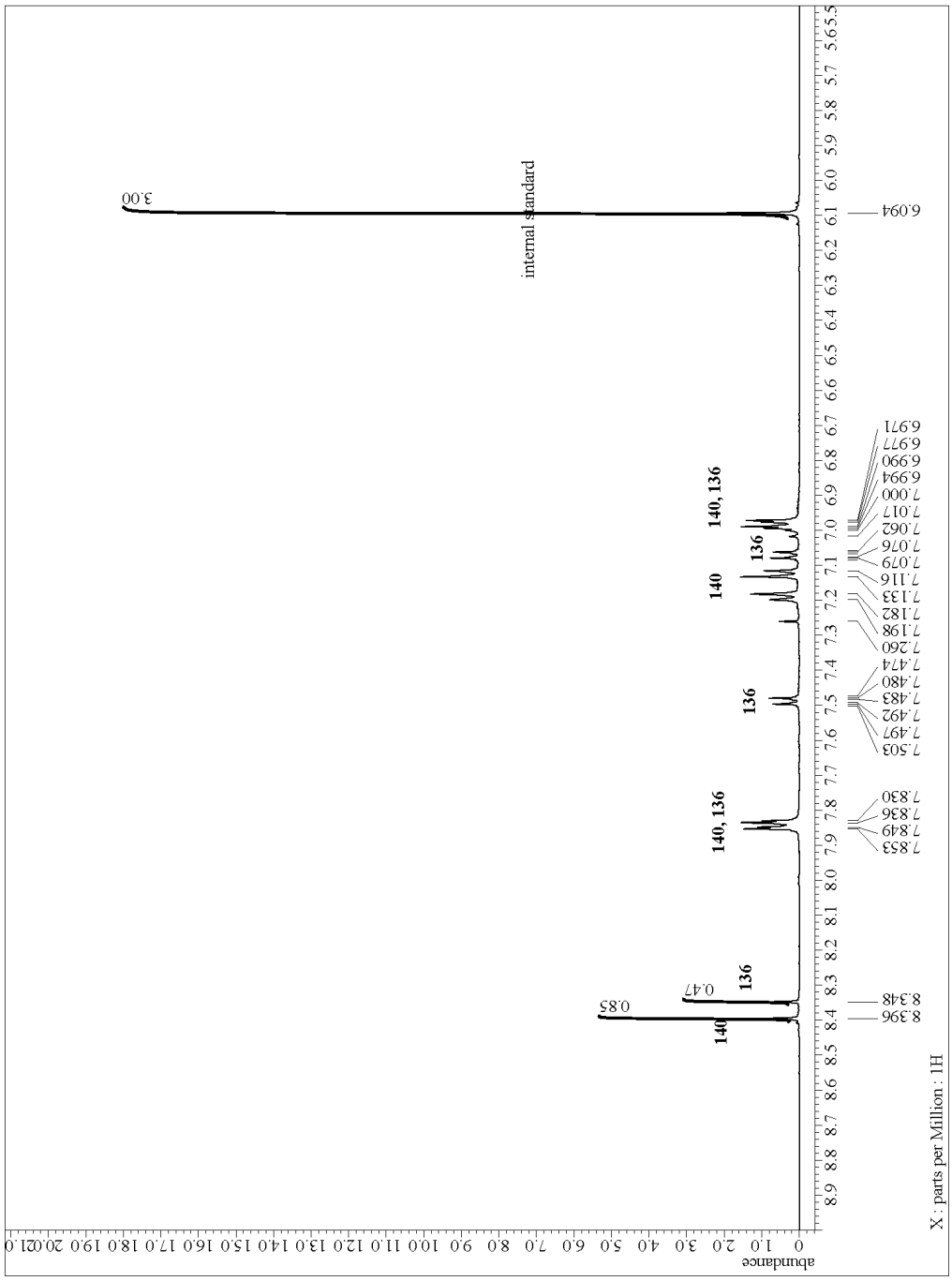

Figure 2.19 ^{1}H NMR spectrum of the fourth isolated fraction from Experiment #4. Imines **136** and **140** are the two major components.

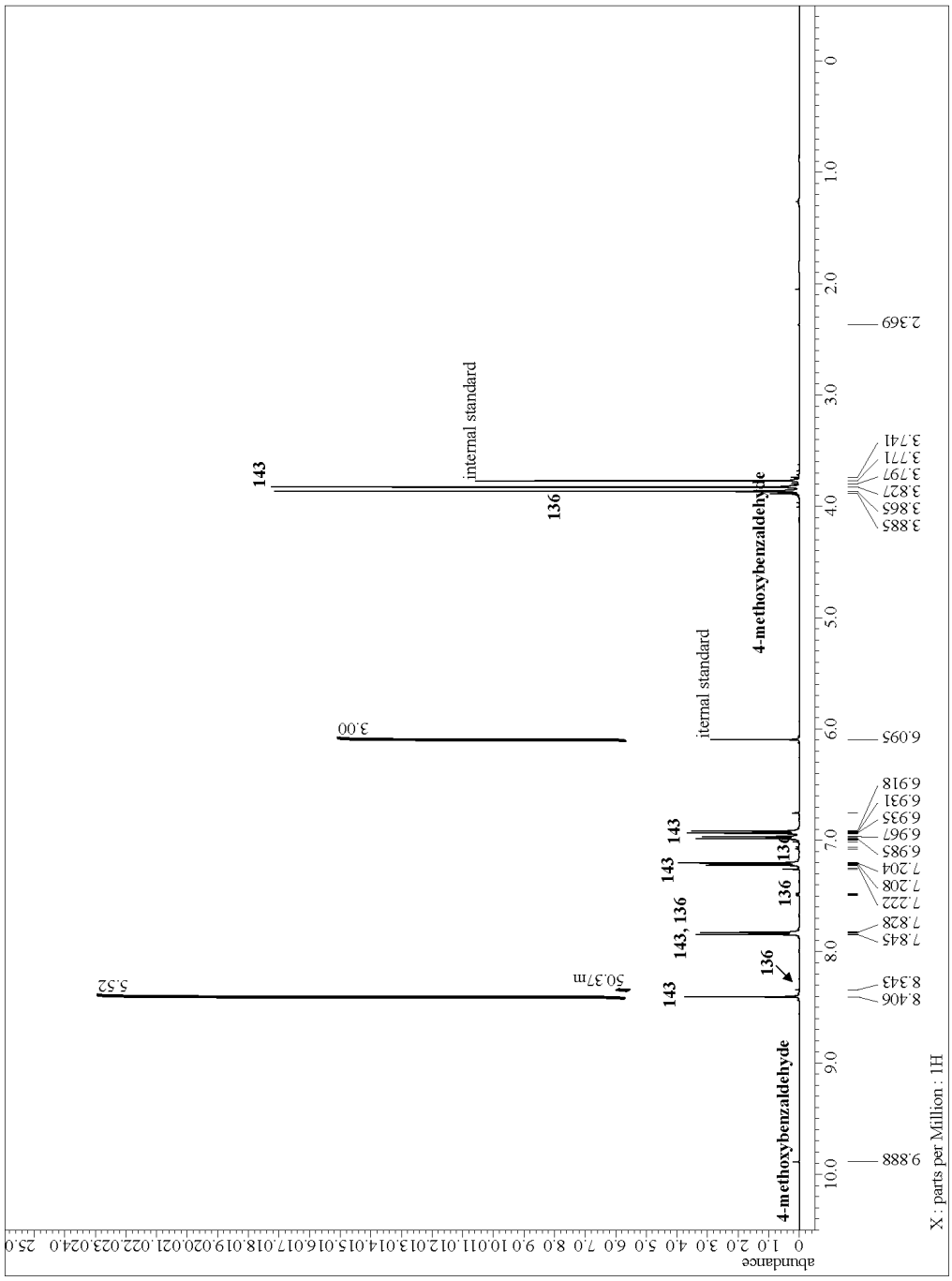

Figure 2.20 ^{1}H NMR spectrum of the fifth isolated fraction from Experiment #5. Imines **136** and **143** are the two major components, with imine **143** being dominant.

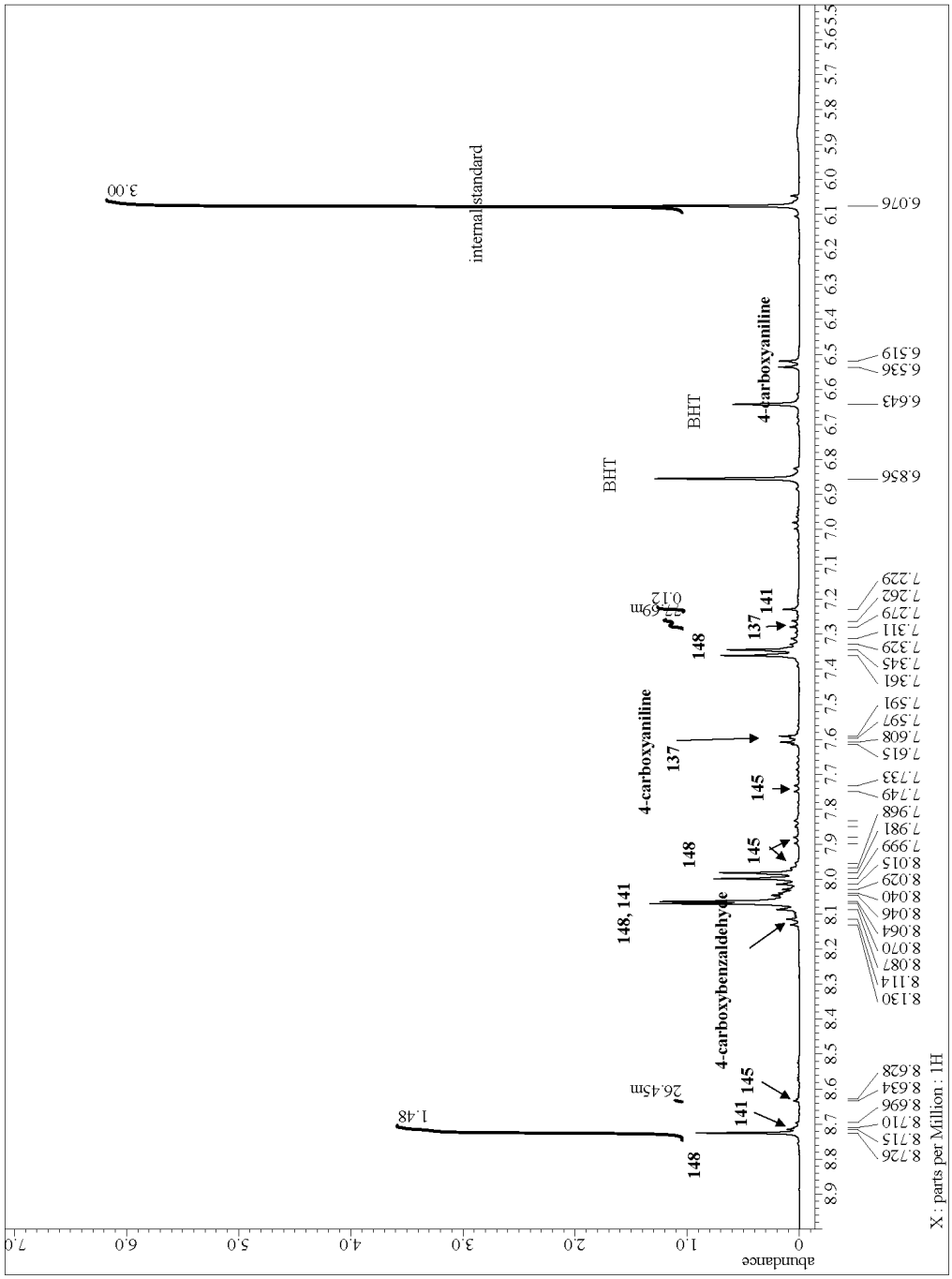

Figure 2.21 ^{1}H NMR spectrum of the sixth isolated fraction from Experiment #5. Imines **137**, **141**, and **145** are the minor constituents, and imine **148** is the major component.

2.4.6 Transmutation of Imines During Column Chromatography

Transmutation of a Mixture of 4-[(Phenylimino)methyl]benzoic acid (**150**) and 4-[(Phenylmethylene)amino]benzoic acid (**149**)

Equimolar amounts of imines **150** (180 mg, 0.799 mmol)[26] and **149** (180 mg, 0.799 mmol)[22] were mixed with silica gel (approx. 0.9 g) and then added on top of a chromatography column, which was pre-loaded with an approx. 10 cm-high layer of oven-dried silica gel. The column was then wrapped with a heating tape and heated to approx. 50 °C. The elution was performed first with a 40:1 hexane/EtOAc (v/v, 400 mL) mixture and then with pure THF (200 mL). Two fractions were isolated. After evaporating the solvent, imine **116** was the dominant product (133 mg, 94% yield) in the first fraction. The second fraction contained imine **148** (202 mg, 92% yield) after using 1-butanol to remove the stabilizer in THF.

148: ^{1}H NMR (DMSO-d_6, 500 MHz): 8.72 (s, 1H), 8.08−8.04 (m, 4H), 8.00−7.97 (m, 2H), 7.36−7.34 (m, 2H) ppm. Spectral data agree with the previous literature report.[21]

116: ^{1}H NMR ($CDCl_3$, 500 MHz): 8.47 (s, 1H), 7.92−7.89 (m, 2H), 7.49−7.46 (m, 3H), 7.42−7.39 (m, 2H), 7.24−7.21 (m, 3H) ppm. Spectral data agree with the previous literature report.[27]

2.5 References

[1] Hsu, C.-W.; Miljanić, O. Š. *Angew. Chem. Int. Ed.* **2015**, *54*, 2219−2222.

[2] For relevance of differential adsorption for the origin of life, see: a) Zaia, D. A. M. *Amino Acids* **2004**, *27*, 113−118; b) Sowerby, S. J.; Cohn, C. A.; Heckl, W. M.; Holm, N. G. *Proc*. *Natl*. *Acad*. *Sci*. *USA* **2001**, *98*, 820−822.

[3] (a) Reek, J. N. H.; Otto, S. *Dynamic Combinatorial Chemistry*, Wiley-VCH, Weinheim, **2010**; (b) Miller, B. L. *Dynamic Combinatorial Chemistry In Drug Discovery, Bioorganic Chemistry, and Materials Science*, Wiley, Hoboken, **2009**; (c) Corbett, P. T.; Leclaire, J.; Vial, L.; West, K. R.; Wietor, J.-L.; Sanders, J. K. M.; Otto, S. *Chem*. *Rev*. **2006**, *106*, 3652–3711; (d) Rowan, S. J.; Cantrill, S. J.; Cousins, G. R. L.; Sanders, J. K. M.; Stoddart, J. F. *Angew*. *Chem*. *Int*. *Ed*. **2002**, *41*, 898–952; *Angew*. *Chem*. **2002**, *114*, 938–993; (e) Ludlow, R. F.; Otto, S. *Chem*. *Soc*. *Rev*. **2008**, *37*, 101–108.

[4] Ji, Q.; Lirag, R. C.; Miljanić, O. Š. *Chem*. *Soc*. *Rev*. **2014**, *43*, 1873–1884.

[5] (a) Safont-Sempere, M. M.; Fernandez, G.; Würthner, F. *Chem*. *Rev*. **2011**, *111*, 5784–5814; (b) Osowska, K.; Miljanić O. Š. *Synlett* **2011**, 1643–1648; (c) Ghosh, S.; Isaacs, L. in *Dynamic Combinatorial Chemistry in Drug Discovery, Bioorganic Chemistry, and Materials Science* (Ed.: B. L. Miller), Wiley, Hoboken, **2010**, pp. 155–168; (d) Northrop, B. H.; Zheng, Y.-R.; Chi, K.-W.; Stang, P. J. *Acc*. *Chem*. *Res*. **2009**, *42*, 1554–1563; (e) Nitschke, J. R. *Acc*. *Chem*. *Res*. **2007**, *40*, 103–112.

[6] (a) Huerta, F. F.; Minidis, A. B. E.; Bäckvall, J. E. *Chem*. *Soc*. *Rev*. **2001**, *30*, 321–331; (b) Vongvilai, P.; Angelin, M.; Larsson, R.; Ramström, O. *Angew*. *Chem*. *Int*. *Ed*. **2007**, *46*, 948–950; *Angew*. *Chem*. **2007**, *119*, 966–968; (c) Vongvilai, P.; Larsson, R.; Ramström, O. *Adv*. *Synth*. *Catal*. **2008**, *350*, 448–452; (d) Vongvilai, P.; Ramström, O. *J*. *Am*. *Chem*. *Soc*. **2009**, *131*, 14419–14425; (e) Sakulsombat, M.; Vongvilai, P.; Ramström, O. *Org*. *Biomol*. *Chem*. **2011**, *9*, 1112–1117; (f) Sakulsombat, M.; Zhang, Y.; Ramström, O. *Chem*. *Eur*. *J*. **2012**, *18*, 6129–6132; (g) Zhang, Y.; Hu, L.; Ramström, O. *Chem*. *Commun*. **2013**, *49*, 1805–1807.

[7] (a) Patzke, V.; von Kiedrowski, G. *ARKIVOC* **2007**, 293–310; (b) del Amo, V.; Philp, D. *Chem*. *Eur*. *J*. **2010**, *16*, 13304–13318; (c) del Amo, V.; Slawin, A. M. Z.; Philp, D. *Org*. *Lett*. **2008**, *10*, 4589–4592; (d) Sadownik, J. W.; Philp, D. *Angew*. *Chem*. *Int*. *Ed*. **2008**, *47*, 9965–9970; (e) Allen, V. C.; Robertson, C. C.; Turega, S. M.; Philp, D. *Org*. *Lett*. **2010**, *12*, 1920–1923.

[8] Osowska, K.; Miljanić, O. Š. *J*. *Am*. *Chem*. *Soc*. **2011**, *133*, 724–726.

[9] (a) Ji, Q.; El-Hamdi, N.; Miljanić, O. Š. *J*. *Chem*. *Educ*. **2014**, *91*, 830–833; (b) Ji, Q.; Miljanić, O. Š. *J*. *Org*. *Chem*. **2013**, *78*, 12710–12716; (c) Osowska, K.; Miljanić, O. Š. *Angew*. *Chem*. *Int*. *Ed*. **2011**, *50*, 8345–8349; See also: (d) Herrmann, A. *Chem*. *Eur*. *J*. **2012**, *18*, 8568–8577; (e) Buchs (née Levrand), B.; Fieber, W.; Vigouroux-Elie, F.; Sreenivasachary, N.; Lehn, J.-M.; Herrmann, A. *Org*. *Biomol*. *Chem*. **2011**, *9*, 2906–2919; (f) Buchs (née Levrand), B.; Godin, G.;

Trachsel, A.; de Saint Laumer, J.-Y.; Lehn, J.-M.; Herrmann, A. *Eur*. *J*. *Org*. *Chem*. **2011**, 681–695.

[10] (a) Lirag, R. C.; Osowska, K.; Miljanić, O. Š. *Org*. *Biomol*. *Chem*. **2012**, *10*, 4847–4850; (b) Hutin, M.; Cramer, C. J.; Gagliardi, L.; Shahi, A. R. M.; Bernardinelli, G.; Cerny, R.; Nitschke, J. R. *J*. *Am*. *Chem*. *Soc*. **2007**, *129*, 8774–8780; (c) Cantrill, S. J.; Chichak, K. S.; Peters, A. J.; Stoddart, J. F. *Acc*. *Chem*. *Res*. **2005**, *38*, 1–9; (d) Meyer, C. D.; Forgan, R. S.; Chichak, K. S.; Peters, A. J.; Tangchaivang, N.; Cave, G. W. V.; Khan, S. I.; Cantrill, S. J.; Stoddart, J. F. *Chem*. *Eur*. *J*. **2010**, *16*, 12570–12581.

[11] (a) Vantomme, G.; Hafezia, N.; Lehn, J.-M. *Chem*. *Sci*. **2014**, *5*, 1475–1483; (b) Hafezi, N.; Lehn, J.-M. *J*. *Am*. *Chem*. *Soc*. **2012**, *134*, 12861–12868; (c) Pérez-Fernández, R.; Pittelkow, M.; Belenguer, A. M.; Sanders, J. K. M. *Chem. Commun.* **2008**, 1738–1740.

[12] (a) Ciesielski, A.; El Garah, M.; Haar, S.; Kovaříček, P.; Lehn, J.-M.; Samorì, P. *Nat*. *Chem*. **2014**, *5*, 1017–1023; For resin-bound DCLs, see: (b) Gromova, A. V.; Ciszewski, J. M.; Miller, B. L. *Chem*. *Commun*. **2012**, *48*, 2131–2133; (c) McNaughton, B. R.; Miller, B. L. *Org*. *Lett*. **2006**, *8*, 1803–1806; See also: (d) Belenguer, A. M.; Friščić, T.; Daya, G. M.; Sanders, J. K. M. *Chem*. *Sci*. **2011**, *2*, 696–700.

[13] Strictly speaking, column chromatography sorts compounds not based on their polarity, but on their affinity for silica gel. Although the two concepts are not the same, there is a strong correlation between them and—in the jargon of preparative

organic chemistry—the two terms are used interchangeably with polar compounds being defined as having a large affinity for silica gel. For the sake of brevity, we will continue this tradition and use the term “polar” to signify compounds which we experimentally found to elute later.

[14] Smith, R. M. *Retention and Selectivity in Liquid Chromatography: Prediction, Standardisation and Phase Comparisons*; Elsevier Science, 1995.

[15] Jin, Y.; Yu, C.; Denman, R. J.; Zhang, W. *Chem. Soc. Rev.* **2013**, *42*, 6634–6654.

[16] (a) Marinković, A. D.; Jovanović, B. Ž.; Assaleh, F. H.; Vajs, V. V.; Juranić, M. I. *J. Mol. Struct.* **2012**, *1011*, 158−165; (b) Zhdanov, Y. A.; Minkin, V. I.; Medyantseva, E. A. *Zh. Obshch. Khim.* **1965**, *35*, 1280−1287.

[17] Bolognese, A.; Diurno, M. V.; Mazzoni, O.; Giordano, F. *Tetrahedron* **1991**, *47*, 7417−7428.

[18] Donthiri, R. R.; Patil, R. D.; Adimurthy, S. *Eur. J. Org. Chem.* **2012**, 4457−4460.

[19] Suresh, R.; Kamalakkannan, D.; Ranganathan, K.; Arulkumaran, R.; Sundararajan, R.; Sakthinathan, S. P.; Vijayakumar, S.; Sathiyamoorthi, K.; Mala, V.; Vanangamudi, G.; Thirumurthy, K.; Mayavel, P.; Thirunarayanan, G. *Spectrochim. Acta, Part A* **2013**, *101*, 239−248.

[20] Walsh, O. M.; Meegan, M. J.; Predergast, R. M.; Al Nakib, T. *Eur. J. Med. Chem.* **1996**, *31*, 989−1000.

[21] Idage, S. B.; Idage, B. B.; Vernekar, S. P. *Polym. Bull.* **1989**, *22*, 371−378.

[22] Marin, L.; Harabagiu, V.; van der Lee, A.; Arvinte, A.; Barboiu, M. *J. Mol. Struct.* **2013**, *1049*, 377−385.

[23] Amaya, T.; Ito, T.; Hirao, T. *Tetrahedron Lett.* **2013**, *54*, 2409−2411.

[24] Naeimi, H.; Rabiei, K. *J*. *Chin*. *Chem*. *Soc*. **2012**, *59*, 208−212.

[25] Miyamura, H.; Morita, M.; Inasaki, T.; Kobayashi, S. *Bull*. *Chem*. *Soc*. *Jpn*. **2011**, *84*, 588−599.

[26] Tabei, K.; Saitou, E. *Bull*. *Chem*. *Soc*. *Jpn*. **1969**, *42*, 2693−2694.

[27] Jiang, L.; Jin, L.; Tian, H.; Yuan, X.; Yu, X.; Xu, Q. *Chem*. *Comm*. **2011**, *47*, 10833−10835.

3 Chapter Three: Iterative Self-sorting of Dynamic Imine Libraries under Three Orthogonal Stimuli

3.1 Introduction

Nature displays plenty of scenarios regarding simplification of complex molecular pools to several molecules or some sub-systems with higher order. For example, oil−water mixture always sorts into oil and water for two isolated layers ultimately; the formation of micelle also manifests the high order of system after the rearrangement of detergent molecules. These phenomena and similar concepts have been classified as "self-sorting" by Isaacs and other research groups since 2003.[1]

Chemists applied the dynamic combinatorial chemistry (DCC)[2] to imitate the same phenomena by utilizing the reversible bond formation such as disulfide bond,[3] imino bond,[4,5] and metal-ligand interaction,[6] to manipulate the direction of equilibrium of components in the systems under thermodynamic or kinetic control. Sanders, Nitschke, and Otto's groups have demonstrated that under thermodynamic control, the redistributed components can result in the most stable species from the dynamic system and form higher order systems.[7] Schalley and Schmittel's groups displayed the integrative/completive self-sorting processes in highly complex systems via supramolecular interaction under thermodynamic control.[8] On the other hand, our group[4,9] and others[10] have unraveled kinetically controlled self-sorting processes. Our protocols utilized chemical oxidation,[11] and physical stimuli such as distillation,[12] adsorption,[13] and precipitation[14] to help kinetic products "leak out" from the imine or

ester libraries with corresponding re-equilibration. Consequently, these [n×n] systems can sort into only n components under these external stimuli.

Nowadays, the highest complexity of the artificial system based on our knowledge is the [5×5] imine library.[12c] In this chapter, I will introduce a [10×10] imine library composed of 10 aldehyde and 10 aniline starting materials, which can afford up to 100 possible imines theoretically and perform the simplification with a set of three stimuli: oxidation, adsorption, and distillation (Scheme 3.1).

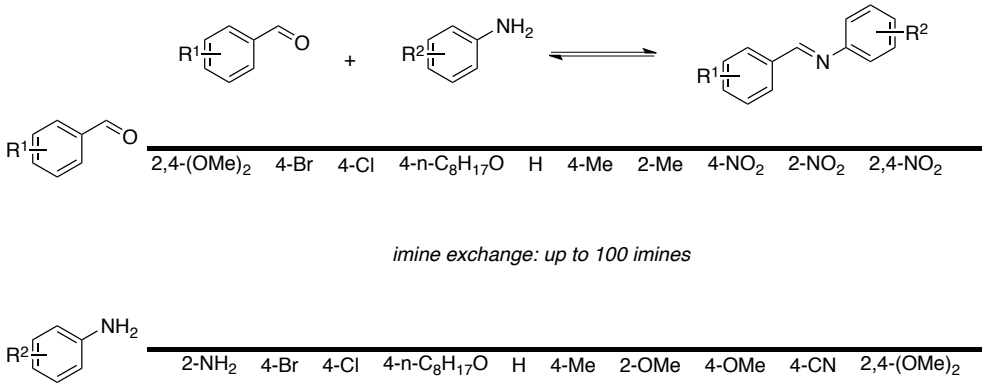

Scheme 3.1 Composition of the starting [10×10] imine library in this study (0.56 mmol each substance).

3.2 Results and Discussion

To avoid bias in our system, we chose only aldehydes and anilines which are soluble in toluene. After this mixture equilibrated in toluene at 65 °C for 12 h, the approximate complexity of our initial library constructed from 10 aldehydes (0.56 mmol each) and 10 anilines (0.56 mmol each) was evaluated using GC/MS and ^{1}H NMR spectroscopy: the former technique revealed 53 imines in the library, the latter 64. During the first self-sorting process, we targeted the imine **90** featuring the most electron rich 2,4-dimethoxybenzaldehyde and 1,2-phenylenediamine by slowly adding an iodine solution in toluene (1 mL/h, 12 h) at 65 °C. Upon slow oxidation, the product, 2,4-

dimethoxyphenylbenzimidazole **97**, precipitated out. After the filtration of the suspension and recrystallization (toluene/acetone, 3:2, v/v) of the crude solid, we obtained **97** in 74% yield (105 mg, 0.41 mmol). This result showed the high degree of self-sorting under kinetic control—irreversible slow oxidation toward the most electron rich imine species with rapid re-equilibration in this [10×10] imine library until all the most electron rich compartments, 2,4-dimethoxybenzaldehyde and 1,2-phenylenediamine, were depleted. The selectivity remained the same as the result we reported in 2012[11] even though the current library had much higher complexity (Scheme 3.2).

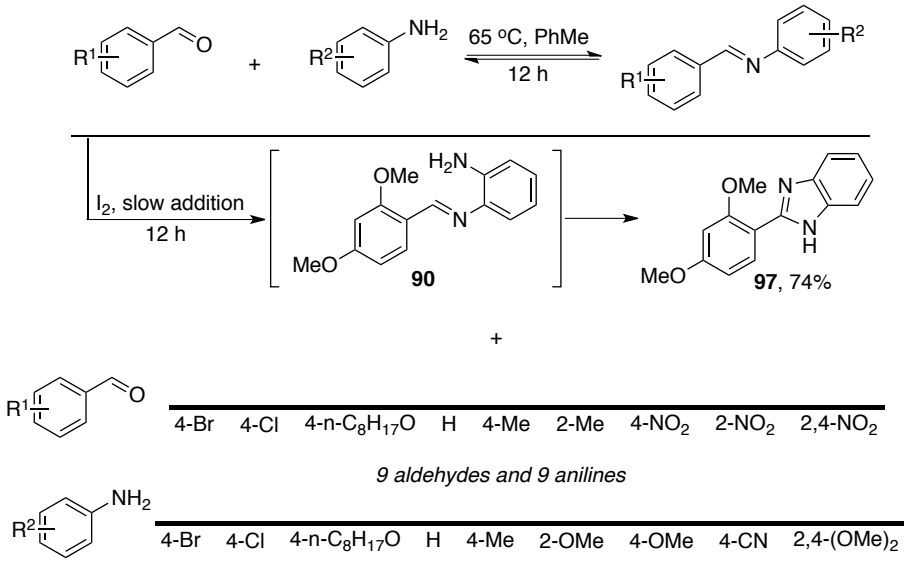

Scheme 3.2 Slow addition of iodine led to the first major component **97** in 74% yield.

In other words, the removal of **90** eliminated 19 possible imines composed of either 2,4-dimethoxybenzaldehyde or 1,2-phenylenediamine as the motifs out of these 100 imines. After collecting the residual imines, composed of 9 aldehydes and 9 anilines, in the system by filtration they were heated at reflux in PhMe with a Dean-Stark trap overnight. This reflux enabled the imines to re-equilibrate and remove excess water to allow a silica gel-based column chromatography to be applied (Scheme 3.3).

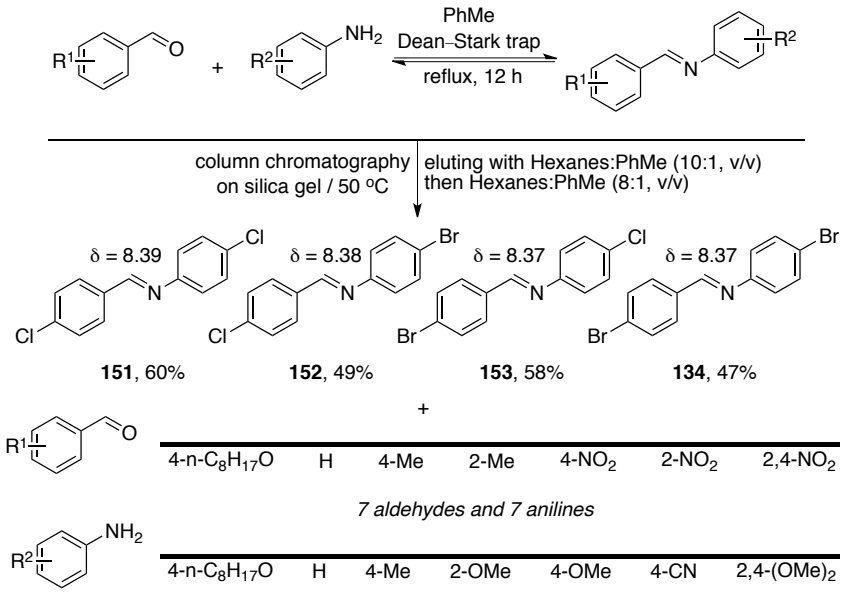

Scheme 3.3 Silica gel-based column chromatography resulted in a [2×2] imine sub-library (**151**, 60%; **152**, 49%; **153**, 58%; **134**, 47%).

After this leftover mixture was re-equilibrated in toluene, the solvent was evaporated under vacuum. The dark brown mixture was pre-adsorbed with ~2.2 g oven-dried silica gel, and then loaded on top of a chromatography column (I.D., 15 mm) which was preloaded with 20 cm high oven-dried silica gel. This column was wrapped with heating tape and heated to approximate 50 °C. This mixture was eluted with 10:1 hexane/toluene (v/v), then 8:1 hexane/toluene (v/v) to afford the first fraction. The product from the first fraction is a [2×2] sub-library containing **134**, **153**, **152**, and **151** in 47% (0.133 mmol/0.28 mmol), 58% (0.161 mmol/0.28 mmol), 49% (0.137 mmol/0.28 mmol), and 60% (0.167 mmol/0.28 mmol) yields, which were determined by the comparison between the integration of the imines and internal standard, 1,3,5-trimethoxybenzene, from ^{1}H NMR respectively (See Supporting Information). According to the GC-FID yield estimation of the initial library, **134** has 0.044 mmol, **153** has 0.021 mmol, **152** has 0.020 mmol, and **151** has 0.049 mmol: the amplification factors after the

column chromatography for each imine are: **134**, 3.023 (0.133 mmol/0.044 mmol); **153**, 7.667 (0.161 mmol/0.021 mmol); **152**, 6.850 (0.137 mmol/0.020 mmol); **151**, 3.408 (0.167 mmol/0.049 mmol). The removal of this sub-system also diminished the imines composed of 4-bormobenzaldehyde, 4-chlorobenzaldehyde, 4-bromoaniline, and 4-chloroaniline as their scaffolds (32 imines in theory) from the [9×9] imine library. However, minor imines were also obtained in the same fraction with trace amount: 4-bromo-*N*-[(2-methylphenyl)methylene]benzenamine **154**, 0.054 mmol; 4-chloro-*N*-[(2-methylphenyl)methylene]benzenamine **155**, 0.056 mmol; *N*-[(2-methylphenyl)methylene]benzenamine **156**, 0.025 mmol; 2-methoxy-*N*-[(2-methylphenyl)methylene]benzenamine **157**, 0.003 mmol). The elution of **134**, **153**, **152**, and **151** triggered the re-distribution of other imines to afford the least polar sub-imine library with total 0.598 mmol of these imines. The second self-sorting of the [9×9] imine library dispensed 53% of halogenated imines out of the system as a sub-imine library (1.120 mmol of imines in total). This showed the limited resolution of silica gel-based column chromatography, which was further exacerbated by the very slight polarity differences between these Br− or Cl− substituted imines. Nevertheless, the amplification of each imine is significant from 3 to 7.7 times larger than their initial amount in the [10×10] imine library. For the following self-sorting process, we eluted the rest of imines out of the column and made the re-equilibration by refluxing the toluene solution with Dean-Stark trap for 12 more hours before the final external stimulus—distillation.

After the re-equilibration of the residual imines, the toluene was evaporated to afford oily dark brown mixture. In the initial library, the least volatile imine **160** was present in the amount of only 0.092 mmol. After the vacuum distillation (50−120 °C,

0.15 mmHg), the distillation residue is the least volatile (heaviest) imine **160** as the major component with 61% yield (0.341 mmol). This amplification of **160** is 3.707. The minor residues are **161** (0.130 mmol) and **162** (trace amount). Consequently, the third distillative self-sorting led to the heaviest−heaviest imine **160** was kept in the original flask with good yield and decent amplification. Theoretically, this final self-sorting process removed up to 19 imines out of the dynamic library.

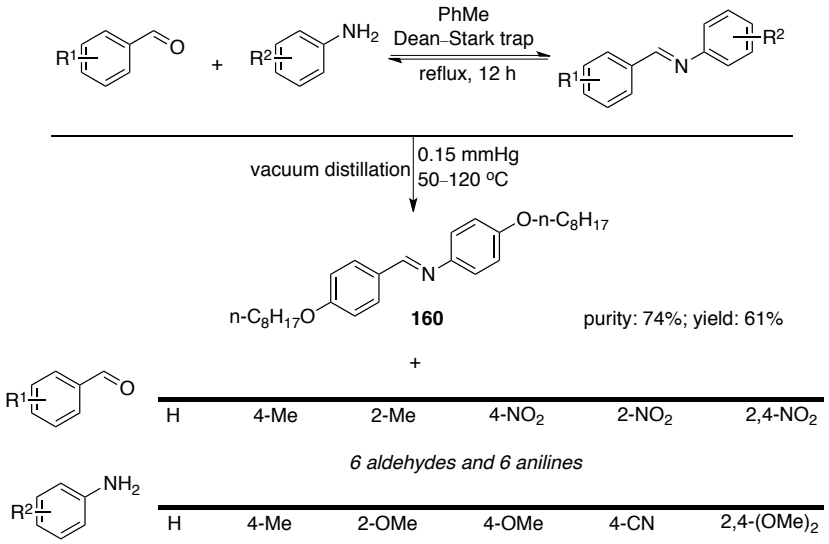

Scheme 3.4 Slow distillation kept the heaviest imine **160** as the major distillation residue (61% yield).

3.3 Conclusion

In conclusion, we successfully utilized three ubiquitous techniques—oxidation, silica gel-based column chromatography, and distillation—to make our [10×10] dynamic imine library sort to **97**, sub-imine library composed of **134**, **152**, **153**, and **151**, and **160**, respectively with reasonable amplification and yield. This experimental design not only successfully expressed the concept of the more "realistic" self-sorting processes of a highly complex multicomponent system, but also merged different stimuli toward the specific chemical and physical properties of the target molecules/sub-systems.

Afterwards, we also separated these major components/sub-systems by filtration, column separation, and distillation. For chemical education, these techniques are affordable and approachable in the organic chemistry lab. This project embraced four important concepts at the same time—oxidation, chromatography, distillation, and equilibrium (Le Châtelier principle) to general chemistry. Nowadays, more possible chemical or physical stimuli such as slow reduction and HPLC are under investigation for the further application with much more complicated systems.

3.4 Experimental Section

3.4.1 General Methods and Materials

Reagents and solvents were purchased from commercial suppliers and used without further purification, except PhMe and hexane, which were dried over molecular sieves. For the first part, the three-necked round bottom flask (50 mL) was used for the slow oxidation. Secondly, the round bottom flask (50 mL) and Dean-Stark trap were used as the standard part of the reaction apparatus for the re-equilibration of the leftover imines. Column chromatography was performed in the same way as the reported procedure.[13] Thirdly, the slow distillation apparatus was operated in the same way as the reported procedure.[12c]

All NMR spectra were collected on JEOL ECX-400, ECA-500, and ECA-600 NMR spectrometers. Chemical shifts are reported in ppm units relative to the residual signal of the solvent ($CDCl_3$: 7.26 ppm, DMSO-d_6: 2.49 ppm). ^{13}C NMR spectra were recorded with simultaneous decoupling of ^{1}H nuclei. The NMR internal standard for yield determination was 1,3,5-trimethoxybenzene (Alfa Aesar, 99%). The melting points

were measured on a Barnstead International Mel-TEMP® apparatus, and are uncorrected. The mass spectra were obtained via LCQ Deca XP Plus from Thermo Finnigan (ESI-MS) or Micromass Autospec Ultima (CI-MS). IR spectra were collected on Thermo Scientific™ Nicolet™ iS™10 FT-IR. For counting number of imines based on GC-MS, Thermo Trace GC-MS was performed under the following conditions: initial temperature was 50 °C for 1 min. The first heating ramp was 30 °C/min to 80 °C and held for 1 min. The second heating ramp was 45 °C/min to 260 °C then 2 °C/min to 300 °C and held for 2 min. For GC-FID analysis, Agilent 7820E spectrometer with a Zebron ZB-5MS capillary column (0.25 mm×0.25 μm×25 m) was utilized under the following conditions: initial temperature was 50 °C for 1 min. The first heating ramp was 30 °C/min to 80 °C and held for 1 min. The second heating ramp was 45 °C/min to 260 °C then 2 °C/min to 300 °C and held for 2 min. Quantification measurements for imines **134**, **153**, **152**, and **151** were based on the integration of their peaks in GC-FID chromatogram and corrected by the corresponding response factor toward the internal standard, biphenyl.

All of the imines have been characterized and reported in the literature, except **161**. Compound **162** was reported without NMR data in the literature. Syntheses and NMR data of **161** and **162** are provided in the following section.

3.4.2 Syntheses of Imines

4-*n*-Octyloxy-*N*-[(4-nitrophenyl)methylene]benzeneamine **162**

Equimolar amounts of 4-nitrobenzaldehyde (84 mg, 0.56 mmol) and 4-*n*-octyloxyaniline (122 mg, 0.56 mmol) were added into a 50 mL round bottom flask, along with PhMe (25 mL). The solution was heated at reflux for 12 h with a Dean-Stark trap.

After that time, PhMe was evaporated in vacuo, and the resulting solid was recrystallized from PhMe/Hexane, to give the title compound as a yellow solid in 72% yield (143 mg).

162: ^{1}H NMR ($CDCl_3$, 500 MHz): 8.58 (s, 1H), 8.33−8.31 (d, 2H), 8.07−8.05 (d, 2H), 7.32−7.29 (m, 2H), 7.36−7.39 (m, 2H), 6.97−6.93 (m, 2H), 3.99 (t, 2H), 1.83−1.77 (m, 2H), 1.50−1.44 (m, 2H), 1.39−1.23 (m, 8H), 0.90−0.88 (m, 3H) ppm. ^{13}C NMR ($CDCl_3$ 125 MHz): 160.0, 154.6, 149.0, 143.4, 142.1, 129.1, 124.1, 122.7, 115.2, 68.4, 31.9, 29.5, 29.4, 26.2, 22.8, 14.2 ppm. Melting point: 60−61 °C. IR (FTIR, neat): 2939 2918, 2853, 1596, 1575, 1516, 1505, 1339, 830 cm^{-1}. LRMS (ESI, positive): Calcd ($[M+H]^+$), 355.20; Found, 355.26.

4-*n*-Octyloxy-*N*-[(2,4-dinitrophenyl)methylene]benzeneamine **161**

Equimolar amounts of 2,4-dinitrobenzaldehyde (108 mg, 0.56 mmol) and 4-*n*-octyloxyaniline (122 mg, 0.56 mmol) were added into a 50 mL round bottom flask, along with PhMe (25 mL). The solution was heated at reflux for 12 h with a Dean-Stark trap. After that time, PhMe was evaporated in vacuo, and the resulting solid was washed with hexane, to give the title compound as a yellow solid in 54% yield (120 mg).

161: ^{1}H NMR ($CDCl_3$, 500 MHz): 9.03 (s, 1H), 8.90 (d, 1H), 8.62 (d, 1H), 8.52 (dd, 1H), 7.39−7.36 (m, 2H), 6.98−6.95 (m, 2H), 4.00 (t, 2H), 1.84−1.78 (m, 2H), 1.50−1.44 (m, 2H), 1.39−1.23 (m, 8H), 0.91−0.88 (m, 3H) ppm. ^{13}C NMR ($CDCl_3$ 125 MHz): 159.9, 149.8, 149.0, 148.2, 142.6, 136.4, 131.2, 127.4, 123.5, 120.5, 155.3, 68.5, 31.9, 29.5, 29.4, 29.3, 26.1, 22.8, 14.2 ppm. Melting point: 69−70 °C. IR (FTIR, neat): 2923, 2856, 1648, 1598, 1573, 1523, 1341, 981, 833 cm^{-1}. HRMS (CI, negative): Calcd, 399.1794; Found, 399.1787

3.4.3 Iterative Self-sorting of the [10×10] Imine Library

Self-Sorting #1: Slow Oxidation

Equimolar amounts of 2,4-dimethoxybenzaldehyde (92 mg, 0.56 mmol), benzaldehyde (56 μL, 0.56 mmol), 4-*n*-octyloxybenzaldehyde (134 μL, 0.56 mmol), 4-chlorobenzaldehyde (78 mg, 0.56 mmol), 4-bromobenzaldehyde (102 mg, 0.56 mmol), *o*-tolualdehyde (65 μL, d = 1.04 g/cm^3, 0.56 mmol), *p*-tolualdehyde (64 μL, d = 1.02 g/cm^3, 0.56 mmol), 2,4-dinitrobenzalehyde (108 mg, 0.56 mmol), 2-nitrobenzaldehyde (84 mg, 0.56 mmol), 1,2-phenylenediamine (60 mg, 0.56 mmol), aniline (50 μL, d = 1.02 g/cm^3, 0.56 mmol), 4-*n*-octyloxyaniline (122 mg, 0.56 mmol), *o*-anisidine (63 μL, d = 1.90 g/cm^3, 0.56 mmol), 4-chloroaniline (70 mg, 0.56 mmol), 4-bromoaniline (94 mg, 0.56 mmol), *p*-anisidine (68 mg, 0.56 mmol), *p*-toluidine (58 mg, 0.56 mmol), 2,4-dimethoxyaniline (86 mg, 0.56 mmol), and 4-aminobenzonitrile (66 mg, 0.56 mmol) were added into a 50 mL three-necked round bottom flask, along with PhMe (25 mL). The mixture was heated at 65 °C for 12 h, followed by slow addition of the iodine solution (149 mg, 0.59 mmol) in 12 mL PhMe at rate 1 mL/h. After the completion of addition, the reaction was kept under 65 °C for 1 h. The brown suspension was allowed to cool to room temperature. The filtration was taken with a silica gel plug and the precipitate was washed with 70 mL toluene, followed by a mixture of hexane and acetone (250 mL, vol/vol = 3:2). The final product was eluted with 300 mL acetone, followed by recrystallization with PhMe/acetone (6 mL / 2 mL) at 60 °C for 20 min then −30 °C for 40 min. The light brown product (105 mg) was obtained as 74% yield.

97: ^{1}H NMR (DMSO-d_6, 500 MHz): 8.44 (s, 1H), 7.81−7.80 (d, $^3J_{H-H}$=8.0 Hz, 2H), 7.30−7.28 (d, $^3J_{H-H}$=7.5 Hz, 2H), 7.22−7.15 (m, 4H), 2.43 (s, 3H), 2.39 (s, 3H) ppm. Spectral data agree with the previous literature report.[11]

Self-Sorting #2: Adsorption-Driven Self-Sorting of [9×9] Imine Library Using Silica Gel-Based Column Chromatography

The filtrate obtained as described in the first section was dried under vacuum to remove solvents. The dried filtrate was added into a 50 mL round bottom flask equipped with a Dean-Stark trap. The mixture was heated with 25 mL PhMe to reflux for 12 h. After the evaporation of PhMe under vacuum, 2.2 g of oven-dried silica gel was added and mixed with the dried filtrate. This mixture was put on the column pre-loaded with ~20 cm high oven-dried silica gel. The column was wrapped with heating tape and heated to around 50 °C. The eluent—first, 10:1 hexane/PhMe (v/v, 220 mL), then 8:1 hexane/PhMe (v/v, 360 mL)—afforded the major sub-library after the evaporation of solvent in vacuo. The yields were calculated by 1,3,5-trimethoxybenzene as the internal standard (268 mg crude, 20.1 mg internal standard).

134: ^{1}H NMR ($CDCl_3$, 600 MHz): 8.37 (s, 1H), 7.76−7.75 (d, 2H), 7.62−7.61 (d, 2H), 7.51−7.50 (d, 2H), 7.10−7.07 (m, 2H) ppm. **153**: ^{1}H NMR ($CDCl_3$, 600 MHz): 8.37 (s, 1H), 7.76−7.75 (d, 2H), 7.51−7.50 (d, 2H), 7.36−7.35 (d, 2H), 7.16−7.14 (m, 2H) ppm. **152**: ^{1}H NMR ($CDCl_3$, 600 MHz): 8.38 (s, 1H), 7.84−7.82 (d, 2H), 7.51−7.50 (d, 2H), 7.46−7.44 (d, 2H), 7.10−7.07 (m, 2H) ppm. **151**: ^{1}H NMR ($CDCl_3$, 600 MHz): 8.39 (s, 1H), 7.84−7.82 (d, 2H), 7.46−7.44 (d, 2H), 7.36−7.35 (d, 2H), 7.16−7.14 (m, 2H) ppm. Spectral data agree with the previous literature reports.[15]

Calculation of the Yields based on the Integration of ^{1}H NMR Spectra

We assumed that the molar contribution of imines in the sub-system is **134**:**153**:**152**:**151** = 1:1:1:1 (each imine has 0.28 mmol) as their quantitative molar amounts. Internal standard 1,3,5-trimethoxybenzene (20.1 mg, 0.120 mmol) was added into 268 mg crude **134**. From the integration of the ^{1}H NMR spectrum (Figure 3.1), the number of moles of **134** was calculated to be 0.120 mmol × 1.11 = 0.133 mmol. Thus, the yield of **134** is 0.133 mmol ÷ 0.28 mmol = 47%. Analogous calculations have been performed for all other imines of interest.

Yield of **153**: 0.120 × 1.34 = 0.161 mmol →→ 0.161 mmol ÷ 0.28 mmol = 58%.

Yield of **152**: 0.120 × 1.14 = 0.137 mmol →→ 0.137 mmol ÷ 0.28 mmol = 49%.

Yield of **151**: 0.120 × 1.39 = 0.167 mmol →→ 0.167 mmol ÷ 0.28 mmol = 60%

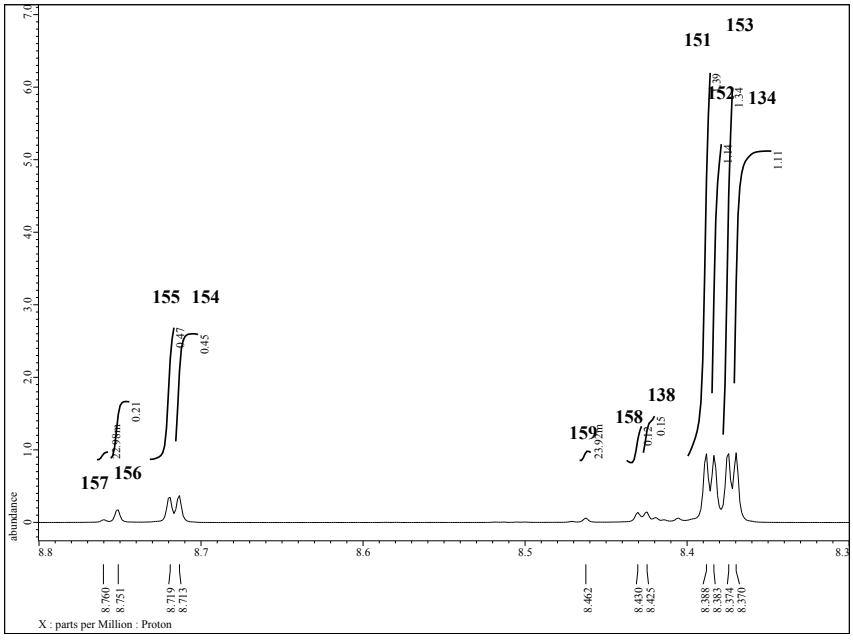

Figure 3.1 ^{1}H NMR spectrum of the first eluted fraction in Self-Sorting #2.

Self-Sorting #3: Distillation-Driven Self-Sorting of the [7×7] Imine Library

The residue of the second section in the column was eluted with 400 mL EtOAc, followed by the evaporation of EtOAc in vacuo. The dried residue was added into a 50 mL round bottom flask equipped with a Dean-Stark trap. The mixture was heated with 25 mL PhMe to reflux for 12 h. After the evaporation of PhMe under vacuum, the residue was transferred to 25 mL round bottom flask and then equipped with a short distillation condenser. The mixture was distilled under vacuum (0.15 mmHg). The distillation followed the following timeframe: 60 °C for 5 d, 80 °C for 3 d, 100 °C for 2 d and 120 °C for 2 d. The distillation resulted in 200 mg of a crude dark brown solid with 4-*n*-octyloxy-*N*-[(4-*n*-octyloxyphenyl)methylene]benzeneamine **160** (0.341 mmol, 74% purity, 61% yield). Minor imines are 4-*n*-octyloxy-*N*-[(2,4-dinitrophenyl)methylene] benzeneamine **161** with 0.13 mmol in 23% yield (26% purity) and 4-*n*-octyloxy-*N*-[(2,4-dinitrophenyl)methylene]benzeneamine **162** in trace amount

160: ^{1}H NMR ($CDCl_3$, 500 MHz): 8.39 (s, 1H), 7.82−7.80 (d, 2H), 7.20−7.18 (d, 2H), 6.97−6.95 (d, 2H), 6.92−6.90 (m, 2H), 4.03−4.00 (t, 2H), 3.98−3.95 (t, 2H), 1.83−1.76 (m, 4H), 1.50−1.43 (m, 4H), 1.37−1.24 (m, 16H), 0.90−0.88 (t, 6H) ppm. **161**: ^{1}H NMR ($CDCl_3$, 500 MHz): 9.03 (s, 1H), 8.90 (d, 1H), 8.62 (d, 1H), 8.52 (dd, 1H), 7.36−7.39 (m, 2H), 6.95−6.98 (m, 2H), 4.00 (t, 2H), 1.78−1.84 (m, 2H), 1.44−1.50 (m, 2H), 1.23−1.39 (m, 8H), 0.88−0.91 (m, 3H) ppm. Spectral data agree with the previous literature report.[16]

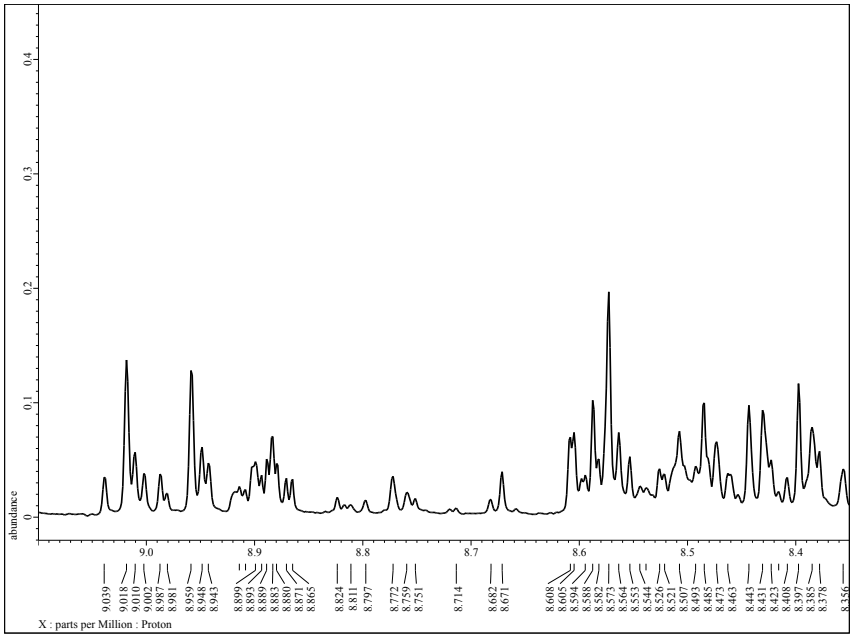

Figure 3.2 Starting mixture of the third step of self-sorting.

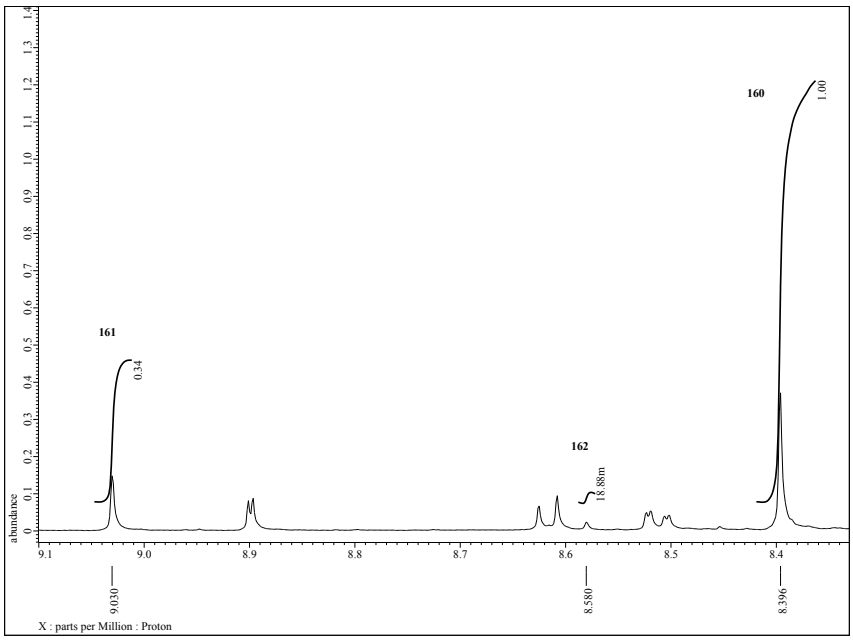

Figure 3.3 Distillation residue from the third step of self-sorting: major imine **160** in 61% yield and minor imine **161** in 23% yield.

3.5 References

[1] Wu, A.; Isaacs, L. *J. Am. Chem. Soc.* **2003**, *125*, 4831−4835.

[2] (a) Corbett, P. T.; Leclaire, J.; Vial, L.; West, K. R.; Wietor, J.-L.; Sanders, J. K. M.; Otto, S. *Chem. Rev.* **2006**, *106*, 3652−3711; (b) Otto, S. *Acc. Chem. Res.* **2012**, *45*, 2200−2210; (c) Reek, J. N. H.; Otto, S. *Dynamic Combinatorial Chemistry*; Wiley, 2010; (d) Belowich, M. E.; Stoddart, J. F. *Chem. Soc. Rev.* **2012**, *41*, 2003−2024.

[3] Black, S. P.; Sanders, J. K. M.; Stefankiewicz, A. R. *Chem. Soc. Rev.* **2014**, *43*, 1861−1872.

[4] Ji, Q.; Lirag, R. C.; Miljanić, O. Š. *Chem. Soc. Rev.* **2014**, *43*, 1873−1884.

[5] Boiocchi, M.; Fabbrizzi, L. *Chem. Soc. Rev.* **2014**, *43*, 1835−1847.

[6] Carnes, M. E.; Collins, M. S.; Johnson, D. W. *Chem. Soc. Rev.* **2014**, *43*, 1825−1834.

[7] (a) Otto, S.; Furlan, R. L. E.; Sanders, J. K. M. *Science* **2002**, *297*, 590−593; (b) Rowan, S. J.; Brady, P. A.; Sanders, J. K. M. *Angew. Chem. Int. Ed. Engl.* **1996**, *35*, 2143−2145; (c) Rowan, S. J.; Hamilton, D. G.; Brady, P. A.; Sanders, J. K. M. *J. Am. Chem. Soc.* **1997**, *119*, 2578−2579; (d) Otto, S.; Furlan, R. L. E.; Sanders, J. K. M. *J. Am. Chem. Soc.* **2000**, *122*, 12063−12064; (f) Nitschke, J. R. *Acc. Chem. Res.* **2007**, *40*, 103−112.

[8] (a) Jiang, W.; Winkler, H. D. F.; Schalley, C. A. *J. Am. Chem. Soc.* **2008**, *130*, 13852–13853; (b) Jiang, W.; Schalley, C. A. *Proc. Natl. Acad. Sci. USA* **2003**, *106*, 10425–10429; (c) Saha, M. L.; Schmittel, M. *Org. Biomol. Chem.* **2012**, *10*,

4651–4684; (d) Mahata, K.; Saha, M. L.; Schmittel, M. *J. Am. Chem. Soc.* **2010**, *132*, 15933–15935; (f) Mahata, K.; Schmittel, M. *J. Am. Chem. Soc.* **2009**, *131*, 16544–16554; (g) Schmittel, M.; Kalsani, V.; Kishore, R. S. K.; Cölfen, H.; Bats, J. W. *J. Am. Chem. Soc.* **2005**, *127*, 11544–11545; (h) M. L. Saha, M. Schmittel, *J. Am. Chem. Soc.* **2013**, *135*, 17743–17746; (i) Saha, M. L.; Mittal, N.; Bats, J. W.; Schmittel, M. *Chem. Commun.* **2014**, *50*, 12189–12192.

[9] Osowska, K.; Miljanić, O. Š. *Synlett* **2011**, 1643−1648.

[10] (a) Mukhopadhyay, P.; Zavalij, P. Y.; Isaacs, L. *J. Am. Chem. Soc.* **2006**, *128*, 14093−14102; (b) Morris, K. L.; Chen, L.; Raeburn, J.; Sellick, O. R.; Cotanda, P.; Paul, A.; Griffiths, P. C.; King, S. M.; O'Reilly, R. K.; Serpell, L. C.; Adams, D. J. *Nat. Commun.* **2013**, *4*, doi: 1038/ncomms2499; For a review, see: Safont-Sempere, M. M.; Fernández, G.; Würthner, F. *Chem. Rev.* **2011**, *111*, 5784−5814.

[11] Osowska, K.; Miljanić, O. Š. *J. Am. Chem. Soc.* **2011**, *133*, 724−727.

[12] (a) Ji, Q.; Miljanić, O. Š. *J. Org. Chem.* **2013**, *78*, 12710−12716; (b) Ji, Q.; El-Hamdi, N. S.; Miljanić, O. Š. *J. Chem. Educ.* **2014**, *91*, 830−833; (c) Osowska, K.; Miljanić, O. Š. *Angew. Chem. Int. Ed.* **2011**, *50*, 8345−8349.

[13] Hsu, C.-W.; Miljanić, O. Š. *Angew. Chem. Int. Ed.* **2015**, *54*, 2219−2222.

[14] Lirag, R. C.; Osowska, K.; Miljanić, O. Š. *Org. Biomol. Chem.* **2012**, *10*, 4847−4850.

[15] **134**: Bolognese, A.; Diurno, M. V.; Mazzoni, O.; Giordano, F. *Tetrahedron* **1991**, *47*, 7417−7428;

153: Subashini, A.; Bhagavannarayana, G.; Ramamurthi, K. *Spectrochim. Acta, Part A* **2012**, *96*, 716−722;

152: Bolognese, A.; Diurno, M. V.; Mazzoni, O.; Giordano, F. *Tetrahedron* **1991**, *47*, 7417−7428;

151: Naeimi, H.; Rabiei, K. *J. Chin. Chem. Soc.* **2012**, *59*, 208−212.

[16] Mohammada, A.-T.; Yeap, G.-Y.; Osman, H. *J. Mol. Struct.* **2015**, *1087*, 88−96.

4 Chapter Four: Characterization and Porosity Measurement on a Fluorinated Noncovalent Organic Framework

4.1 Introduction

Materials whose voids can accommodate guest molecules are considered porous and can be classified as microporous (< 2 nm), mesoporous (2−50 nm), and macroporous (> 50 nm) based on pore size. Crystalline and amorphous porous materials (including polymeric frameworks) have been extensively utilized in catalysis, gas separation, storage, and filtration.[1,2,3] For example, zeolites, the crystalline aluminumsilicates, can capture CO_2,[4] convert methanol and ammonia to dimethylamine[5], and separate air into N_2 and O_2.[6] Noria, the amorphous waterwheel-like organic solid, manifests the selective adsorption of CO_2 over N_2.[3] These applications of porous materials require permanent porosity, high thermal and chemical stability, and high surface areas. The earliest porous materials, zeolites (also known as aluminosilicates), have been comprehensively investigated and applied in chemical and petroleum industries.[7,8] Since applications such as adsorption and ion exchange were widely studied, the corresponding artificial zeolite syntheses was also well-developed. Since the 1990s people have designed organic linker-based porous materials, which featured various functionalities, topologies, and metal-versatile networks. There are three categories of porous frameworks with organic components: covalent organic frameworks (COFs), [9] metal-organic frameworks (MOFs),[10] and noncovalent organic frameworks (nCOFs).[11] In the following section, I will briefly introduce the current development and applications of each category of porous materials and mainly focus on nCOFs.

4.1.1 Covalent Organic Frameworks

Covalent organic frameworks are constructed by organic ligands that fabricate crystalline organic polymer networks. In 2005, Yaghi et al. reported the first two crystalline organic polymer networks with discrete pores fabricated by the dehydration of 1,4-benzenediboronic acids (BDBA) or the condensation of BDBA and 2,3,6,7,10,11-hexahydroxytriphenylene (HHTP)—**COF-1** and **COF-5** were synthesized respectively (Scheme 4.1).[12] Powder X-ray diffraction studies of **COF-1** and **COF-5** manifested their crystallinity and N_2 sorption isotherms revealed high surface areas according to the BET model (**COF-1**: 711 m^2 g^{-1} and **COF-5**: 1590 m^2 g^{-1}). The calculated pore diameters are 15 Å and 27 Å, respectively.

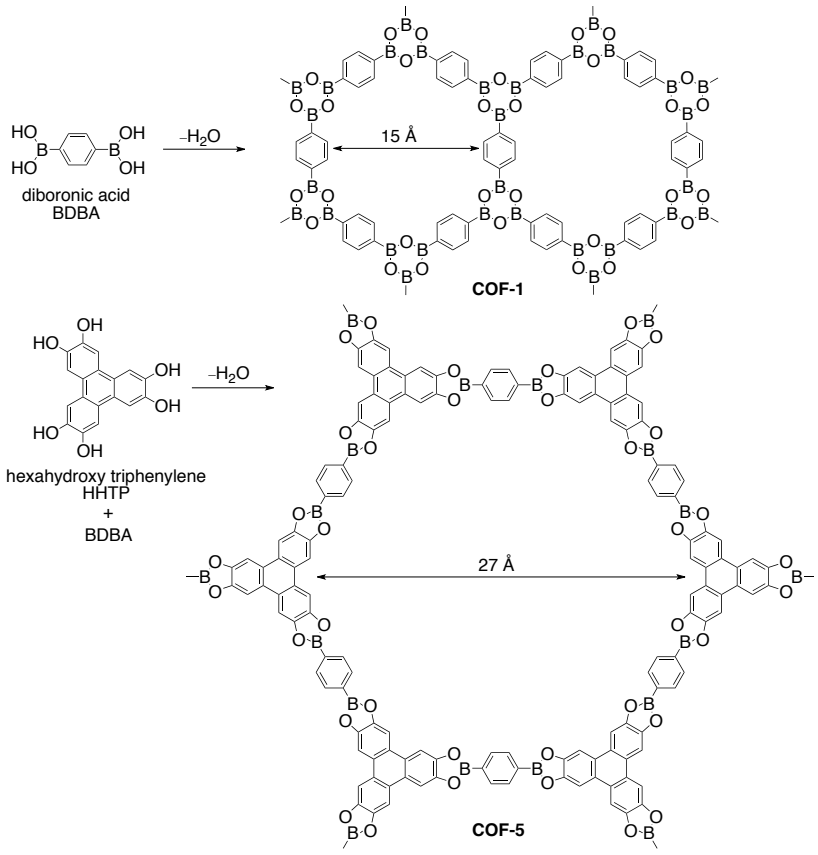

Scheme 4.1 Syntheses of the first two crystalline organic polymers with discrete pores.

Moreover, Yaghi et al. extended the building blocks from boronic acids to borosilicates,[13], imino bonds,[14] and hydrazone[15] to construct **COF-202**,[13] **COF-300**,[14] and **COF-42**[15] (Scheme 4.2). These COFs all have high surface areas in the Brunauer-Emmett-Teller (BET) model (**COF-202**: 2690 m^2 g^{-1}, **COF-300**: 1360 m^2 g^{-1}, **COF-42**: 710 m^2 g^{-1}) and provided the concept of the design of COFs with different building blocks and the potential application on gas separation and gas adsorption.

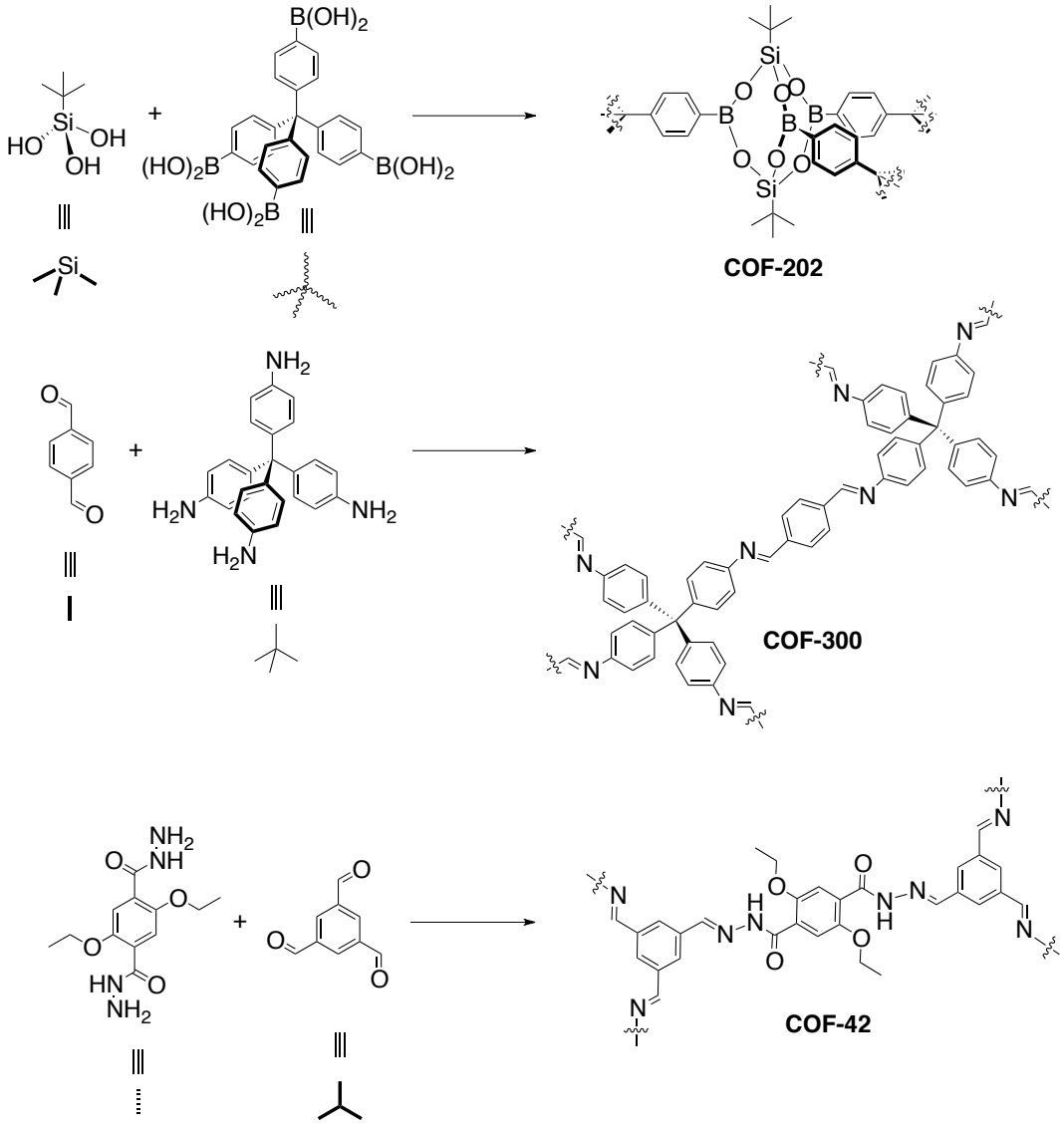

Scheme 4.2 Various building blocks give different COFs.

COFs have been considered as potential materials for gas adsorption/storage because of their high surface areas. Their capabilities in adsorption of gases such as CO_2, H_2, and CH_4 have been investigated widely.[16] Some COFs could have water tolerance during the process of gas separation/adsorption process and have lower regeneration energy than MOFs. For example, Banerjee et al. reported two COFs (**TpPa-1** and **TpPa-2**) fabricated by the condensation of 1,3,5-triformylphloroglucinol (Tp) with *p*-phenylenediamine (Pa-1) and 2,5-dimethyl-*p*-phenylenediamine (Pa-2), respectively.[17] They both showed a tolerance to acids and bases. For the CO_2 uptake, **TpPa-1** and **TpPa-2** could accommodate 78 and 64 $cm^3\ g^{-1}$ at 273 K and 1 bar. Moreover, CO_2/N_2 selective adsorption is a more important concern to remove the primary greenhouse gas from the atmosphere. Zhong et al. screened the selective adsorption of CO_2 and N_2 from 46 primary COFs.[18] Moreover, Han and coworkers constructed a perfluorinated covalent triazine-based organic framework featuring the selective adsorption of CO_2 over N_2.[19] Based on the publication of the non-fluorinated COF, **CTF-1,** in 2008,[20] they incorporated fluorine into **CTF-1** by using tetrafluoroterephthalonitrile as the building block instead and obtained the fluorinated **CTF-1**, **FCTF-1** (Scheme 4.3).[19] The selectivity of CO_2/N_2 (v/v, 10:90) calculated by ideal absorbed solution theory (IAST) is 31:1 at 298 K under 1 bar.

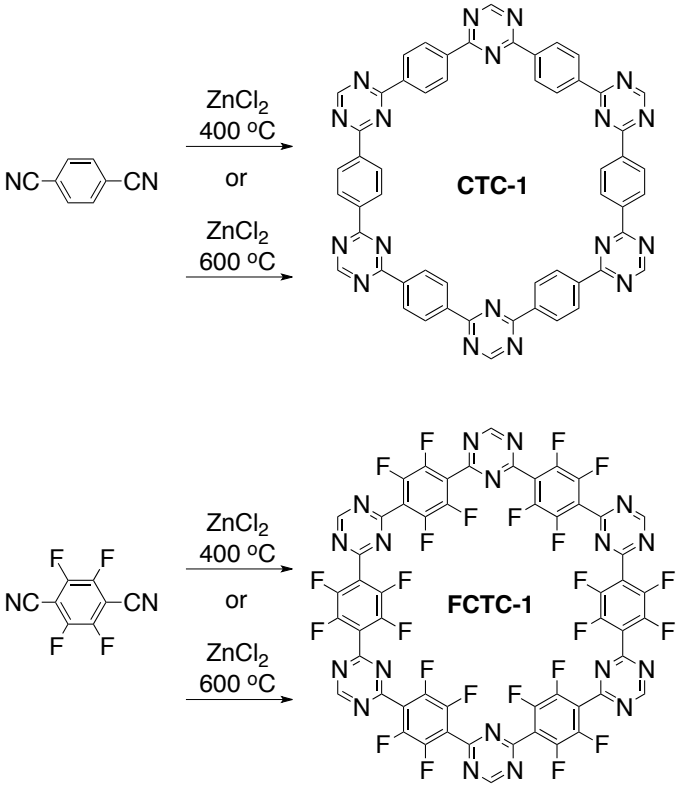

Scheme 4.3 Syntheses of **CTC-1** and perfluorinated **CTC** (**FCTC-1**).

4.1.2 Metal Organic Frameworks

In comparison to zeolites, metal-organic frameworks (MOFs) have the flexibility of design, which could possess the desired functional groups on the organic building blocks. These frameworks have applications in gas separation, gas storage, and catalysis.[10] In 1999, Yaghi et al. reported the first highly stable and porous metal-organic framework: **MOF-5** (Scheme 4.4).[21] They constructed **MOF-5** by adding triethylamine into the solution of 1,4-benzenedicarboxlic acid and $Zn(NO_3)_2$ in the *N,N'*-dimethylformamide (DMF)/chlorobenzene. The single X-ray diffraction data of **MOF-5** displayed that one Zn(II) formed the ZnO_4 tetrahedral cluster with the four deprotonated hydroxyls of 1,4-benzenedicarboxylic acids. Eight clusters fortify a huge cavity which has a diameter of 18.5 Å. The calculated surface area of Langmuir model is 2900 $m^2\ g^{-1}$.

The thermogravimetric analysis of **MOF-5** showed no weight loss up to 410 °C. In 2004, Yaghi group reported another MOF with much higher surface area: **MOF-177** (Scheme 4.4).[23] **MOF-177** was constructed by heating a (*N*,*N*-diethylformamide) DEF solution of 4,4',4''-benzene-1,3,5-triyl-tribenzoic acid (H_3BTB) and $Zn(NO_3)_2$ $6H_2O$ to 100 °C for 23 h. The single crystal structure displayed that one Zn(II) formed the tetrahedron (ZnO_4) with four deprotonated hydroxyls of BTB. The pore diameter is 10.8 Å. With the calculation of its N_2 adsorption isotherm data, the Langmuir surface area of **MOF-177** was given as 4500 m^2 g^{-1}. For CO_2 capture and separation,[22] Long et al. manifested that two representative MOFs synthesized by Yaghi et al. (**MOF-177**[23] and **Mg-MOF-74** (Scheme 4.4)[24]) featured the selective adsorption toward CO_2 over N_2 at different temperature.[25] Based on the calculation with IAST model, **Mg-MOF-74** revealed a relatively higher selectivity factor of 148.1 at 50 °C and **MOF-177** showed the much lower selectivity (even its Langmuir surface area is 4500 m^2 g^{-1}).

MOFs have also been applied in catalysis.[10] For example, Cohen et al. reported the Cr-metalated MOF, **UiO-66-CrCAT**, which is the catalyst for the oxidation of secondary alcohols to ketones (Scheme 4.5).[26] **UiO-66-CrCAT** displays its capability to be the environmental friendly catalyst toward the alcohol oxidation. It can catalyze the oxidation with only 0.5−1 mol% metal loading in high yields (70%−99%) and the catalyst is reusable and recyclable.

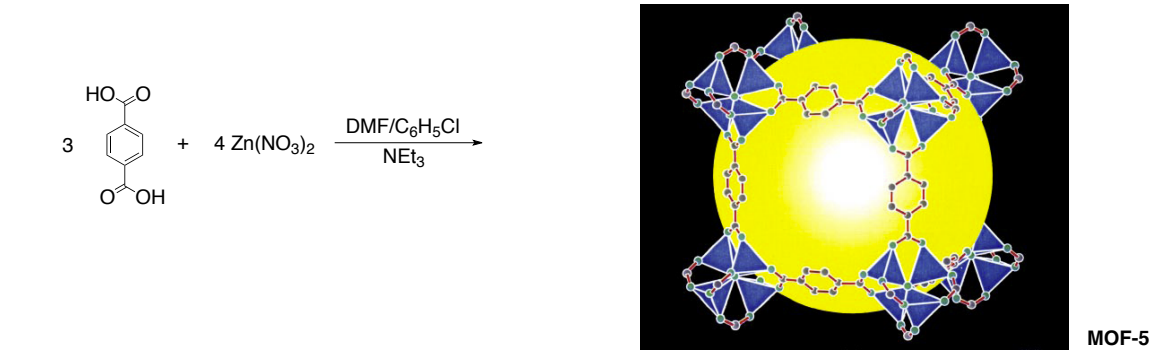

Scheme 4.4 Syntheses of **MOF-5**, **MOF-177**, and **Mg-MOF-74**.

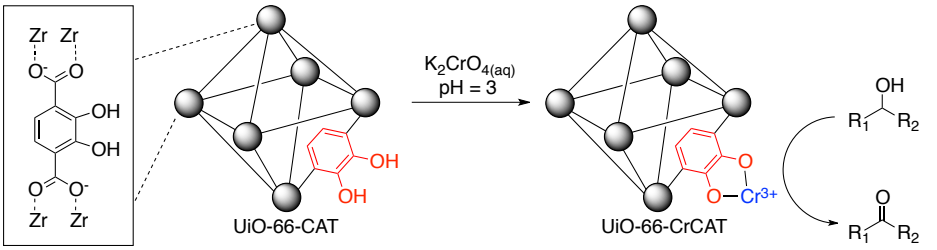

Scheme 4.5 UiO-66-CrCAT catalyzed oxidation of secondary alcohols to ketones.

4.1.3 Noncovalent Organic Frameworks

Other than COFs and MOFs, porous organic molecules are relatively less-developed and still have potentials with further application capability. Cooper et al. mentioned the following features of porous organic molecules: solution processability, ligand combination, flexibility, and diverse modification.[27] They classified porous molecules as intrinsically or extrinsically porous. The intrinsically porous materials were defined as those containing permanent pores in isolated molecules; the extrinsically porous materials emerge through inefficient packing among molecules, wherein the porosity cannot be attributed to an isolated molecule. Even though the porous organic molecules are not as well-investigated as porous networks, the synthetic diversification of porous molecules is still valuable and has some more unraveled areas.

4.1.3.1 Intrinsically Porous Molecular Crystals

In 2002, Atwood et al. reported a hexagonal close-packed arrangement of calix[4]arene containing a permanent cavity, which accommodated small molecules such as methane, Freons, and chloroform (Figure 4.1).[11a] Intramolecular hydrogen bonds led to the cone formation of this calix[4]arene; three cones rearranged to form a spherical trimer. They have demonstrated that the van der Waals interaction resulted in the host-guest interaction between cage and these small molecules. This cage compound also displayed the compositional stability up to 202 °C with CF_3Br as its adsorbate without weight loss (CF_3Br boiling point is −58 °C).

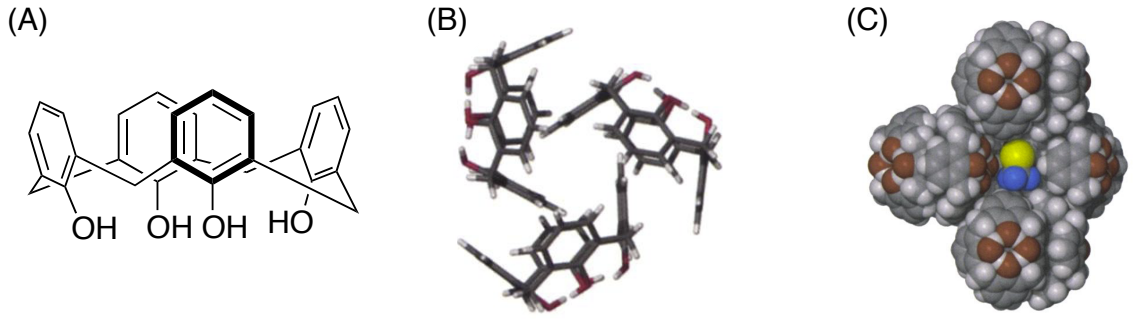

Figure 4.1 (A) Chemical structure of calix[4]arene. (B) Capped-stick representation view of trimeric arrangement of calix[4]arene. (C) Space-filling representation of CF_3Br@calix[4]arene. (B) and (C) were reproduced with the permission from Science AAAS. Colors: C, gray; H, white; O, dark red; F, blue; and Br, yellow.

Cooper and coworkers first demonstrated that covalently bonded organic cages can assemble into crystalline microporous materials (Figure 4.2).[11b] A series of intrinsically porous organic cage compounds were accomplished via imino bond formation; these intrinsic organic cages also formed the porous materials through the noncovalent interactions. In Figure 4.2b, the crystal packing showed that the molecular unit provided the molecular voids (intrinsic porosity); in Figure 4.2c, among these cages, the inefficient packing led to the extrinsic pores (yellow rod between adjacent cages). The interlocking of three cyclohexyl groups on adjacent cages resulted in the window-to-window packing and fabricated the diamondoid-pore network. This intrinsically microporous material has the surface area as 624 $m^2\ g^{-1}$ in BET model and 730 $m^2\ g^{-1}$ in Langmuir model. Its thermogravimetric analysis (TGA) showed no weight loss up to 398 °C. They also demonstrated that this porous material can adsorb small molecules such as hydrogen gas, methane, and carbon dioxide.

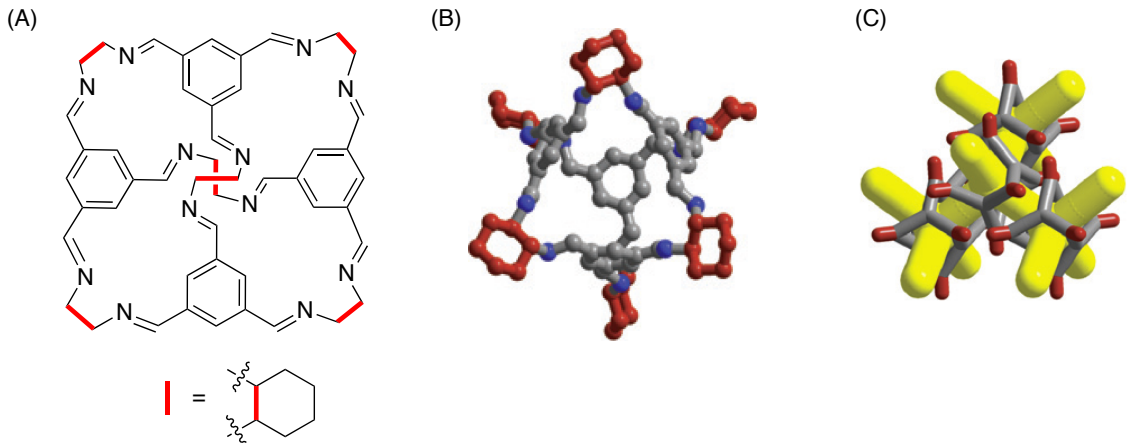

Figure 4.2 (A) Chemical structure of Cooper's porous imine-based capsule. (B) Crystal structure of the single unit. (C) Packing mode of this compound showed the window to window packing. (B) and (C) were reprinted by permission from Macmillan Publishers Ltd: Nature Mater. **2009**, *8*, 973−978, copyright 2009. Colors: C, gray; N, blue; cyclohexyl, red.

Mastalerz et al. focused on the imine and boronic ester chemistry to build up cage compounds with intrinsic porosity. For example, in Scheme 4.6, the [4+6] imine cage formation between triaminotriptycenes and salicylic dialdehydes resulted in an adamantoid cage with a high surface area: 1566 $m^2 g^{-1}$ (Langmuir) and 1375 $m^2 g^{-1}$ (BET); the selective adsorption of this compound toward CO_2 and methane is 10:1 by weight.[28] The corresponding post-modification of this material—the nucleophilic substitution—was also reported by the same group.[29] Recently, Mastalerz et al. constructed a [12+8] boronic ester cage compound using 12 triptycene tetraols and 8 triboronic acid and they obtained the single crystal X-ray structure. The diameter of the pore is 2.6 nm (mesoporous pore) and the surface area is 4246 $m^2 g^{-1}$ (Langmuir) and 3758 $m^2 g^{-1}$ (BET). This boronic ester cage has the highest surface area to date.

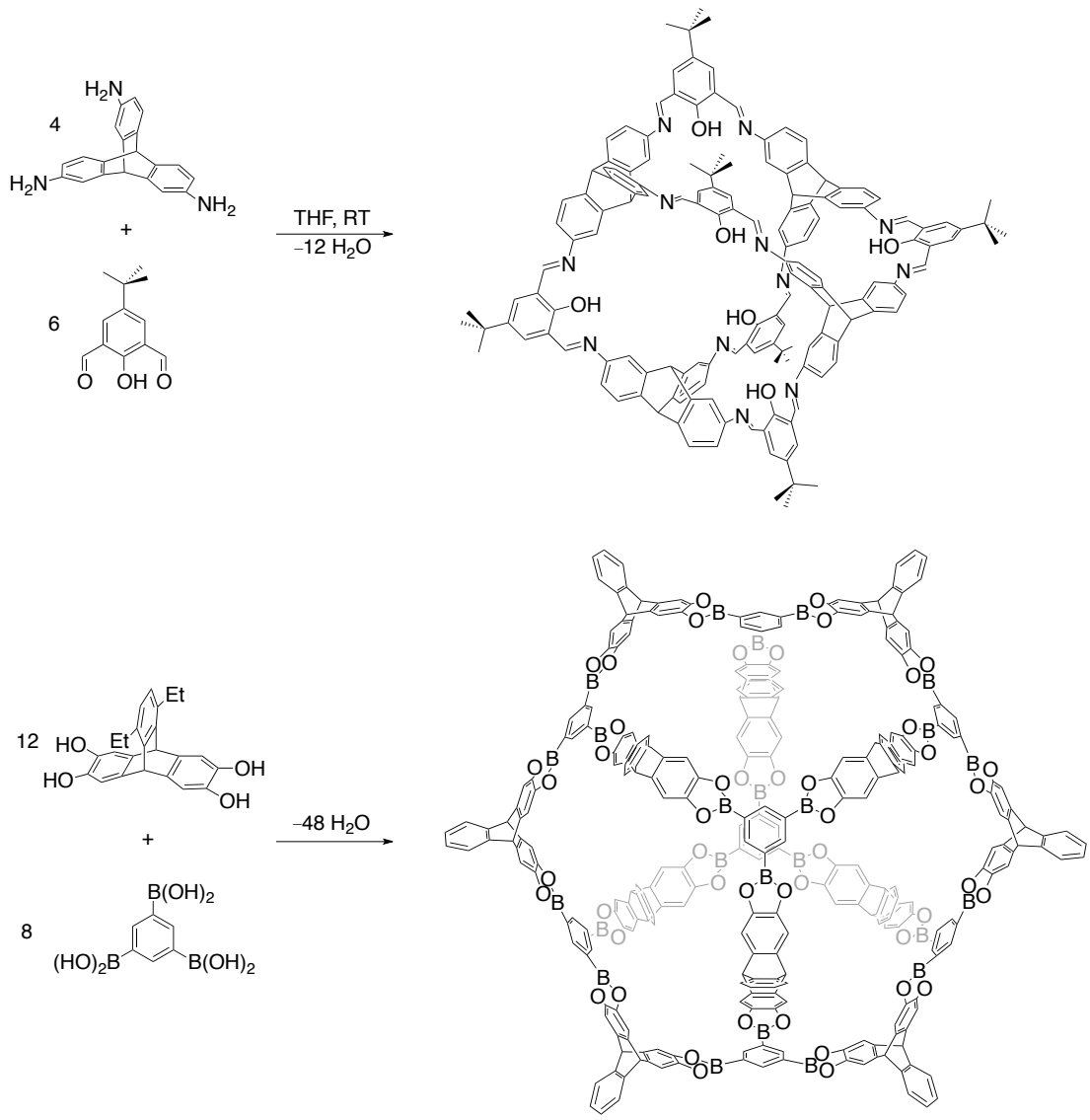

Scheme 4.6 Synthesis of [4+6] imine cage compound (top) and [12+8] boronic ester cage (bottom).

4.1.4 Extrinsically Porous Materials

Extrinsic pores are constructed by the inefficient packing of organic molecules, wherein the porosity is not intrinsic to any individual isolated molecule. One of the comprehensively studied extrinsically porous materials is *tris-o*-phenylenedioxycyclotriphosphazene (TPP) featuring a phosphazene (P_3N_3) core with three orthogonal catechol rings (Figure 4.3A).[30] According to the crystal structure and

gaseous sorption isotherms, this one-dimensional hexagonal porous material could accommodate small molecules such as CO_2 and CH_4. Besides the innovative design of new molecules, McKeown et al. searched the Cambridge Structural Database and found the potential noncovalent organic frameworks, 3,3'-4,4'-tetrakis(trimethylsilylethyl) biphenyl (4TMSEBP) (Figure 4.3B).[31] Based on the crystallographic data of this compound, the structure showed that its internal void has 11 Å as the diameter. With the gas sorption measurement, the BET surface area of 4TMSEBP was calculated as 278 m^2 g^{-1} and this porous material could adsorb N_2 as 4.4 mmol g^{-1} when $P/P_o = 1$ (P, absolute pressure; P_o, saturation pressure). The crystals of 4TMSEBP utilized the CH−π interactions between aromatic protons and the p orbital of acetylene (CH−C distance, < 2.90 Å) to build these extrinsic pores.

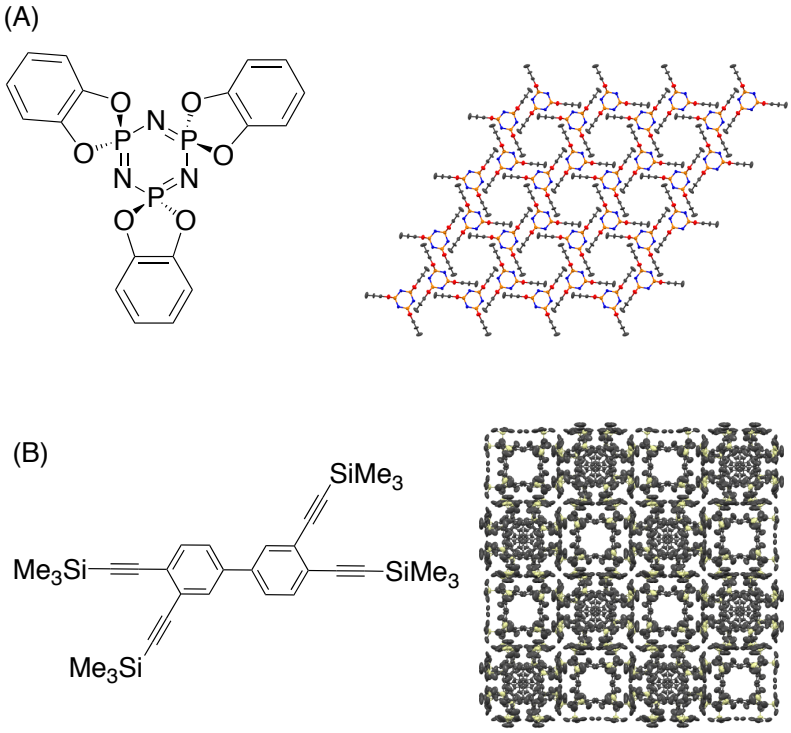

Figure 4.3 (A) Chemical structure of TPP and its crystal structure with extrinsic pores. (B) Chemical structure of 4TMSEBP and its crystal structure with extrinsic pores.

Hydrogen-bonding is a very common interaction widely utilized in organic frameworks to fortify the porosity. Chen and Zhong's groups synthesized several hydrogen-bonded organic frameworks (HOFs) with extrinsic pores.[32,33] Chen et al. reported the first HOF (**HOF-1**) composed of 2,4-diaminotriazine as the building unit, which conducted the one-dimensional channels via multiple hydrogen bonds.[32] **HOF-1** is stable up to 420 °C and its surface area is 359 m^2 g^{-1} in BET model based on the calculation from the N_2 sorption isotherm data. Moreover, **HOF-1** can selectively separate C_2H_2 from C_2H_4; the selectivity molar ratio of C_2H_2/C_2H_4 is 7.6 at 273 K under 1 atm.

Zhong's group also reported a noncovalent organic framework, **HOF-8**, fabricated by the organic building block N^1,N^3,N^5-tris(pyridin-4-yl)benzene-1,3,5-tricarboxamide (TPBTC) with a three dimensional microporous structure.[33] Not only is thermal stability increased to 350 °C, but **HOF-8** also exhibited highly selective CO_2 and benzene adsorption at ambient temperature.

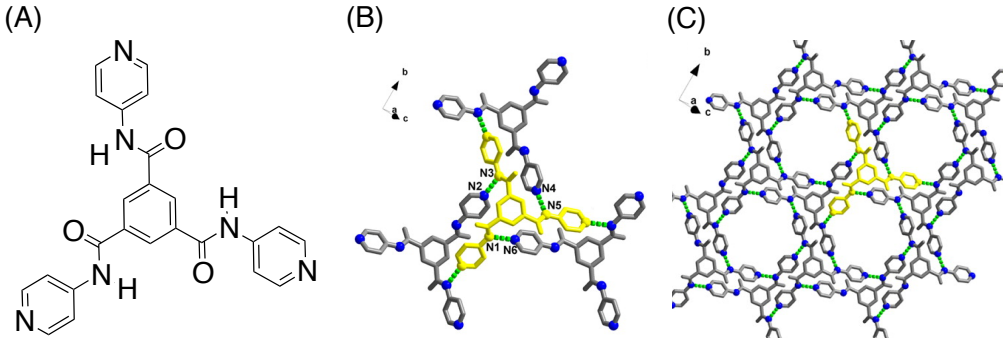

Figure 4.4 (A) Molecular structure of TPBTC. (B) Intramolecular hydrogen-bonding mode. (C) 2D layer structure of **HOF-8**.

Mastalerz's group synthesized the most porous extrinsic organic framework with BET surface area of 2796 m^2 g^{-1}.[34] They utilized the triptycene trisbenzimidazolone

(TTBI) as their building unit to construct the ribbon-like structure with one-dimensional pore channels (Figure 4.5). TGA measurement showed the high thermal stability of TTBI up to 440 °C; the characteristic sorption data unveiled that TTBI preferably adsorbed CO_2 rather than CH_4.

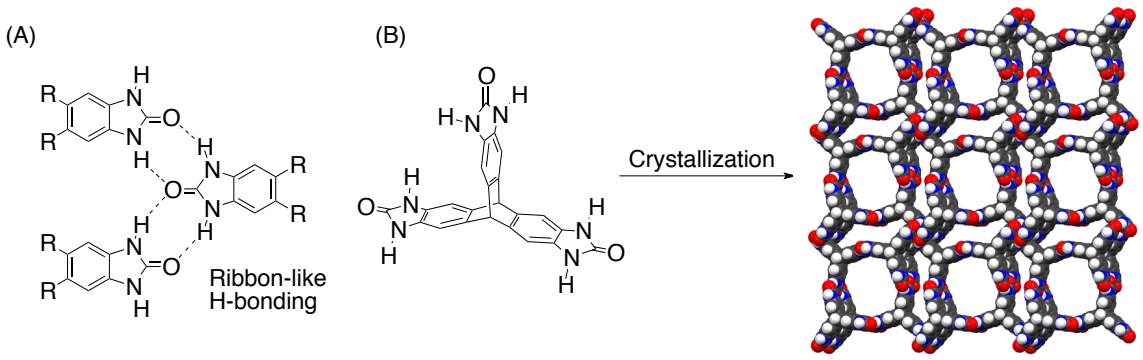

Figure 4.5 (A) Ribbon-like structure fabricated by H-bonding of 4,5-disubstituted benzimidazolones. (B) Crystal structure of TTBI. Colors: C, gray; H, white; O, red; N, blue.

Our group reported a fluorinated noncovalent organic framework, which was built up from a fluorinated trispyrazole molecule, resulting in an extrinsically porous material with high surface area (1,159 $m^2\ g^{-1}$, BET).[35] The structure was fortified with the combination of [N−H···N] hydrogen bonds between the terminal pyrazoles and the [π···π] stacking between the electron-poor tetrafluorobenzenes and the electron-rich pyrazoles (Figure 4.6); these noncovalent interactions also led to compositional stability up to 360 °C without weight loss. According to the variable-temperature PXRD, this trispyrazole porous material retained its structure and porosity stable up to 250 °C without significant pattern change. For the gas adsorption, this fluorinated porous material showed high affinity toward fluorocarbons and CFCs (up to 2.52 moles per mole of trispyrazole porous material).

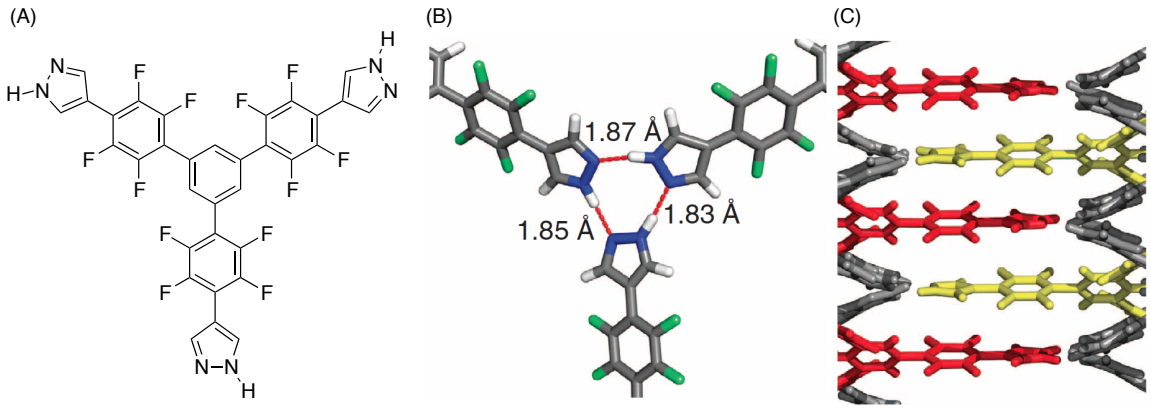

Figure 4.6 (A) Molecular structure of tripyrazole ligand. (B) [N−H···N] hydrogen-bonding between three pyrazole rings. (C) [π···π] stacking between electron-rich pyrazole and electron-poor tetrafluorobenzene.

4.1.5 Selective Adsorption of CO_2

Some porous molecular crystals show selective adsorption of CO_2 over N_2, in a manner similar to COFs and MOFs.[3] For instance (Scheme 4.7), Atwood et al. unraveled the selective adsorption of CO_2 presented by the waterwheel-like compound, the noria, which was reported by Nishikubo et al. in 2006[36]. This amorphous intrinsic pore manifested higher affinity toward CO_2 (9 wt% uptake at 18 bar, 298 K) over N_2 (1 wt% uptake at 18 bar, 298 K).[3]

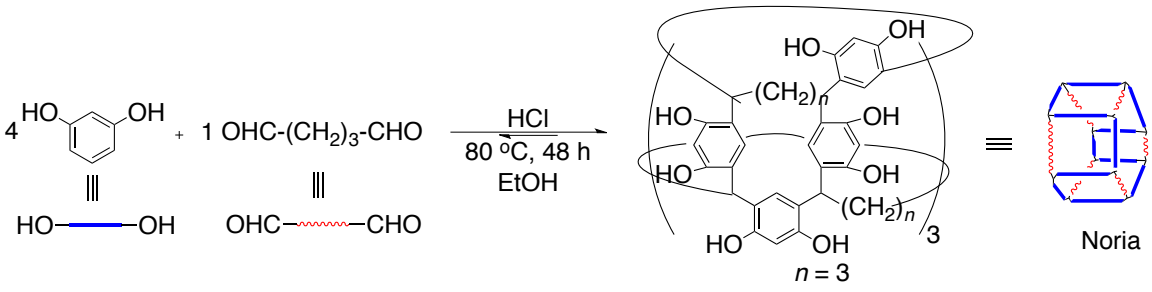

Scheme 4.7 Synthesis of noria—the waterwheel-like amorphous porous molecule.

Coskun et al. reported azo-based organic polymers that retained high selective adsorption of CO_2 over N_2 at high temperature (323 K, CO_2/N_2 = 288.1).[2a] The azo group

successfully decreased the affinity toward N_2 at higher temperature and the selectivity could be up to CO_2/N_2, 288.1:1, based on the IAST or CO_2/N_2 mixture (15%/85%).

These two examples displayed the potential applications of porous molecules, especially the gas separation of CO_2 over N_2. In the following section, I will show the characteristic studies of the fluorinated porous material—4,4',4''-(benzene-1,3,5-tris(2,3,5,6-tetrafluorophenyl 1*H*-tetrazole) **163** and the selective adsorption of CO_2.

4.2 Result and Discussion

4.2.1 Recrystallization and Characterization of 4,4',4''-(benzene-1,3,5-tris(2,3,5,6-tetrafluorophenyl 1*H*-tetrazole) 163

According to the adsorptive properties of trispyrazole-based fluorinated porous material,[36] we were inspired to unravel the possible porosity of another perfluroinated ligand derivative. With the innovative input of Dr. Popov,[37,38] the ligand—4,4',4''-(benzene-1,3,5-tris(2,3,5,6-tetrafluorophenyl 1*H*-tetrazole) **163**—was synthesized by the following steps (Scheme 4.8): upon complexation of 2,3,4,5-tetrafluorobenzocyanide with CuCl and KO^{t}Bu in the DMF solution, followed then the coupling reaction with 1,3,5-triiodobenzne catalyzed by $Pd(PPh_3)_4$, precursor **163** was obtained.

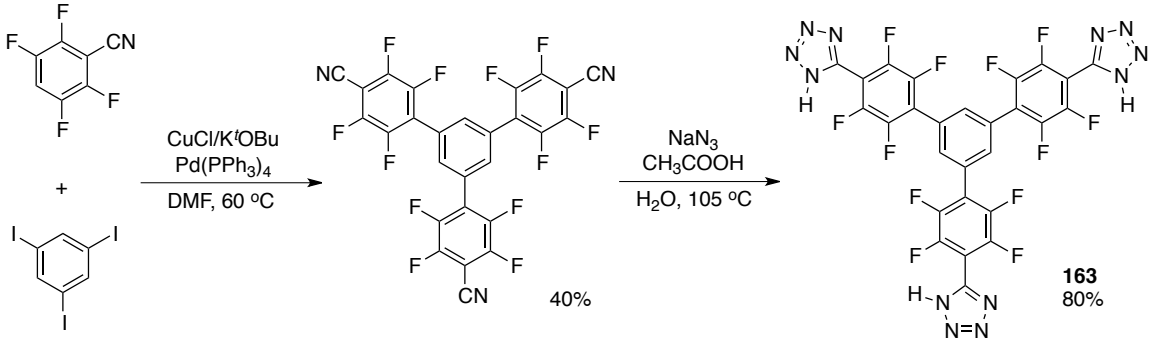

Scheme 4.8 Synthetic route to **163**.

This precursor was treated with NaN_3 and $ZnCl_2$ in the water solution with acetic acid to form the tristetrazole **163**. After the slow evaporation of mixed solvent (MeOH/PhMe, vol/vol 4:1) with **163**, we successfully obtained needle-like crystals. With the use of synchrotron radiation, the single-crystal X-ray diffraction data of **163** was collected and revealed a 3D structure. In Figure 4.7, the propeller-like crystal structure showed that it has a 3-fold rotation axis, and the torsion angles between the central ring and three tetrafluorobenzenes are all 50.88° (C4−C5−C8−C9); the molecule is not planar, and torsion angles between tetrafluorobenzene and tetrazoles are −34.51° (defined as angles C6−C2−C1−N4). The pore diameter is 12.1 Å (Figure 4.8B), displaying the microporous structure of **163**. Each molecule has six [N−H···N] hydrogen bonds (1.84 Å) between two adjacent layers of terminal tetrazoles (Figure 4.8A). The distance between the central benzenes of the adjacent layers is 4.97 Å, showing no apparent [π···π] stacking for extra secondary interaction in this framework, even though these two centroids are parallel (Figure 4.8A). In the same layer (Figure 4.9), the adjacent molecules have electrostatic interaction between C−F···C'−F' whose torsion angle is 0° and the distance is 3.30 Å.

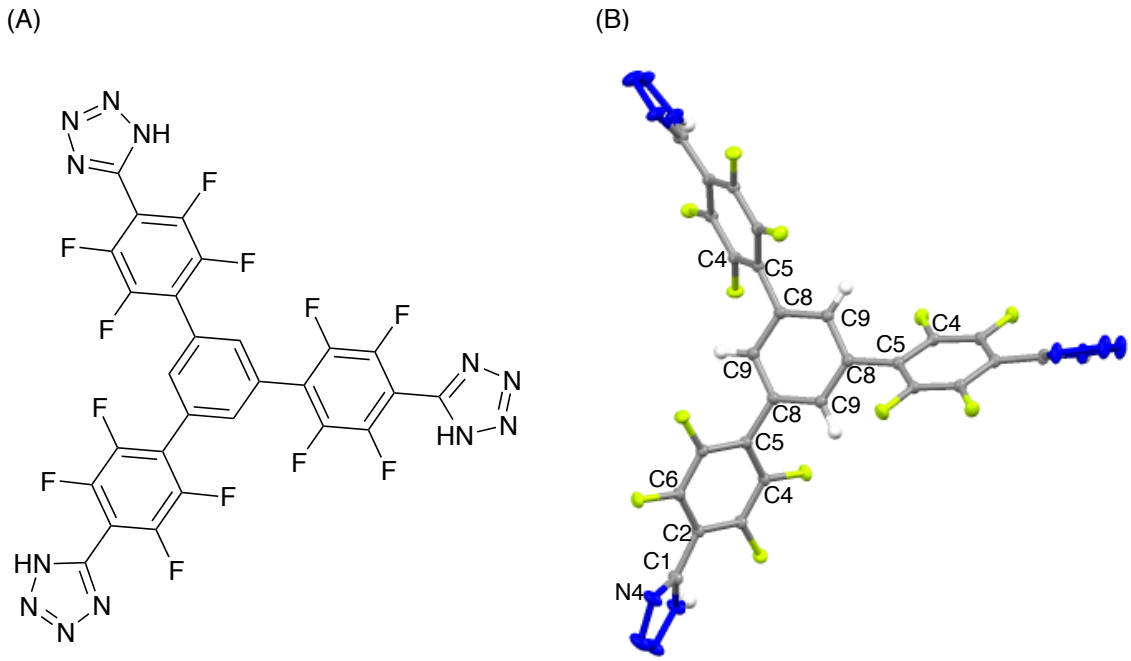

Figure 4.7 (A) Chemical structure of **163**. (B) Crystal structure of **163** shows the C_3 symmetry. The torsion angles are 50.9° (C4−C5−C8−C9) and −34.5° (C6−C2−C1−N4).

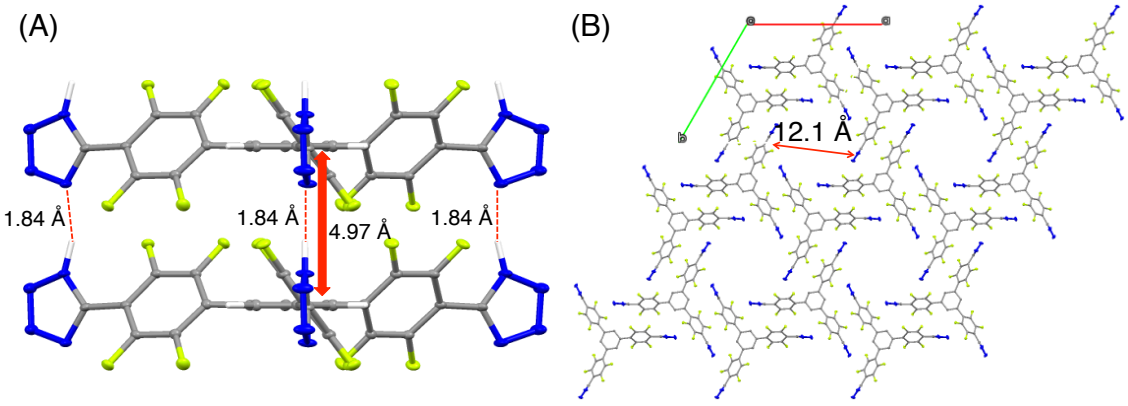

Figure 4.8 (A) [N−H···N] hydrogen bonds between two adjacent layers: 1.84 Å. (B) One-dimensional pore of **163** with 12.1 Å as its diameter.

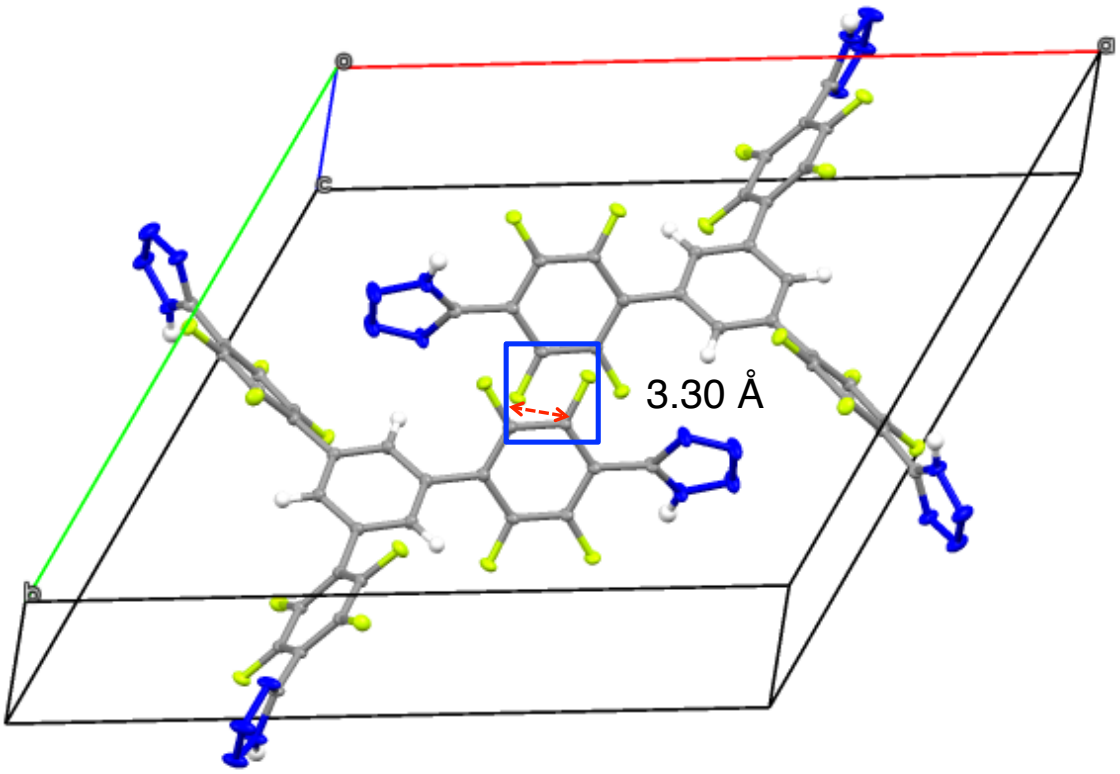

Figure 4.9 In the same layer, the adjacent molecules have electrostatic interaction between C−F···C'−F'. The distance is 3.30 Å and the torsion angle is 0°. Element colors: C—gray, F—yellow, N—blue, H—light gray.

Compound **163** is light yellow and was recrystallized from MeOH/PhMe at ambient temperature. We further preceded the powder X-ray diffraction (PXRD) of **163** after the evaporation of residual solvents from **163** under vacuum at 120 °C for 15 h. The unchanged PXRD patterns showed the same structure of the desolvated **163** as the solvated one.

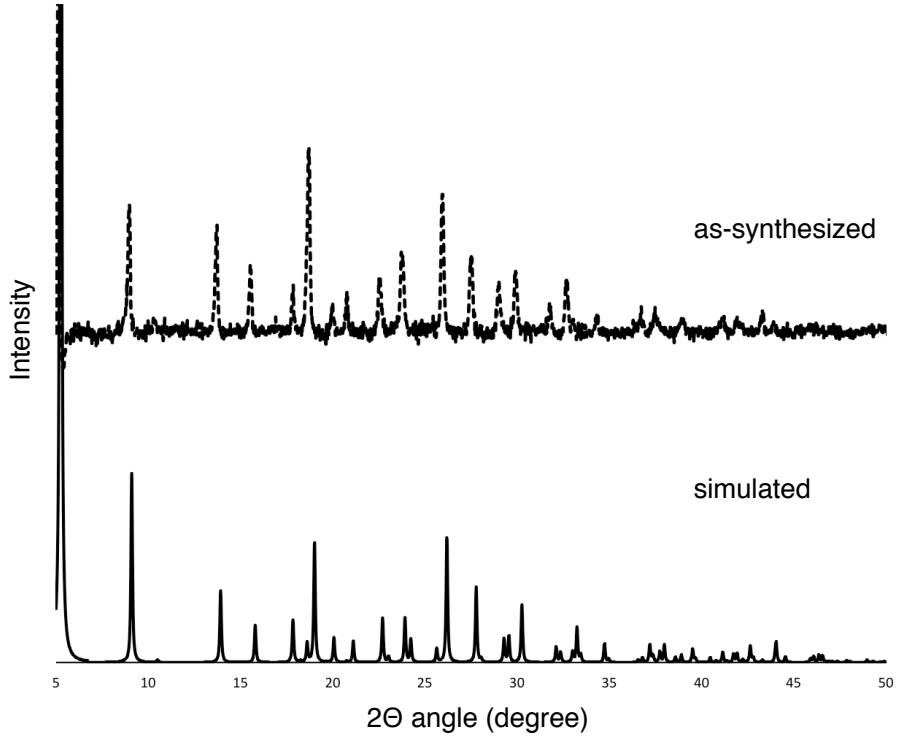

Figure 4.10 Powder X-ray diffraction patterns of **163**: as-synthesized vs. simulated from single crystal X-ray data.

Thermogravimetric analysis (TGA) of **163** was performed under air and nitrogen (Figure 4.10). Compound **163** did not lose any weight until 270 °C, suggesting that no significant amounts of synthesis solvent have been incorporated into the crystal. At 270 °C, compound **163** loses approximately 18% of its weight, under both nitrogen and air. For higher temperature, **163** loses ~50% weight under nitrogen at 600 °C and ~95% weight under air at 575 °C.

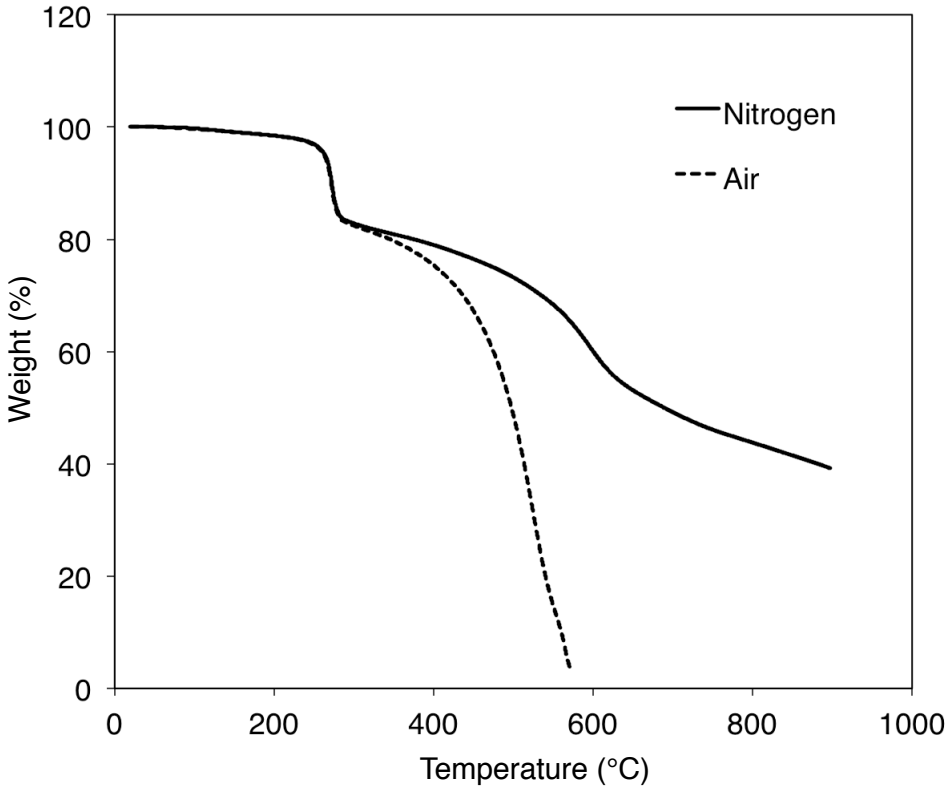

Figure 4.11 Thermogravimetric analysis of **163** under N_2 and air.

Gas sorption measurement of **163** was performed using CO_2 and N_2 at several temperatures (CO_2: 195 K, 273 K, 298 K; N_2: 77 K, 195 K, 273 K, 298 K). In Figure 4.12 (left), the isotherm of N_2 adsorption showed the lower adsorbed quantity than the CO_2 adsorption isotherm of **163** (Figure 4.12, right) which showed type I adsorption isotherm. Based on the CO_2 sorption isotherm, Langmuir surface area of **163** was calculated as 283 $m^2\ g^{-1}$. At 195 K (760 mmHg), **163** shows higher adsorption of CO_2 than N_2: the adsorbed quantity ratio of **163** is CO_2:N_2, 15:1, in mmol g^{-1} (Figure 4.13, left; Table 4.1) and 21:1 in weight percent (Figure 4.13, right). The CO_2 heat of adsorption of **163** is ~14.7 kJ mol^{-1} (For detailed calculation, see experimental section).

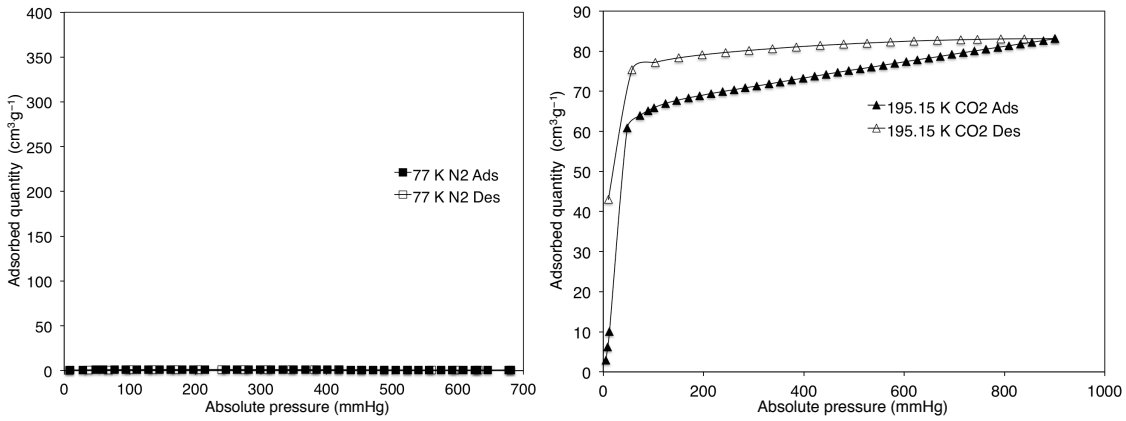

Figure 4.12 Left: nitrogen adsorption isotherm of **163** at 77 K. Right: CO_2 adsorption isotherm of **163** at 195 K. Langmuir surface area is 283 m^2 g^{-1}.

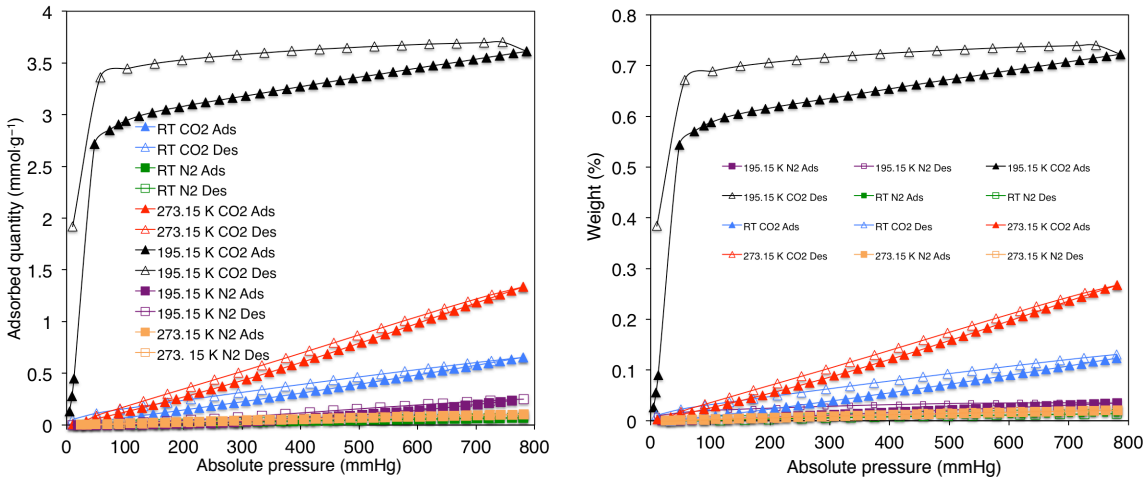

Figure 4.13 Compound **163** has selective adsorption of CO_2 and N_2 under 195 K, 273 K, and ambient temperature. Left: adsorbed quantity in mmol g^{-1}. Right: uptake in weight percent.

4.2.2 Comparison between Tristetrazole Framework 163 and Trispyrazole Framework 164

According to their single-crystal structure of **164** (Figure 4.6), each molecule of **164** interacts with twelve adjacent molecules to form six [N−H···N] hydrogen bonds and six [π···π] stacking interactions. The torsion angle of the adjacent tetrafluorobenzene and pyrazole rings is ~10° and the interplanar angle between the central benzenes is

approximately 10°. The corresponding [π···π] stacking, whose distance is ~3.68 Å, resulted from the efficient interplanar interaction in framework **164**. Framework **163** has six [N−H···N] hydrogen bonds with two neighbors from the adjacent layers. The non-planar geometry of **163** between the central ring and the arm conducts the "layer to layer" hydrogen bonding from the interplanar tetrazoles. The adjacent layers in **163** have no [π···π] stacking, wherein the electron-poor tetrafluorobenzenes could not stack with the electron-rich tetrazoles efficiently. The less rigid noncovalent bonding in framework **163** resulted in the closer packing among the unit building blocks. Diameter of pore in each framework also shows the smaller pore size of **163** (**163**, 12.1 Å; **164**, 16.9 Å). Based on their nitrogen adsorption isotherms, trispyrazole framework **164** has much higher surface area (1159 $m^2 g^{-1}$)[35] than compound **163** (283 $m^2 g^{-1}$); both frameworks retain the type I adsorption isotherm (**164** toward N_2, **163** toward CO_2).

Gas \ T (K)	77 K [a]	195 K [b]	273 K [b]	Ambient Temperature [b]
$V(CO_2)$ [mmol g^{-1}]	N/A	3.59 mmol g^{-1}	1.30 mmol g^{-1}	0.64 mmol g^{-1}
$V(N_2)$ [mmol g^{-1}]	0.03 mmol g^{-1}	0.24 mmol g^{-1}	0.10 mmol g^{-1}	0.07 mmol g^{-1}

Table 4.1 Comparison of CO_2 and N_2 absorbed quantity (mmol g^{-1}) of **163** under different temperatures. [a] at 680 mmHg; [b] at 760 mmHg.

4.3 Conclusion

Crystalline tristetrazole ligand **163** was successfully obtained via the recrystallization from MeOH/PhMe (vol/vol, 4:1) at ambient temperature. From the

single-crystal X-ray diffraction data, compound **163** shows the Langmuir surface area of, 283 m^2 g^{-1} based on its CO_2 adsorption isotherm. Moreover, **163** has selective adsorption of CO_2—14 times more than N_2 in mmol g^{-1} at 195 K under 780 mmHg. This noncovalent organic framework **163** fabricated by the perfluorinated tristetrazole ligand fortifies smaller pores with lower porosity, and displays decent selectivity between CO_2 and N_2. The thermal stability of **163** is up to 270 °C. These two properties of **163**—heat tolerance and selective adsorption—not only manifested the durability of this fluorinated porous material, but also extended the function of fluorinated porous materials from high affinity of fluorocarbons/CFCs to selective affinity toward one of the greenhouse gas sources—CO_2.

4.4 Experimental Section

4.4.1 General Methods and Materials

Synthesis of tristetrazole **163** is based on Dr. Ilja Popov's dissertation and has been published.[37,38] Recrystallization solvents (MeOH and PhMe) were obtained from commercial sources and used without further purification. Single-molecule X-ray diffraction data was collected at ChemMatCARS beamline at Advanced Photon Source in Argonne National Laboratory. Thermogravimetric analysis (TGA) was obtained with a TA Instruments TGA 2050 thermogravimetric analyzer under N_2 or air with the temperature ramping rate 2 °C/min. Gas adsorption measurements and data were proceeded with ASAP 2020. PXRD data was collected using PANalytical X'Pert PRO diffractometer.

4.4.2 Crystal Data of 163

Table 4.2 Crystal data and structure refinement for **163**

Empirical formula	C27.36 H6 F12 N12 O0.36	
Formula weight	736.52	
Temperature	100(2) K	
Wavelength	0.40651 Å	
Crystal system	Trigonal	
Space group	P -3	
Unit cell dimensions	a = 19.4179(17) Å	α = 90°.
	b = 19.4179(17) Å	β = 90°.
	c = 4.9668(4) Å	γ = 120°.
Volume	1621.9(3) $Å^3$	
Z	2	
Density (calculated)	1.508 Mg/m^3	
Absorption coefficient	0.049 mm^{-1}	
F(000)	730	
Crystal size	0.09×0.01×0.01 mm^3	
Theta range for data collection	2.400° to 22.082°.	
Index ranges	$-34 \le h \le 32$, $-33 \le k \le 34$, $-8 \le l \le 5$	
Reflections collected	25026	
Independent reflections	5588 [*R*(int) = 0.0457]	
Completeness to theta = 14.117°	95.0 %	
Absorption correction	None	
Refinement method	Full-matrix least-squares on F^2	
Data / restraints / parameters	5588 / 2 / 170	
Goodness-of-fit on F^2	1.023	
Final R indices [I>2sigma(I)]	R_1 = 0.0491, wR_2 = 0.1497	
R indices (all data)	R_1 = 0.0707, wR_2 = 0.1633	
Extinction coefficient	n/a	
Largest diff. peak and hole	0.652 and −0.334 $eÅ^{-3}$	

4.4.3 Gas Sorption Isotherms

The micrometrics ASAP 2020 accelerated surface area and porosimetry system was used to perform gas sorption measurements. Samples were pre-treated under vacuum for 24 h at ambient temperature and then transferred to the sample tube (~100 mg), which was then capped by a TranSeal^{TM}. During the degas process, samples were heated to 120 ˚C under high vacuum for 6 h. N_2 isotherms were measured using a liquid nitrogen bath (77 K), isopropanol-dry ice bath (195 K), ice-water bath (273 K), and water bath at ambient temperature (298 K). CO_2 isotherms were performed under 195 K, 273 K, and 298 K.

4.4.4 Calculation of CO_2 Adsorption Heat, Q_{st}

Method (A) Virial-type Thermal Equation

Virial-type equation of gas solid adsorption expression[39,40] was utilized to calculate the CO_2 adsorption heat of **163** at 273 K and 298 K. Retrieved adsorption data were fitted to the following equation: $\ln P = \ln N + \frac{1}{T}\sum_{i=0}^{m} a^i N^i + \sum_{i=0}^{n} b^i N^i$. P represents pressure (in Pa), N is adsorbed quantity (in mmol g^{-1}), and T is the temperature in Kelvin; then, a and b are virial coefficients, and m and n are the number of virial coefficients (a and b) needed for proper fitting of corresponding isothermal data.[18] After this proper fitting, the adsorption heat can be evaluated using this equation: $Q_{st} = -R\sum_{i=0}^{m} a^i N^i$, where R is the gas constant (8.314 J mol^{-1} K^{-1}). The detail of calculation process is shown in the following steps:

We made the equation $\ln P = \ln N + \frac{1}{T}\sum_{i=0}^{5} a^i N^i + \sum_{i=0}^{n2} b^i N^i$, then converted to $P = e\text{^}(\ln N + \frac{1}{T}\sum_{i=0}^{5} a^i N^i + \sum_{i=0}^{n2} b^i N^i)$. After all adsorption data from 273 K and 298 K

were fitted to this equation, we applied the retrieved a_0, a_1, a_2, a_3, a_4, and a_5 into $Q_{st} = -R\sum_{i=0}^{m} a^i N^i$. The Q_{st} at 50 mmHg is 14.79 kJ mol^{-1}.

Method (B) Langmuir-type Expression

The other method that can be also considered to evaluate the CO_2 heat adsorption is the single- or dual-site Langmuir-type expression: $N = \frac{q_{sat,A} b_A P}{1+b_A P} + \frac{q_{sat,B} b_B P}{1+b_B P}$.[41] N is the adsorbed quantity (mmol g^{-1}). q_{sat} is the saturated adsorbed quantity (mmol g^{-1}). b is the parameter in the Langmuir adsorption isotherm (Pa^{-1}). P is the pressure in the isotherm (Pa). With CO_2 adsorption isotherm of **163** at 273 K and 298 K, there are no perceptible inflections. Thus, the CO_2 adsorption is considered as single-site Langmuir model. The corresponding equation for data fitting is $N = \frac{q_{sat,A} b_A P}{1+b_A P}$. Here are two approaches we utilized to calculate the heat of adsorption:

(1) With the approximation, this expression can be simply converted to simple linear expression with these assumptions:

(i) Absolute pressure is close to 0 Pa. (ii) bP is much smaller than 1.

$N = \frac{q_{sat,A} b_A P}{1+b_A P}$, is simplified to $N = q_{sat,A} b_A P$. N is equal to q (adsorbed quantity in the isotherm), and the equation becomes: $\frac{q}{q_{sat}} = b_A P$, where q_{sat} is constant so that the equation can be converted to: $\alpha(V) = b_A P$, where $b_A = b_0 e\text{^}(\frac{E}{RT})$, α is the constant, and V is adsorbed quantity (mmol g^{-1}). The final expression is: $\alpha(V) = b_0 \exp(\frac{E}{RT}) P$, where E is the heat of adsorption (J mol^{-1}).

Based on CO_2 adsorption isotherm at 273 K and 298 K, we chose the absorption

under 50 mmHg for both measurements. Thus, the expression became:

At 273 K: $\alpha(1.31) = b_0[e\text{^}(\frac{E}{R(273)})]\times 50$;

At 298 K: $\alpha(0.76) = b_0[e\text{^}(\frac{E}{R(298)})]\times 50$.

These two equations were then divided and α, b_0, and 50 were eliminated. The simplified equation converted to: $\frac{1.31}{0.76} = \frac{e\text{^}(\frac{E}{R(273)})}{e\text{^}(\frac{E}{R(298)})}$, then combined with natural logarithm: $\ln\left(\frac{1.31}{0.76}\right) = \frac{E}{R}(\frac{1}{273} - \frac{1}{298})$. The adsorption heat of CO_2, E, was obtained as 14.73 kJ mol^{-1}. The isosteric heat of adsorption, Q_{st}, is 14.73 kJ mol^{-1}.

(2) We directly fitted the adsorption data to this equation, $N = \frac{q_{sat,A}b_A P}{1+b_A P}$, at 273 K and 298K. E was calculated as 14.66 kJ mol^{-1}. The isosteric heat, Q_{st}, is 14.66 kJ mol^{-1}.

4.5 References

[1] Akhtar, F.; Andersson, L.; Ogunwumi, S.; Hedin, N.; Bergström, L. *J. Eur. Ceram. Soc*. **2014**, *34*, 1643−1666.

[2] (a) Patel, H. A.; Hyun Je, S.; Park, J.; Chen, D. P.; Jung, Y.; Yavuz, C. T.; Coskun, A. *Nat. Commun.* **2013**, *4*, doi: 10.1038/ncomms2359; (b) Jeon, Y.-M.; Armatas, G. S.; Heo, J.; Kanatzidis, M. G.; Mirkin, C. A. *Adv. Mater.* **2008**, *20*, 2105−2110.

[3] Tian, J.; Thallapally, P. K.; Dalgarno, S. J.; McGrail, P. B.; Atwood, J. L. *Angew. Chem. Int. Ed.* **2009**, *48*, 5492−5495.

[4] Bae, T.-H.; Hudson, M. R.; Mason, J. A.; Queen, W. L.; Dutton, J. J.; Sumida, K.; Micklash, K. J.; Kaye, S. S.; Brown, C. M.; Long, J. R. *Energy Environ. Sci.* **2013**, *6*, 128−138.

[5] Abrams, L.; Corbin, D. R.; Shannon, R. D. Zeolite rho and ZK-5 catalysts for conversion of methanol and ammonia to dimethylamine. U.S. Patent 4,814,503, March 21, 1989.

[6] Corbin, D. R. Gas separation process. U.S. Patent 7,169,212, January 30, 2007.

[7] Yilmaz, B.; Trukhan, N.;w Müller, U. *Chin*. *J*. *Catal*. **2012**, *33*, 3−10.

[8] Themed issue of *Chem*. *Soc. Rev.* **2016**, *45*, 584−7127.

[9] Feng, X.; Ding, X.; Jiang, D. *Chem*. *Soc*. *Rev*. **2012**, *41*, 6010−6022.

[10] (a) Farrusseng, D. *Metal-Organic Frameworks: Applications from Catalysis to Gas Storage;* Wiley-VCH: Weinheim, Germany 2011; (b) MacGillivray. L. R. *Metal-Organic Frameworks: Design and Applications;* Wiley: Hoboken, NJ,

2010; (c) Special issue of *Chem*. *Soc*. *Rev*. **2009**, *38*, 1201−1508; (d) Special issue of *Chem*. *Rev*. **2012**, *112*, 673−1268.

[11] (a) Atwood, J. L.; Barbour, L. J.; Jerga, A. *Science* **2002**, *296*, 2367−2369; (b) Tozawa, T.; Jones, J. T. A.; Swamy, S. I.; Jiang, S.; Adams, D. J.; Shakespeare, S.; Clowes, R.; Bradshaw, D.; Hasell, T.; Chong, S. Y.; Tang, C.; Thompson, S.; Parker, J.; Trewin, A.; Bacsa, J.; Slawin, A. M. Z.; Steiner, A.; Cooper, A. I. *Nature Mater.* **2009**, *8*, 973−978; (c) Mitra, T.; Jelfs, K. E.; Schmidtmann, M.; Ahmed, A.; Chong, S. Y.; Adams, D. J.; Cooper, A. I. *Nature Chem.* **2013**, *5*, 276−281.

[12] Côté, A. P.; Benin, A. I.; Ockwig, N. W.; O'Keeffe, M.; Matzger, A. J.; Yaghi, O. M. *Science* **2005**, *310*, 1166−1170.

[13] Hunt, J. R.; Doonan, C. J.; LeVangie, J. D.; Côté, A. P.; Yaghi, O. M. *J. Am. Chem. Soc.* **2008**, *130*, 11872−11873.

[14] Uribe-Romo, F. J.; Hunt, J. R.; Furukawa, H.; Klöck, C.; O'Keeffe, M.; Yaghi, O. M. *J. Am. Chem. Soc.* **2009**, *131*, 4570-4571.

[15] Uribe-Romo, F. J.; Doonan, C. J.; Furukawa, H.; Oisaki, K.; Yaghi, O. M. *J. Am. Chem. Soc.* **2011**, *133*, 11478−11481.

[16] Zeng, Y.; Zou, R.; Zhao, Y. *Adv. Mater.* **2016**, *28*, 2855−2873.

[17] Kandambeth, S.; Mallick, A.; Lukose, B.; Mane, M. V.; Heine, T.; Banerjee, R. *J. Am. Chem. Soc.* **2012**, *134*, 19524−19527.

[18] Tong, M.; Yang, Q.; Xiao, Y.; Zhong, C. *Phys. Chem. Chem. Phys.* **2014**, *16*, 15189−15198.

[19] Zhao, Y.; Yao, K. X.; Teng, B.; Zhang, T.; Han, Y. *Energy Environ. Sci.* **2013**, *6*, 3684−3692.

[20] Kuhn, P.; Antonietti, M.; Thomas, A. *Angew. Chem. Int. Ed.* **2008**, *47*, 3450−3453.

[21] Li, H.; Eddaoudi, M.; O'Keeffe, M.; Yaghi, O. M. *Nature* **1999**, *402*, 276−279.

[22] Sumida, K.; Rogow, D. L.; Mason, J. A.; McDonald, T. M.; Bloch, E. D.; Herm, Z. R.; Bae, T.-H.; Long, J. R. *Chem. Rev.* **2012**, *112*, 724−781.

[23] Chae, H. K.; Siberio-Perez, D. Y.; Kim, J.; Go, Y.; Eddaoudi, M.; Matzger, A. J.; O'Keeffe, M.; Yaghi, O. M. *Nature* **2004**, *427*, 523−527.

[24] Britt, D.; Furukawa, H.; Wang, B.; Glover, T. G.; Yaghi, O. M. *Proc. Natl. Acad. Sci. USA* **2009**, *106*, 20637−20640.

[25] Mason, J. A.; Sumida, K.; Herm, Z. R.; Krishna, R.; Long, J. R. *Energy Environ. Sci.* **2011**, *4*, 3030−3040.

[26] Fei, H.; Shin, J.; Meng, Y. S.; Adelhardt, M.; Sutter, J.; Meyer, K.; Cohen, S. M. *J. Am. Chem. Soc.* **2014**, *136*, 4965−4973.

[27] Holst, J. R.; Trewin, A.; Cooper, A. I. *Nature Chem.* **2010**, *2*, 915−920.

[28] Mastalerz, M.; Schneider, M. W.; Oppel, I. M.; Presly, O. *Angew. Chem. Int. Ed.* **2011**, *50*, 1046−1051.

[29] Schneider, M. W.; Oppel, I. M.; Griffin, A.; Mastalerz, M. *Angew. Chem. Int. Ed.* **2013**, *52*, 3611−3615.

[30] Sozzani, P.; Bracco, S.; Comotti, A.; Ferretti, L.; Simonutti, R. *Angew. Chem. Int. Ed.* **2005**, *44*, 1816−1820.

[31] Msayib, K. J.; Book, D.; Budd, P. M.; Chaukura, N.; Harris, K. D. M.; Helliwell, M.; Tedds, S.; Walton, A.; Warren, J. E.; Xu, M.; McKeown, N. B. *Angew. Chem. Int. Ed.* **2009**, *48*, 3273−3277.

[32] He, Y.; Xiang, S.; Chen, B. *J. Am. Chem. Soc.* **2011**, *133*, 14570−14573.

[33] Luo, X.-Z.; Jia, X.-J.; Deng, J.-H.; Zhong, J.-L.; Liu, H.-J.; Wang, K.-J.; Zhong, D.-C. *J. Am. Chem. Soc.* **2013**, *135*, 11684−11687.

[34] Mastalerz, M.; Oppel, I. M. *Angew. Chem. Int. Ed.* **2012**, *51*, 5252−5255.

[35] Chen, T.-H.; Popov, I.; Kaveevivitchai, W.; Chuang, Y.-C.; Chen, Y.-S.; Daugulis, O.; Jacobson, A. J.; Miljanić, O. Š. *Nat. Commun.* **2014**, *5*, doi: 10.1038/ncomms6131.

[36] Kudo, H.; Hayashi, R.; Mitani, K.; Yokozawa, T.; Kasuga, N. C.; Nishikubo, T. *Angew. Chem. Int. Ed.* **2006**, *45*, 7948−7952.

[37] Popovs, I. Ph. D. Dissertation, University of Houston, Houston, TX, May 2014.

[38] Chen, T.-H.; Popov, I.; Kaveevivitchai, W.; Chuang, Y.-C.; Chen, Y.-S.; Jacobson, A. J.; Miljanić, O. Š. *Angew. Chem. Int. Ed.* **2015**, *54*, 13902−13906.

[39] Czepirsky, L.; Jagiello, J. *Chem. Eng. Sci.* **1989**, *44*, 797−801.

[40] Sumida, K.; Rogow, D. L.; Mason, J. A.; McDonald, T. M.; Bloch, E. D.; Herm, Z. R.; Bae, T.-H.; Long, J. R. *Chem. Rev.* **2012**, *112*, 724−781.

[41] Mason, J. A.; Sumida, K.; Herm, Z. R.; Krishna, R.; Long, J. R. *Energy Environ. Sci.* **2011**, *4*, 3030−3040.